2012

Microstructure study of the rare-earth intermetallic compounds R5(SixGe1-x)4 and R5(SixGe1-x)3

Qing Cao
Iowa State University

Microstructure study of the rare-earth intermetallic compounds $R_5(Si_xGe_{1-x})_4$ and $R_5(Si_xGe_{1-x})_3$

by

Qing Cao

A dissertation submitted to the graduate faculty

in partial fulfillment of the requirements for the degree of

DOCTOR OF PHILOSOPHY

Major: Materials Science and Engineering

Program of Study Committee:

L. Scott Chumbley, Major Professor

Vitalij K. Pecharsky

Karl A. Gschneidner, Jr.

Alan M. Russell

Gordon J. Miller

Iowa State University

Ames, Iowa

2012

TABLE OF CONTENTS

ABSTRACT

The unique combination of magnetic properties and structural transitions exhibited by many members of the $R_5(Si_xGe_{1-x})_4$ family (R = rare earths, $0 \leq x \leq 1$) presents numerous opportunities for these materials in advanced energy transformation applications. Past research has proven that the crystal structure and magnetic ordering of the $R_5(Si_xGe_{1-x})_4$ compounds can be altered by temperature, magnetic field, pressure and the Si/Ge ratio. Results of this thesis study on the crystal structure of the Er_5Si_4 compound have for the first time shown that the application of mechanical forces (i.e. shear stress introduced during the mechanical grinding) can also result in a structural transition from Gd_5Si_4-type orthorhombic to $Gd_5Si_2Ge_2$-type monoclinic. This structural transition is reversible, moving in the opposite direction when the material is subjected to low-temperature annealing at 500 ˚C.

Successful future utilization of the $R_5(Si_xGe_{1-x})_4$ family in novel devices depends on a fundamental understanding of the structure-property interplay on the nanoscale level, which makes a complete understanding of the microstructure of this family especially important. Past scanning electron microscopy (SEM) observation has shown that nanometer-thin plates exist in every $R_5(Si_xGe_{1-x})_4$ (“5:4”) phase studied, independent of initial parent crystal structure and composition. A comprehensive electron microscopy study including SEM, energy dispersive spectroscopy (EDS), selected area diffraction (SAD), and high resolution transmission electron microscopy (HRTEM) of a selected complex 5:4 compound based on Er rather than Gd, $(Er_{0.9}Lu_{0.1})_5Si_4$, has produced data supporting the assumption that all the platelet-like features present in the $R_5(Si_xGe_{1-x})_4$ family are hexagonal $R_5(Si_xGe_{1-x})_3$ (“5:3”)

phase and possess the same reported orientation relationship that exists for the Gd_5Ge_4 and $Gd_5Si_2Ge_2$ compounds, i.e. $[010](10\bar{2})_m \parallel [10\bar{1}0](1\bar{2}11)_p$. Additionally, the phase identification in $(Er_{0.9}Lu_{0.1})_5Si_4$ carried out using X-ray powder diffraction (XRD) techniques revealed that the low amount of 5:3 phase is undetectable in a conventional laboratory Cu Kα diffractometer due to detection limitations, but that extremely low amounts of the 5:3 phase can be detected using high resolution powder diffraction (HRPD) employing a synchrotron source. These results suggest that use of synchrotron radiation for the study of $R_5(Si_xGe_{1-x})_4$ compounds should be favored over conventional XRD for future investigations.

The phase stability of the thin 5:3 plates in a Gd_5Ge_4 sample was examined by performing long-term annealing at very high temperature. The experimental results indicate the plates are thermally unstable above 1200˚C. While phase transformation of 5:3 to 5:4 occurs during the annealing, the phase transition is still fairly sluggish, being incomplete even after 24 hours annealing at this elevated temperature. Additional experiments using laser surface melting performed on the surface of a $Ho_5(Si_{0.8}Ge_{0.2})_4$ sample showed that rapid cooling will suppress the precipitation of 5:3 plates.

Bulk microstructure studies of polycrystalline and monocrystalline Gd_5Ge_3 compounds examined using optical microscopy, SEM and TEM also show a series of linear features present in the Gd_5Ge_3 matrix, similar in appearance in many ways to the 5:3 plates observed in $R_5(Si_xGe_{1-x})_4$ compounds. A systematic microscopy analysis of these linear features revealed they also are thin plates with a stoichiometric composition of Gd_5Ge_4 with an

orthorhombic structure. The orientation relationship between the 5:3 matrix and the precipitate 5:4 thin plates was determined as $[10\bar{1}0]\,(1\bar{2}11)_m \parallel [010]\,(10\bar{2})_p$.

CHAPTER 1. Introduction

General Introduction

The possibility of producing devices that utilize the magnetocaloric effect as an alternate technology for refrigeration, rather than the common gas compression/expansion method, has long been of interest. In order to be commercially viable, the first criterion a suitable material must exhibit is that the magnetocaloric effect be present in a temperature range that is of primary interest. For example, cooling slightly below room temperature (~ 250 K - 290 K) is of particular interest because of the potential impact on energy savings and environmental concerns for common refrigerators and air-conditioners. The second criterion is that the material possess a large magnetocaloric effect, since the larger the effect the greater the potential for improved energy efficiency. The rare-earth based intermetallic system $R_5(Si_xGe_{1-x})_4$, is a material that satisfies both criteria. Thus, this family of alloys has captured the attention of scientists all over the world and has led to extensive research on the magnetic properties and microstructures of this system of intermetallic compounds. In addition, there is increasing interest in other families of rare-earth based intermetallic compounds, namely, the $R_5(Si_xGe_{1-x})_3$-type compounds, because the particular structures of these materials lend themselves to modifications through chemical means, allowing researchers to experiment and test a wide array of modified structures that exhibit rich physical and chemical properties. Some important information and knowledge about the magnetocaloric effect and both families of $R_5(Si_xGe_{1-x})_4$ and $R_5(Si_xGe_{1-x})_3$ are provided in this chapter as research background. At the end of this chapter, the motivations of this study

are presented.

Discovery of Magnetocaloric Effect (MCE)

The magnetocaloric effect (MCE) is a magneto-thermodynamic phenomenon in which a reversible change in temperature of a suitable material is caused by exposing the material to a changing magnetic field. This is also known by low temperature physicists as adiabatic demagnetization, due to the application of the process specifically to affect a temperature drop. The MCE is an intrinsic property of all magnetic materials and is due to the coupling of the magnetic sublattice with the magnetic field, which changes the magnetic part of the entropy of a solid. The effect was first observed in iron by the German physicist Emil Warburg in 1880 [1] and the fundamental principle of the MCE and its practical use to reach ultralow temperature was suggested by Debye (1926) [2] and Giauque (1927) [3] independently.

Fundamentals of MCE

For a magnetic solid, the total entropy S(T,H) at constant pressure is a function of both the magnetic field strength H and the absolute temperature T. The total entropy S of a magnetic solid consists of three contributions, the magnetic part S_M which is also a function of H and T, the lattice part S_L, and the electronic part S_E, which are independent of the magnetic field strength H:

$$S(T,H) = S_M(T,H) + S_L(T) + S_E(T)$$

The relation between the entropy S and the absolute temperature T in a ferromagnet near its

Curie temperature T_C (magnetic ordering temperature) is illustrated schematically in Figure 1[4]. The solid lines represent the total entropy in two different magnetic fields: $H_0 = 0$ and $H_1 > 0$. The horizontal arrow shows ΔT_{ad} and the vertical arrow shows ΔS_M when the magnetic field is changed from H_0 to H_1. The dotted line shows the combined lattice and electronic (non-magnetic) entropy, and dashed lines show the magnetic entropy in the two fields. S_0 and T_0 are zero field entropy and temperature, respectively, S_1 and T_1 are entropy and temperature at the elevated magnetic field H_1.

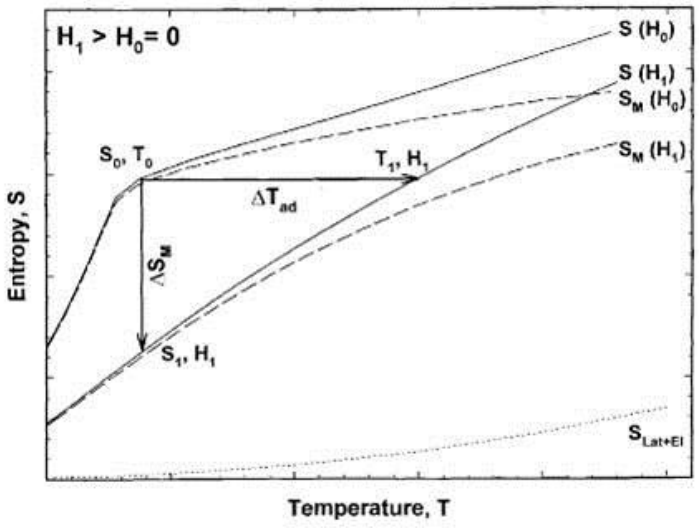

Figure 1. The S-T diagram illustrating the existence of the magnetocaloric effect. (From Ref. [4])

Similar to isothermal compression of a gas, during which the positional disorder and the corresponding component of the total entropy are decreased, exposing a ferromagnet to a change of a magnetic field from zero H_0 to a higher field H_1 near its Curie temperature Tc results in magnetic ordering, which will reduce the disorder of a spin system, thus lowering the magnetic part of the total entropy which is shown as ΔS_M in Figure 1. Reversibly, like the isothermal expansion of a gas, isothermal demagnetization will restore the zero field

magnetic entropy. When a gas is compressed adiabatically, its total entropy remains constant, whereas velocities of the constituent gas molecules, and the temperature of the gas, increase. Likewise, after a ferromagnet experiences adiabatic magnetization (demagnetization), the sum of the lattice and electronic entropies must change by the opposite of the change of magnetic entropy, leading to an increase (decrease) of temperature $\Delta T_{ad,}$ Therefore, $\Delta T_{ad.}$ and ΔS_M are two quantitative measures of the magnetocaloric effect.

The quantities ΔT_{ad} and ΔS_M are correlated with magnetization M, the magnetic field strength H, the heat capacity C, and the absolute temperature T by one of Maxwell's relations: [5]

$$(\frac{\partial M}{\partial T})_H = (\frac{\partial S}{\partial H})_T \quad (1)$$

For an isothermal-isobaric process, the integration of equation (1) gives

$$\Delta S_M = \int_{H_1}^{H_2} (\frac{\partial M}{\partial T})_H \, dH \quad (2)$$

The specific heat capacity C at constant magnetic field strength H can be expressed as equation (3):

$$C_H = T(\frac{\partial S}{\partial T})_H \quad (3)$$

Combining equation (1) and (3) yields:

$$C_H dT = -T\left(\frac{\partial M}{\partial T}\right)_H dH \quad (4)$$

A finite adiabatic change in magnetic field thus produces a temperature change given by:

$$\Delta T_{ad} = -\int_{H_1}^{H_2} \frac{T}{C_H} (\frac{\partial M}{\partial T})_H \, dH \quad (5)$$

Equations (2) and (5) are important if one is to understand the behavior of the MCE in

solids. They also serve as a guide for the search for new materials with a large magnetocaloric effect. Since for paramagnets and simple ferromagnets, $(\frac{\partial M}{\partial T})_H < 0$, then ΔS_M should be negative (Eq. 2), and ΔT_{ab} should be positive (Eq. 5), which also agrees with Figure 1. Additionally, in ferromagnets $\left|(\frac{\partial M}{\partial T})_H\right|$ has the largest value at T_C and, therefore, $|\Delta S_M|$ should peak at T_C. The behavior of ΔT_{ad} is similar to that of $|\Delta S_M|$, i.e it will peak at T_C.

Application of MCE : Magnetic Refrigeration

Global warming and energy shortages due to increasing world-wide energy consumption are driving efforts to find new ways to save energy. As mentioned in Gschneidner and Pecharsky's review [6], 15% of the total worldwide energy consumption involves the use of refrigeration (air conditioning, refrigeration, freezing, chilling, etc). Magnetic refrigeration as a cooling technology has the potential to lower energy consumption by 20-30% over conventional vapor compression technology. Therefore, interest in magnetic refrigeration has grown considerably over the past ten years. Magnetic refrigeration has a number of advantages in additional to lower energy consumption, being a solid-state cooling technology that has the potential to be more environmentally friendly than vapor compression methods. The technique also can be used to attain extremely low temperature (well below 1K), as well as achieve cooling in the ranges used in common refrigerators, depending on the design of the system.

The history of magnetic refrigeration can be traced to the middle of the last century, when Collins and Zimmerman [7] built and tested magnetic refrigerators operating between ~1

and 0.73K by periodically magnetizing and demagnetizing iron ammonium alum. The first near-room-temperature continuously operating magnetic refrigerator was reported by Brown in 1976 [8], which made it clear that magnetic refrigeration had the potential to be utilized at significantly higher temperatures and achieve much larger temperature spans. Ever since then the development of prototype magnetic refrigerators has spread to numerous universities and institutes across the globe. More than 25 prototype magnetic refrigerators capable of operating with varying degrees of efficiency at room temperature have been built and tested to date. Prototypes show a cooling power of up to 600 W and a temperature span of up to 50˚C, depending on the magnetic flux density and the amount of magnetocaloric material used. The most advanced and important of all current prototypes are the three devices made by the Astronautics Corporation of America in 1998 [9], 2003 [10], and 2007 [11], which seem to be setting the trend for magnetic refrigeration development.

The basic operating principle of an adiabatic demagnetization refrigerator (ADR) is the use of a strong magnetic field to control the entropy of a volume of material, often called the "refrigerant". The thermodynamic cycle during the process of magnetic refrigeration is performed as a refrigeration cycle, analogous to the Carnot cycle, and can be described from a starting point where the magnetocaloric substance, (i.e. the refrigerant) is introduced into a magnetic field. The refrigerant starts in thermal equilibrium with the refrigerated environment. The cycle mainly consists of four steps as shown in Figure 2 [12].

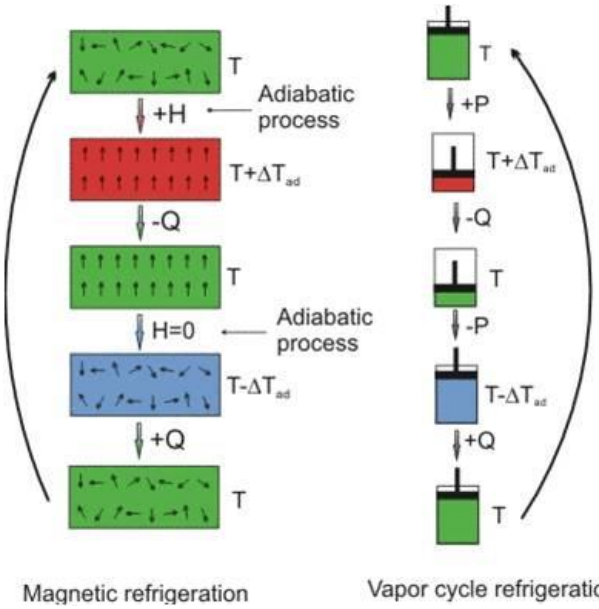

Figure 2. Analogy between magnetic refrigeration and vapor cycle or conventional refrigeration. H = externally applied magnetic field; Q = heat quantity; P = pressure; ΔT_{ad} = adiabatic temperature variation. (From Ref. [12])

- **Adiabatic magnetization:** A magnetocaloric substance is placed in an insulated environment. An increasing external magnetic field (+H) causes the magnetic dipoles of the atoms to align. The stronger the external magnetic field, the more aligned the dipoles become, corresponding to lower entropy and heat capacity because the material has effectively lost some of its internal degrees of freedom. Since the substance is placed in an insulated environment, overall energy is not lost and total entropy is not reduced (according to thermodynamic laws), i.e it is an isentropic process. The net result is that the substance heats ($T + \Delta T_{ad}$).

- **Isomagnetic enthalpic transfer:** The added heat can then be removed (-Q) by a fluid or gas — gaseous or liquid helium, for example. The magnetic field is held

constant to prevent the dipoles from reabsorbing the heat. Once sufficiently cooled, the magnetocaloric substance and the coolant are separated.

- **Adiabatic demagnetization:** The magnetocaloric substance is returned to another adiabatic (insulated) condition so the total entropy remains constant. However, this time the magnetic field is decreased to zero, the heat capacity of the refrigerant rises again because the degrees of freedom associated with orientation of the dipoles are once again liberated, thereby lowering the overall temperature of the system and, thus, the refrigerant cools via an adiabatic temperature change. Energy (and entropy) transfers from thermal entropy to magnetic entropy (disorder of the magnetic dipoles).

- **Isomagnetic entropic transfer:** After the magnetic field is removed, the magnetocaloric substance is placed in thermal contact with the environment being refrigerated. Because the magnetocaloric substance is cooler than the refrigerated environment (by design), heat energy migrates into the magnetocaloric substance (+Q).

In practice, the magnetic field is decreased slowly in order to provide continuous cooling and keep the sample at an approximately constant low temperature. Once the field falls to zero, or to some low limiting value determined by the properties of the refrigerant, the cooling power of the adiabatic demagnetization refrigerator vanishes, and heat leaks will cause the refrigerant to warm.

Magnetocaloric Materials

Interest in the MCE and the number of related publications worldwide increased dramatically after the discovery of the giant MCE in $Gd_5Si_2Ge_2$ in 1997 [13]. The great variety of magnetocaloric materials can be grouped into three main families: the 4f lanthanide metals and their intra-lanthanide alloys and compounds; the 3d transition metals and their alloys and compounds; and mixed 4f lanthanide - 3d transition metal materials. Of these groups the 4f lanthanide family holds the most promise for eventual commercial applications.

When comparing the measured MCE in different 4f lanthanide metals including Nd [14], Gd [8, 9, 15-18], Tb [17,18], Dy [15-18], Ho [16-18], Er [18], and Tm [18,19], Gd has the largest near room–temperature MCE and has been successfully used as a magnetic refrigerant to provide cooling between ~270 and ~310K [8, 9]. Tb and Dy show a somewhat lower MCE, but could still be used as magnetic refrigerant materials. Other lanthanides metals are considered unusable as magnetic refrigerants because of their low MCE. The intra-lanthanide alloys are prepared by arc-melting two lanthanide metals together, such as $Gd_{1-x} - Dy_x$, where x = 0.12, 0.28, 0.44, and 0.70 [20], $Gd_{0.84}Er_{0.16}$ [21], $Gd_{1-x} - Y_x$, where x = 0.25, 0.48, and 0.52 [16, 22, 23], $Gd_{0.85}Tb_{0.15}$ [24]. The addition of one lanthanide metal to another can adjust the magnetic ordering temperature and, therefore, the maximum MCE and the range of operating temperatures.

The magnetic-ordering temperature and MCE of various lanthanide compounds including lanthanide dialuminides RAl_2 (R = Dy, Er [25,26], and Ho [26]]), GdPd [15,27], zinc alloy

$Gd_{0.75}Zn_{0.25}$ [24], $Gd_5(Si_xGe_{1-x})_4$ [13, 28, 29], etc. have been directly measured or indirectly calculated from the measured magnetization or heat capacity, both as a function of temperature and magnetic field. Among these lanthanide compounds, $Gd_5(Si_xGe_{1-x})_4$ compounds are unique as good candidates for magnetic refrigerant materials not only due to their large magnetocaloric effects, but also because of two additional features. The first is that their Curie temperature can be tuned between ~ 20 K and ~ 300 K by manipulating the chemical composition, namely the Si to Ge ratio [29]. The second is that the giant magnetocaloric effect in the $Gd_5(Si_xGe_{1-x})_4$ alloys ($0 \leq x \leq 0.5$) is reversible, i.e. it does not disappear after the first application of the magnetic field [4].

The Curie points of 3d transition metals are much higher than room temperature, such as Fe (1042 K), Co (1386 K), and Ni (633 K). Additionally, the MCE in transition metal–based alloys is smaller than is seen in lanthanide-based alloys for the same temperature range. These factors make 3d transition metals unlikely candidates for use as magnetic refrigerant materials below 300 K, but they may be useful materials for magnetic refrigerators/heat pumps rejecting heat well above room temperature. The Curie temperatures of 3d transition metals can be decreased dramatically by mixing with 4f lanthanides. For example, $TbNi_2$ orders ferromagnetically at 38 K, $ErCo_2$ exhibits a first order magnetic/structural transition at 31 K, and Er_3Ni orders at 6 K. However, since these temperatures are far below room temperature, compounds such as these are not good candidates for magnetic refrigerant materials. A detailed review about the magnetic properties of 3d transition metals, their alloys and compounds, and mixed 4f lanthanide - 3d transition metal materials can be found in [30].

Literature Review

The $R_5(Si_xGe_{1-x})_4$ Family of Intermetallic Compounds

The $R_5(Si_xGe_{1-x})_4$ (hereafter referred to as "5:4") family of intermetallic compounds (R = rare-earth metal) was first studied nearly half a century ago by Smith et al [31]. Both the silicides R_5Si_4 and germanides R_5Ge_4 (except La, Ce, Pr, Nd, and Lu silicides) [32] were initially assigned to the layered Sm_5Ge_4 crystal structure[33]. However, Holtzberg et al. [34] discovered that the crystal structures of R_5Si_4 and R_5Ge_4 were in fact different, and described the inequality between the two phases. They also found an unknown intermediate phase in $Gd_5(Si_xGe_{1-x})_4$ alloys for $0.24 \leq X \leq 0.5$ which was later determined to have a monoclinic structure at room temperature by Pecharsky and Gschneidner [28] . In 1997 a giant magnetocaloric effect, at least two times greater than any normal magnetic material, was discovered in the intermediate phase $Gd_5Si_2Ge_2$ [13], creating a firestorm in the field of magnetic refrigeration research and resulting in continued extensive studies on the $R_5(Si_xGe_{1-x})_4$ system thereafter. Since then the crystal structure, magnetic properties, phase transformation, and thermodynamic properties of various $R_5(Si_xGe_{1-x})_4$ alloys including Ce [35], Sm [36], Gd [37], Ho [38], Er [39] and Yb [40] have been systematically studied by several research groups.

The majority of $R_5(Si_xGe_{1-x})_4$ compounds have layered structures [41] with the building blocks being essentially equivalent sub-nanometer thick two-dimensional slabs. There are some (Si, Ge) – (Si, Ge) covalent-like bonds between these slabs, and the arrangement states of these bonds determine the crystallographic and magnetic structures of the

compounds. Since the $Gd_5(Si_xGe_{1-x})_4$ system is the most studied compound of the $R_5(Si_xGe_{1-x})_4$ family and also is quite representative of the series of alloys, it is chosen as the representative for most of the subsequent discussions. There are three crystal structures in $Gd_5(Si_xGe_{1-x})_4$ system at room temperature (Figure 3): (1) Sm_5Ge_4-type orthorhombic structure (termed O(II), Pnma, $0 \leq x \leq 0.2$) with no inter-slab Si(Ge)-Si(Ge) bonds (Figure 3a); (2) $Gd_5Si_2Ge_2$-type monoclinic structure (termed M, $P112_1/2$, $0.24 \leq x \leq 0.5$,) with alternating strongly and weakly interacting slabs since one half of the inter-slab bonds are connected and the other half are broken (Figure 3b); and (3) Gd_5Si_4-type orthorhombic structure (termed O(I), Pnma, $0.5 < x \leq 1$) with all the inter-slab Si(Ge)-Si(Ge) bonds connected (Figure 3c). A graphical summary of recent data concerning the room-temperature crystal structures of the $R_5(Si_xGe_{1-x})_4$ family as a function of compositions is shown in Figure 4 [42].

A number of factors have been shown to affect the crystal structure and magnetic ordering of the $R_5(Si_xGe_{1-x})_4$ intermetallic compounds, namely temperature, applied magnetic field , pressure and chemical composition. Levin et al [43] observed that Gd_5Ge_4 is antiferromagnetic in a zero magnetic field below ~ 130 K, but it will transform into the ferromagnetic state both reversibly (above 20 K) and irreversibly(below 10 K) depending on the applied magnetic field, the temperature and the direction of their changes. The effect of Si content in the $R_5(Si_xGe_{1-x})_4$ compounds, termed the chemical pressure [42] arises due to the different atomic sizes of isoelectronic Si and Ge. The unit cell volume decreases when Si substitutes for Ge and results in an effect equivalent to the application of external pressure [44]. However, X-ray magnetic circular dichroism (XMCD) studies on a series

$Gd_5(Si_xGe_{1-x})_4$ [45] indicated that a similar volume change results in ~ 3 times larger increase in T_c with Si doping than with applied pressure, which means Si doping enhances the formation of the ferromagnetic low-volume O(I) phase by more than simply reducing the unit cell volume.

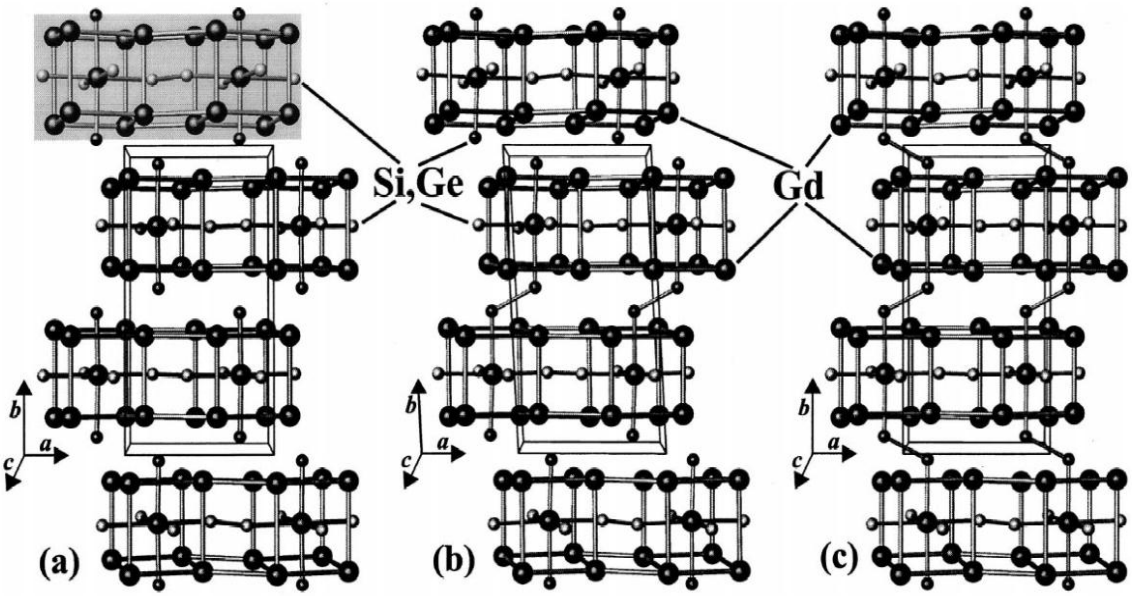

Figure 3. Three types of crystal structure in $Gd_5(Si_xGe_{1-x})_4$ system: (a) Sm_5Ge_4-type orthorhombic (Pnma), (b) $Gd_5Si_2Ge_2$ -type monoclinic ($P112_1/a$), (c) Gd_5Si_4-type orthorhombic (Pnma), Large black spheres represent Gd atoms, small gray spheres represent intra-slab Si (Ge) atoms, small black spheres represent the Si (Ge) atoms, which are responsible for the inter-slab bonds. (From Ref. [41])

The intense interest in the $R_5(Si_xGe_{1-x})_4$ system is not only due to the giant magnetocaloric effect [13, 46, 47], but also can be ascribed to a number of other unusual features observed in these compounds, such as colossal magnetostriction [48, 49] and giant magnetoresistance [50-52]. These extreme behaviors are due to a strongly coupled magnetic–structural first-order transition. The magnetic-structural phase diagram of the $Gd_5(Si_xGe_{1-x})_4$ system, which shows the magnetic and structural phase transformation in different composition regions

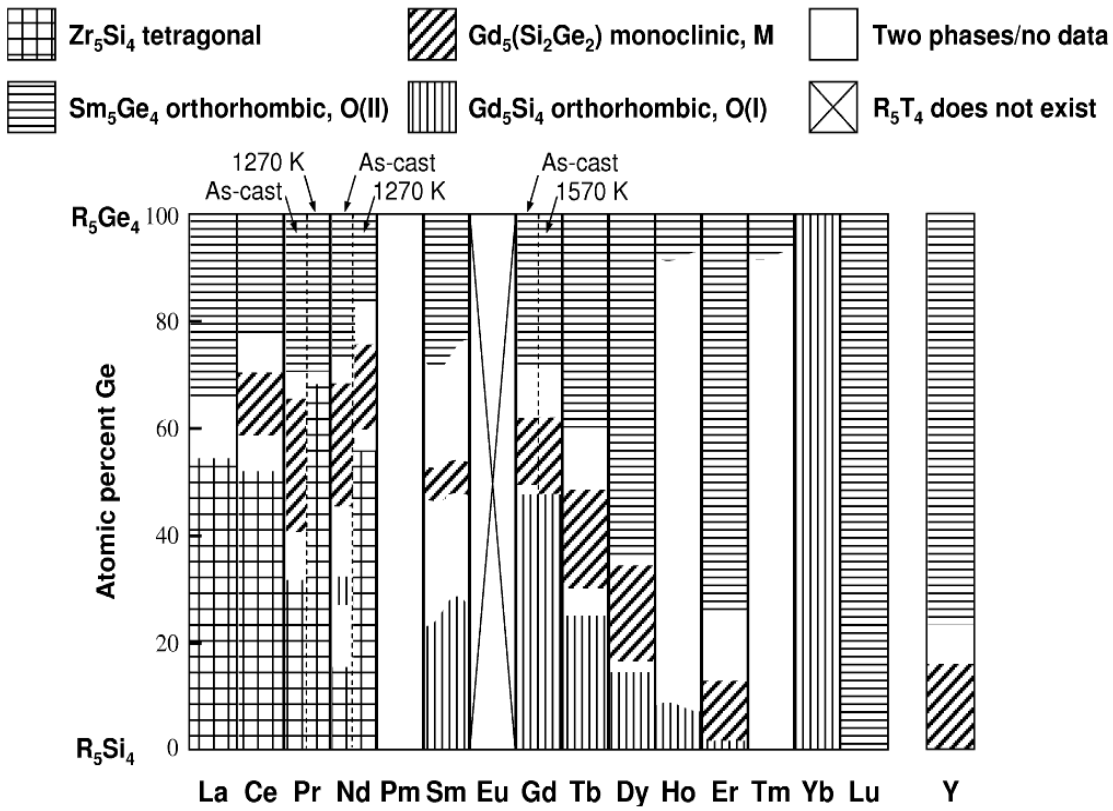

Figure 4. Room temperature crystal structure of $R_5(Si_xGe_{1-x})_4$ family. (From Ref. [42])

with respect to temperature in zero magnetic field, is shown in Figure 5 [37]. As shown in this diagram, the $Gd_5(Si_xGe_{1-x})_4$ compound possesses a Gd_5Si_4-type orthorhombic structure over the whole composition range at low temperatures. In the Si-rich region ($0.507 \leq x \leq 1$), the compound transforms from a ferromagnetic (FM) to a paramagnetic (PM) state above 300K without changing its crystal structure. In the intermediate composition range ($0.4 < x \leq 0.503$), the transformation of the magnetic structure from FM to PM is coupled with a crystallographic structure transition from Gd_5Si_4-type orthorhombic structure to $Gd_5Si_2Ge_2$-type monoclinic structure. For the Ge-rich region ($0 < x \leq 0.3$), upon heating, the low-temperature ferromagnetic form with an O(I) structure transforms to an antiferromagnetic (AFM) state with a Sm_5Ge_4-type orthorhombic structure (called O(II)), which is also a

coupled magnetostructural phase transition. Further heating of the compound causes a magnetic disordering and transforms it into a paramagnetic state without a coupled structure transition.

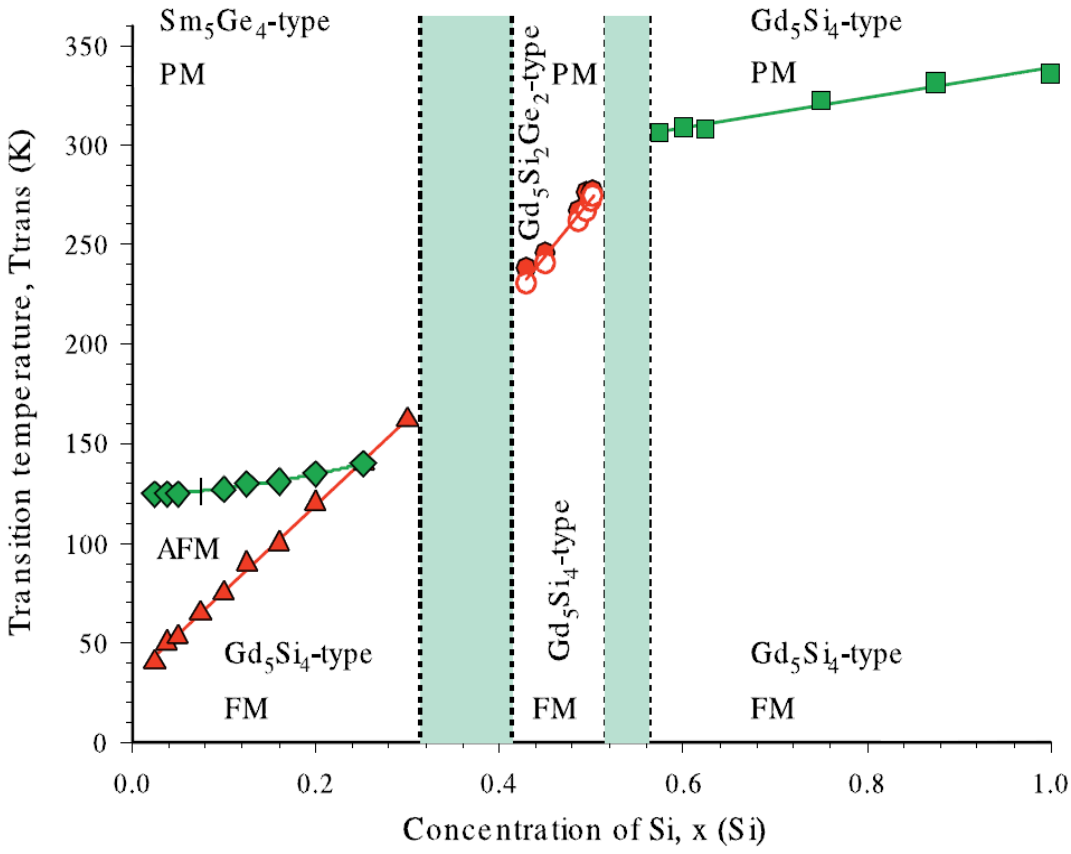

Figure 5. The magnetic-structural phase diagram of $Gd_5(Si_xGe_{1-x})_4$ system. (From Ref. [37])

Er_5Si_4 is a particularly interesting member of the $R_5(Si_xGe_{1-x})_4$ family. Contrary to most of compounds in this family that have a strong magnetostructural coupling, the magnetic and structural transition of Er_5Si_4 is unusually decoupled by ~ 190 K, with a magnetic ordering transition occurring at 32 K, while the structural transition from O(I) to M crystal structure occurs at ~ 220 K [53, 54]. The Er_5Si_4 also is unique in that the temperature dependent structural sequence is opposite that of other representatives of the $R_5(Si_xGe_{1-x})_4$ family,

where the reversible Gd_5Si_4-type orthorhombic to $Gd_5Si_2Ge_2$-type monoclinc distortion occurs on cooling, not upon heating [55]. The results of high applied hydrostatic pressure experiments performed on polycrystalline [56] and monocrystalline Er_5Si_4 [57] showed an extraordinary sensitivity of Er_5Si_4 to pressure. The crystal structure transition (O(I)→M) temperature T_t decreases rapidly at an exceptionally high rate of dT_t/dP = -30K/kbar when pressure increases. This strong pressure dependence may be due to the absence of a magnetic ordering anomaly in the vicinity of the structural transition. The magnetization isotherms of single crystal Er_5Si_4 indicate that the easy magnetization direction is along the b-axis [57].The magnetic and crystallographic P-T phase diagram of Er_5Si_4 is shown in Figure 6 [56].

In 1997 a series of alloys in the $Gd_5(Si_xGe_{1-x})_4$ system, where $0 \leq x \leq 0.5$ was reported [13, 28, 58] to exhibit at least two to four times greater magnetocaloric effect than the normal magnetic materials. Termed giant magnetocaloric effect (GMCE) materials, the effect comes from the first- order nature of the phase transition, in which the entropy is increased at constant temperature by the utilization of the enthalpy of phase transformation. Thus it is a coupled magnetic-structural phase transformation, while for other normal magnetic materials the magnetocaloric effect comes from the second-order phase transition, which does not have such an enthalpy change [41]. The Curie temperature of the $Gd_5(Si_xGe_{1-x})_5$ system can be tuned between ~ 20 and ~ 300 K by changing the Si to Ge ratio. According to Equation (5) mentioned previously, lower heat capacity gives larger MCE at the transition temperature. Therefore, although the GMCE is observed in both Ge-rich, and intermediate regions of Ge concentration the largest GMCE occurs at x = 0.24

since the lowest heat capacity at the transition temperature occurs at this point [41].

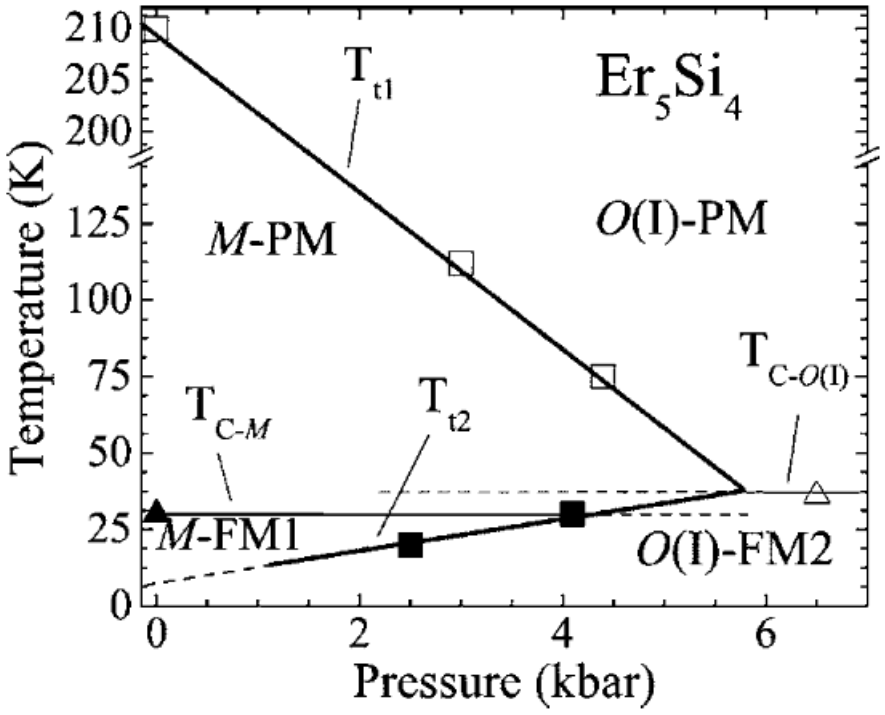

Figure 6. The magnetic and crystallographic P-T phase diagram of Er_5Si_4. Open squares represent the high-temperature O(I)↔ M transformation (T_t), whereas solid squares are used for the low temperature pressure-induced O(I) reentrance (T_{t2}). Both sets of values are extracted from linear thermal expansion (LTE) data. Solid triangle for the pure M phase at ambient pressure and open triangle for the pure O(I) phase at high pressure. Thick solid lines depict the magnetic and/or crystallographic phase boundaries, and dotted lines are used for the magnetic ordering of the minority phase involved in the first-order crystallographic transformation. (From Ref. [56])

The $R_5(Si_xGe_{1-x})_3$ Family of Intermetallic Compounds

Rare-earth-based intermetallic compounds based on the formula $R_5(Si_xGe_{1-x})_3$ (hereafter referred to as "5:3" compounds), where R is one of rare-earth metals, is another family with rich physical properties that present the researcher with a wide variety of options by which

to study the interplay between crystal structure and magnetism in the solid-state materials. The first publication about alloys in the $R_5(Si_xGe_{1-x})_3$ family appeared in 1960 [59] and reported the crystal structure of Y_5Si_3 and Y_5Ge_3. Although studies about $R_5(Si_xGe_{1-x})_3$ occurred several years earlier than initial research in $R_5(Si_xGe_{1-x})_4$ alloys, the depth and width of the research in the former is far behind the latter.

The intermetallic compounds $R_5(Si_xGe_{1-x})_3$ crystallize in the Mn_5Si_3-type hexagonal $D8_8$ structure with the space group $P6_3/mcm$ [59-62]. The unit cell consists of two formulae and the rare-earth atoms occupy two non-equivalent crystallographic sites, 4d and 6g [59, 63, 64]. It was later discovered that site 6g has a lower magnetic moment than site 4d due to crystal field effects [65]. For example, the erbium magnetic moments in Er_5Si_3 are $8.3\mu_B$ for site 4d and 5.2 μ_B for site 6g [66]. A stereoscopic drawing of the Mn_5Si_3-type hexagonal $D8_8$ is shown in Figure 7 [67].

Soon after identification of the crystal structure, researchers began to explore the magnetic properties of the $R_5(Si_xGe_{1-x})_3$ compounds [68-70]. Magnetic susceptibility measurements for Nd, Gd and Dy germanides and silicides [68] indicated there is a ferromagnetic spin ordering for rare earth atoms in the crystallographic 6g sites, and an antiferromagnetic ordering in the 4d sites. It is interesting to note that the published Neel temperatures of the same $R_5(Si_xGe_{1-x})_3$ compound vary significantly, which may be due to the discrepancies in the measurement methods and the quality of the tested samples. Buschow and Fast [69] found the paramagnetic to antiferromagnetic transition of the polycrystalline Gd_5Ge_3 occurred at 48 K. Takanori et al [71] reported the Neel temperature of the single crystal Gd_5Ge_3 is $T_N = 76$ K, and the magnetic moments in the antiferromagnetic phase tend to be

aligned in the c-plane. Dhar et al [72] observed that the single crystal Gd_5Ge_3 orders antiferromagnetically below 80 K. Linear thermal expansion measurements performed on a

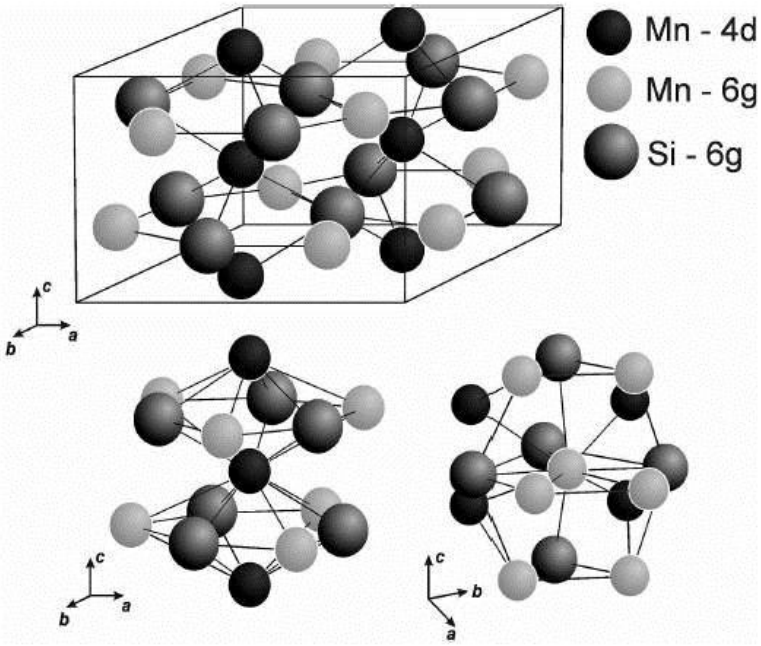

Figure 7. The crystal structure of Mn_5Si_3 and the atomic surrounding of Mn atoms at the different crystallographic sites. One unit cell is outlined by the rectangular parallelepiped. (From Ref. [67])

polycrystalline Gd_5Ge_3 sample showed a crystal structure transition that coincides with the magnetic transition [73], but the authors suggested that this was a second-order transition. This coupling between magnetism and crystal structure was recently confirmed by Mudryk et al. [74]. Additionally, it was found that the Gd_5Ge_3 compound prepared from low-purity Gd shows a lower Neel temperature than that of a Gd_5Ge_3 alloy prepared using high-purity Gd, which suggested that interstitial impurities affect the strength of the antiferromagnetic interaction [74]. Besides the gadolinium-based 5:3 compounds, the magnetic properties of other rare-earth intermetallics have also been studied. Neutron diffraction experiments

performed on Er_5Si_3 show a Neel temperature equal to 20 K [66]. Magnetic measurements on a Nd_5Ge_3 single crystal found that Nd_5Ge_3 is in the antiferromagnetic state below T_N = 51 K, and an irreversible magnetic-field-induced antiferromagnetic to ferromagnetic transition was observed below 26 K [75].

$R_5(Si_xGe_{1-x})_3$ Linear Features in $R_5(Si_xGe_{1-x})_4$ Matrix

A review of all the studies concerning the microstructure of $R_5(Si_xGe_{1-x})_4$ systems reveals a linear feature present in every $R_5(Si_xGe_{1-x})_4$ compound ever studied. The linear features were first observed in Gd_5Si_4, $Gd_5Si_2Ge_2$, and Gd_5Ge_4 by Szade [76] using scanning electron microscopy (SEM) and Auger electron spectrometer (AES). They were described as sets of parallel lines with a fixed angular relationship between them (Figure 8) occurring on the surface of as-grown single crystals. Back-reflection Laue results showed the lines were not parallel to any crystallographic directions with low indices. Later, Meyers et al [77] showed the linear features were not a surface feature associated with the growth structure of the crystals but a separate second phase existing throughout the bulk of the material, with a stoichiometric composition $Gd_5(Si_xGe_{1-x})_3$. This composition corresponds to intermetallic phases of elemental ratios 5:3 that exist in both the Gd-Si and Gd-Ge systems. While Szade's experimental results found the composition of the linear features in $Gd_5Si_2Ge_2$ to be high in Gd and low in both Si and Ge, Meyers (who used the more exact method of x-ray spectroscopy) found the linear features to be high in Gd and low in Si with the Ge level being approximately the same as compared to the composition of the 5:4 matrix (Figure 9). The findings of Meyers were later supported by Ugurlu, et al [78].

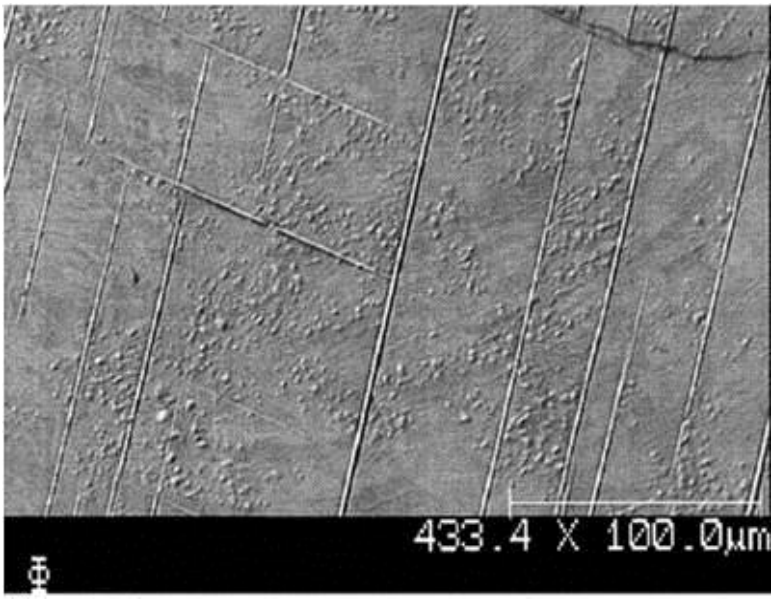

Figure 8. The SEM image of the linear features on the surface of Gd_5Si_4. (From Ref. [76])

Subsequent studies by Ugurlu et al [78] proved the linear features are neither lines nor rods but are actually two-dimensional cross-sections of thin plate structures. TEM results [78-80] clearly show these thin plates have a hexagonal crystal structure and have been described as an atypical Widmanstatten structure. While Manekar [81] suggested that the hexagonal electron diffraction patterns observed in [78-80] might be attributed to an unusual twinning mechanism in an orthorhombic structure, direct evidence for the hexagonal identification in the form of a convergent beam electron diffraction (CBED) pattern of the [0001] showing six-fold symmetry as reproduced in Figure 10 from [82] and high-resolution TEM studies (Figure 11) of [80] conclusively show no evidence of the orthorhombic twinning required by [81] that might result in a pseudo-hexagonal structure. The orientation relationship the 5:3 thin plates possess with the 5:4 matrix was determined as $[10\bar{1}0](1\bar{2}11)p \parallel [010](10\bar{2})_m$

by Ugurlu et al and a displacive-diffusional mechanism was proposed for the formation of the 5:3 plates and reported in [80].

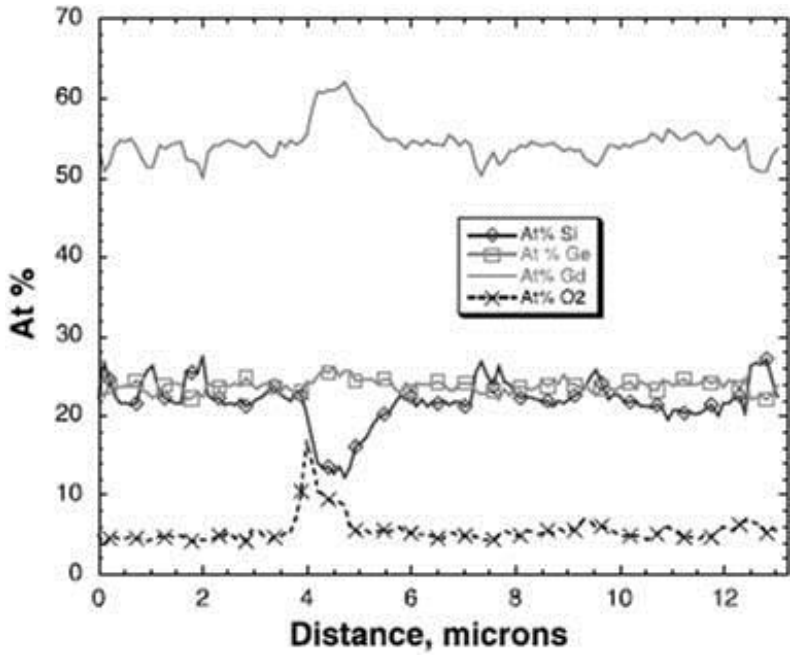

Figure 9. EDS line scan across a linear feature in $Gd_5Si_2Ge_2$. (From Ref. [77])

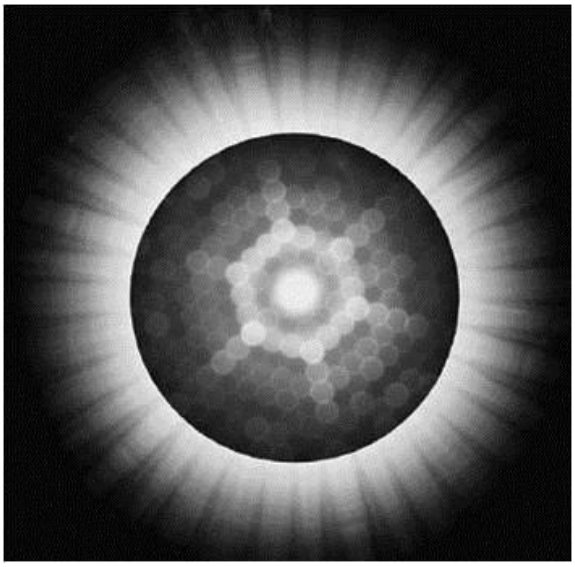

Figure 10. CBED of a $Gd_5(Si,Ge)_3$ thin plate showing the six-fold symmetry of the hexagonal crystal structure. B = [0001]. (From Ref. [82])

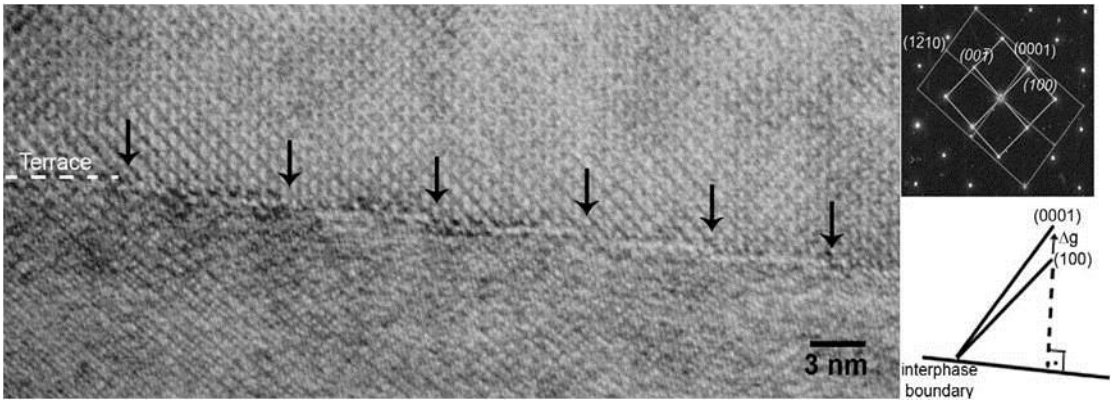

Figure 11. HRTEM image taken from a Gd_5Ge_4 single crystal showing the ledge-wise interface between the thin plates and the matrix. Corresponding SAD and misfit between phases is consistent with $[10\bar{1}0](1\bar{2}11)p \parallel [010](10\bar{2})_m$ orientation relationship. (risers shown with black arrows and one terrace shown with dashed line). (From Ref. [80])

The 5:3 plates possess an extremely high length-to-thickness aspect ratio, extending tens (and often hundreds) of microns in two directions but with a thickness usually on the order of tens to hundreds of nanometers. This morphology allows rapid growth in the two favorably oriented directions and results in the formation of terraces on the interface boundary between the 5:4 matrix and the 5:3 plates in the thin direction [80]. The atomic mobility is low perpendicular to the interface, but high along the risers in the approximate direction of interface. Interestingly, the presence of thin plates assumed to be 5:3 has been confirmed in essentially every examined alloy in the $R_5(Si_xGe_{1-x})_4$ family including R = Gd, Tb, Dy, Er [79,83], Yb, and Ho [84] (Figure 12). The precipitation of 5:3 plates appears relatively independent of the initial crystal structure and composition of the parent matrix [79, 82]. Somewhat surprising was that alloy compositions specifically chosen in an attempt to avoid 5:3 formation still possessed 5:3 plates whenever the 5:4 phase was present, pointing to an unusual stability of the 5:3 plates within a 5:4 matrix [85].

Although the 5:3 plates are prevalent in all alloys of the $R_5(Si_xGe_{1-x})_4$ system, their low volume percentage often prevents them from being detected using laboratory x-ray diffraction and / or magnetization measurements, which explains why studies that do not employ microscopy as a characterization technique claim that various 5:4-based alloys are phase-pure [38, 86]. In addition, the small size scale of the plates makes it difficult to properly identify this phase unless transmission electron microscopy is used.

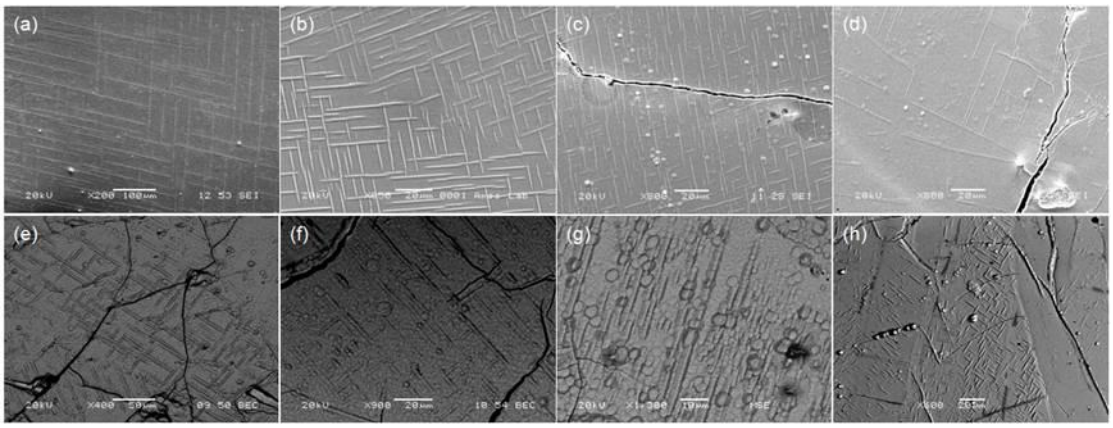

Figure 12. 5:3 plates in several studied rare-earth systems, (a)Gd_5Ge_4, (b)Er_5Si_4, (c)Tb_5Ge_4, (d)Dy_5Si_4, (e)$Ho_5(Si_{0.8}Ge_{0.2})_4$, (f)Ce_5Ge_4, (g)Yb_5Ge_4, (h)Gd_5Si_4. (Merged images from Ref. [79, 83, 84])

Recent work by researchers in England [87] involving magnetic measurements has shown that the 5:3 plates play a significant role in the magnetic transformations. The scanning Hall probe imaging performed on a $Gd_5Si_2Ge_2$ showed that the 5:3 plates serve as nucleation sites within the room temperature paramagnetic 5:4 matrix for the formation of ferromagnetic domains upon cooling (Figure 13). This suggests that if one can control the number and distribution of the plates the unique magnetic properties of the parent matrix can be enhanced.

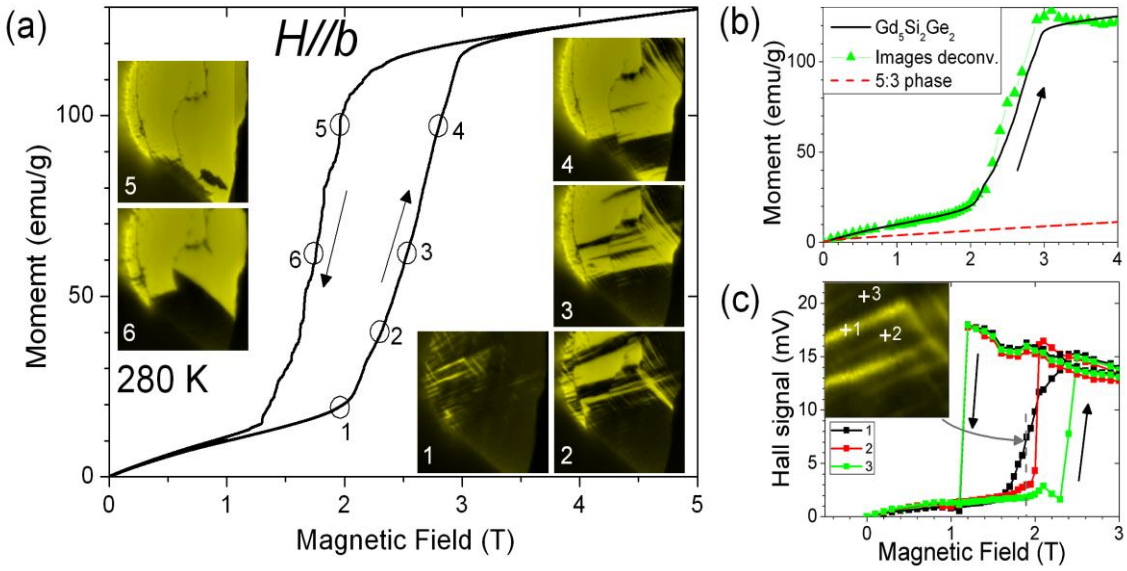

Figure 13. Seeding of the FM transition in the [010] face of $Gd_5Si_2Ge_2$ by the 5:3 platelets. a) Bulk M-H loop at 280 K. Insets are Hall images showing nucleation on thin plates. b) M-H curves illustrating difference of signal for 5:4 and 5:3 at 280K. c) Local M-H curves at 280K. Inset shows magnified region from image 1 in part a). (From Ref. [87])

Motivation of the Study and Dissertation Organization

This dissertation begins with a general introduction, literature review, and motivation for the study as a background to the research in Chapter 1. Chapters 2-5 are written in the alternate format consisting of four original manuscripts, followed by a general conclusion presented as Chapter 6. References cited in each chapter are presented immediately after each chapter.

Given the importance of microstructure in terms of providing nucleation sites for magnetic and structural transitions, it is important to understand not only what phases are present in the microstructure of the $R_5(Si_xGe_{1-x})_4$ compounds but how the amount of, and balance

between the possible phases present in such a complex system is affected by things such as sample preparation and examination technique. Equally important is a basic understanding of the balance that exists between the $R_5(Si_xGe_{1-x})_4$ and the $R_5(Si_xGe_{1-x})_3$ compounds, since these two structures seem to be intimately related. Thus, several experiments and examinations have been conducted to broaden the knowledge base concerning these families of complex materials.

It has been confirmed by numerous experimental results that the crystal structure and magnetic ordering of the $R_5(Si_xGe_{1-x})_4$ compounds can be altered by a number of factors, namely temperature, applied magnetic field, pressure and chemical composition (i.e Si to Ge ratio). While the cause may be different the general resultant effect is to subject the crystal structure to an applied strain, resulting in expansion / contraction of the lattice and the breaking / forming of interslab Si(Ge)-Si(Ge) bonds. It is thus entirely logical to expect that direct application of strain via mechanical means should result in the same effect. Mechanical grinding is a traditional method for providing such a direct strain, and has the additional advantage of being easy to perform. The Er_5Si_4 compound was chosen as the experimental object due to its particularly high sensitivity to the applied hydrostatic pressure [56, 88]. The effects of mechanical grinding and subsequent low temperature annealing on the crystallographic structure of Er_5Si_4 are presented in Chapter 2.

Although a linear feature is precipitated as a second phase in every studied $R_5(Si_xGe_{1-x})_4$, the exact composition and crystallographic structure of the linear feature and its orientation relationship with respect to the 5:4 matrix has only been positively confirmed for the Gd-base system. Due to the similarities in crystal structure, microstructure, phase diagram,

atomic bonding, etc., it has always been assumed that the linear features seen in other $R_5(Si_xGe_{1-x})_4$ type alloys are also 5:3 phases, possessing the same orientation relationship and formation characteristics as those detailed for the Gd-base system, but little work has been done to conclusively prove this assumption. In fact, the linear features appearing in the 5:4 matrix possessing the Sm_5Ge_4-type orthorhombic structure (O(II)) and $Gd_5Si_2Ge_2$-type monoclinic structure (M) are the only ones that have been studied in detail and conclusively identified as $R_5(Si_xGe_{1-x})_3$. Thus, to test the validity of the basic assumption that all 5:4 compounds possess 5:3 impurity plates, a lutetium-doped erbium silicide $(Er_{0.9}Lu_{0.1})_5Si_4$ was chosen for examination. If the basic assumption is to be disproven this alloy presents the most likely exception to the rule since the $(Er_{0.9}Lu_{0.1})_5Si_4$ possesses the O(I) structure (previously unstudied as regards the nature of the observed linear features), and is also one where substitution occurs in the rare-earth metal content rather than in simply changing the Si/Ge ratio. A complete characterization of the microstructure present in the $(Er_{0.9}Lu_{0.1})_5Si_4$ was performed using SEM and TEM. The detailed results of this study are presented in Chapter 3.

The 5:3 plates, their exact composition, crystallographic structure, and the orientation relationship they possess with the 5:4 matrix have been determined in studies by Meyer [77] and Ugurlu [78-80, 83] and a formation mechanism of these plates has been suggested. However, the exact conditions under which these plates form and the driving force for their formation are yet unknown. The high degree of stability noted for the plates [85] suggests a strong kinetic driving force in much the same way martensitic transformations occur in opposition to equilibrium thermodynamic considerations. Further study of the 5:3 thin

plates to define their formation temperature and range of stability is needed if one is to manipulate and control the structure. To address these issues, research was carried out to investigate the stability of 5:3 plates as a function of high temperature annealing. The extent to which the formation of 5:3 plates can be enhanced or suppressed under rapid cooling conditions was also investigated using laser surface melting. The detailed results of these experiments are presented in Chapter 4.

It has been shown that the minor precipitate $R_5(Si_xGe_{1-x})_3$ phase always coexists with the parent $R_5(Si_xGe_{1-x})_4$ phase in the form of platelets, even when compositions are chosen in an attempt to purposefully avoid the formation of $R_5(Si_xGe_{1-x})_3$[85]. Given the strong tendency of the 5:4 compound to contain 5:3, it would be useful to understand what happens if $R_5(Si_xGe_{1-x})_3$ becomes the parent phase. Although researchers have shown a gradual increase of interest in the family of $R_5(Si_xGe_{1-x})_3$ compounds, all of the experiments which have been implemented thus far are focused on the magnetic measurements and no information about the microstructures has been reported. To better understand the microstructure-property relationships which exist, a comprehensive study in the microstructure of the $R_5(Si_xGe_{1-x})_3$ compounds is necessary. An initial study concerning the microstructures of both polycrystalline and monocrystalline Gd_5Ge_3 specimens has been carried out using optical and electron microscopy (SEM, TEM). The results are discussed and presented in Chapter 5.

Because of the difficulties discussed in [82], conventional x-ray diffraction methods often do not possess the sensitivity to unambiguously identify the precipitate 5:3 plates. Considering their importance as “seeds” for the nucleation and growth of ferromagnetic

domains in the 5:4 matrix, conventional microscopy techniques suffer in that they only examine a relatively small area if one is to control and monitor the number, distribution, and size of the plates in order to tailor the microstructure for engineering implications, microscopy methods need to be coupled with techniques that obtain more of a bulk assessment of the phase percentages present. Therefore, finding a suitable materials characterization method that can provide a reliable bulk analysis for the small amount of 5:3 plates is required. The manuscript attached in the Appendix discusses the feasibility of using different bulk diffraction techniques to determine the existence of the 5:3 platelets and suggests possible future uses of high resolution synchrotron radiation for the study of $R_5(Si_xGe_{1-x})_3$ and $R_5(Si_xGe_{1-x})_4$ compounds.

References

[1] E. Warburg, Ann. Phys., 13 (1881) 141.

[2] P. Debye, Ann. Phys., 81 (1926) 1154.

[3] W. F. Giauque, J. Amer. Chem. Soc., 49 (1927) 1864.

[4] V. K. Pecharsky, K. A. Gschneidner Jr., J. Magn. Magn. Mater., 200 (1999) 44.

[5] A. H. Morrish, The physical Principles of Magnetism, Wiley, New York, 1965 (Chapter 3).

[6] K. A. Gschneidner, Jr., V. K. Pecharsky, Int. J. Refrig., 31 (2008) 945.

[7] S.C. Collins, F. J. Zimmerman, Phys. Rev., 90 (1953) 991.

[8] G. V. Brown, J. Appl. Phys., 47 (1976) 3673.

[9] C. B. Zimm, A. Sternberg, C. Jastrab, V. K. Pecharsky, K. A. Gschneidner Jr., M. Osborne and I. Anderson, Adv. Cryog. Eng., 43 (1998) 1759.

[10] C. B. Zimm, A. Sternberg, A. G. Jastrab, A. M. Boeder, L. M. Lawton, J. J. Chell,

2003. Rotating bed magnetic refrigeration apparatus. U.S. Patent, 6,526,759.

[11] C. B. Zimm, J. Auringer, A. Boeder, J. Chells, S. Russek, A. Sternberg, Proceedings of the Second International Conference on Magnetic Refrigeration at Room Temperature, 2007 April 11-13, Portoroz, Slovenia. International Institute of Refrigeration, Paris, pp 341.

[12] http://en.wikipedia.org/wiki/Magnetic_refrigeration

[13] V. K Pecharsky and K. A. Gschneidner Jr., Phys. Rev. Lett., 78 (1997) 4494.

[14] C. B. Zimm, P. M. Ratzmann, J. A. Barclay, G. F. Green, J. N. Chafe, Adv. Cryog. Eng., 36 (1990) 763.

[15] A. M. Tishin, K. A. Gschneidner Jr., V. K. Pecharsky, Phys. Rev. B, 59 (1999)503.

[16] B. R. Gopal, R. Chahine, T. K. Bose, Rev. Sci. Instr., 68 (1997) 1818.

[17] S. Y. Dan'kov, Y. I. Spichkin, A. M. Tishin, J. Magn. Magn. Mater., 152 (1996) 208.

[18] M. D. Kuz'min, A. M. Tishin, Cryogenics, 33 (1993) 868.

[19] C. B. Zimm, J. A. Barclay, H. H. Harkness, G. F. Green, and W. G. Patton, Cryogenics, 29 (1989) 937.

[20] A. Smaili, R. Chahine, J. Appl. Phys., 81 (1997) 824.

[21] A. M. Tishin, Cryogenics, 30 (1990) 720.

[22] M. F¨oldeaki , R. Chahine, B. R. Gopal, T. K. Bose, X. Y. Liu, et al., J. Appl. Phys., 83 (1998) 2727.

[23] M. F¨oldeaki, W. Schnelle, E. Gmelin, P. Benard, B. Koszegi, et al., J. Appl. Phys., 82 (1997) 309.

[24] Y. Shao, J. Zhang, J. K. L. Lai, C. H. Shek, J. Appl. Phys., 80 (1996)76.

[25] P. J. Von Ranke, V. K. Pecharsky, K. A. Gschneidner Jr., Phys. Rev. B, 58 (1998) 12110.

[26] T. Hashimoto, K. Matsumoto, T. Kurihara, T. Numazawa, A. Tomokiyo, et al., Adv. Cryog. Eng., 32 (1986) 279.

[27] K. A. Gschneidner Jr., H. Takeya, J. O. Moorman, V. K. Pecharsky, Appl. Phys. Lett., 64 (1994) 253.

[28] V. K. Pecharsky and K. A. Gschneidner Jr., J. Alloys Compd., 260 (1997) 98.

[29] V. K. Pecharsky and K. A. Gschneidner Jr., Appl. Phys. Lett., 70 (1997) 3299.

[30] K. A. Gschneidner Jr, V. K. Pecharsky and A. O. Tsokol, Rep. Prog. Phys., 68 (2005)

1479.

[31] G. S. Smith, A. G. Tharp, and Q. Johnson, Nature, 210 (1966) 1148.

[32] G. S. Smith, A. G. Tharp, and Q. Johnson, Acta Crystallogr., 22 (1967) 940.

[33] G. S. Smith, Q. Johnson, A. G. Tharp, Acta Crystallogr., 22 (1967) 269.

[34] F. Holtzberg, R. J. Gambino, and T. R. McGuire, J. Phys. Chem. Solids, 28 (1967) 2283.

[35] H. Zhang, Ya. Mudryk, Q. Cao et al., J. Appl. Phys., 107 (2010) 013909.

[36] K. Ahn, V. K. Pecharsky et al., Phys. Rev. B, 76 (2007) 014415.

[37] A. O. Pecharsky, K. A. Gschneidner, Jr. et al., J. Alloy. Compd., 338 (2002) 126.

[38] A. M. Pereira, J. B. Sousa et al., Phys. Rev. B, 77 (2008) 134404.

[39] A. O. Pecharsky, K. A. Gschneidner, Jr. et al., Phys. Rev. B, 70 (2004) 144419.

[40] K. Ahn, A. O. Tsokol et al, Phys. Rev. B, 72 (2005) 054404.

[41] V. K. Pecharsky, and K. A. Gschneidner Jr., Adv. Mater., 13 (2001) 683.

[42] V. K. Pecharsky and K. A. Gschneidner, Jr., Pure Appl. Chem., 79 (2007) 1383.

[43] E. M. Levin, K. A. Gschneidner, Jr., V. K. Pecharsky, Phys. Rev. B, 65 (2002) 214427.

[44] Y. Mudryk, Y. Lee, T. Vogt, K. A. Gschneidner, Jr., V. K. Pecharsky, Phys. Rev. B, 71 (2005)174104.

[45] Y. C. Tseng, D. Haskel, J. C. Lang, S. Sinogeikin, Ya. Mudryk, V. K. Pecharsky, and K. A. Gschneidner, Jr., Phys. Rew. B, 76 (2007) 014411.

[46] A. Giguere, M. Foldeaki, B. R. Gopal, R. Chahine, T. K. Bose, A. Frydman, J. A. Barclay, Phys. Rev. Lett., 83 (1999) 2262.

[47] L. Morellon, C. Magen, P. A. Algarabel, M. R. Ibarra, and C. Ritter, Appl. Phys. Lett., 79 (2001) 1318.

[48] C. Magen, L.Morellon, P. A. Algarabel,C. Marquina and M. R. Ibarra, J.Phys.: Condens. Matter, 15 (2003) 2389.

[49] V. K. Pecharsky, A. P. Holm, K. A.Gschneidner Jr and R. Rink, Phys. Rev. Lett., 91 (2003) 197204.

[50] E. M. Levin, V. K. Percharsky, K. A. Gschneidner Jr., P. Tomlinson, J. Magn. Magn. Mater., 210 (2000) 181.

[51] J. B. Sousa, M. E. Braga, F. C. Correia, F. Carpinteiro, L. Morellon, P. A. Algarabel,

and M.R. Ibarra, Phys. Rev. B, 67 (2003) 134416.

[52] M. Zou M, V. K. Pecharsky, K. A. Gschneidner Jr, Ya. Mudryk, D. L. Schlagel, T. A. Lograsso, Phys. Rev. B, 80 (2009) 174411.

[53] C. Ritter, C.Magen, L. Morellon, P. A. Algarabel, M. R. Ibarra, V. K. Pecharsky, A. O. Tsokol, K.A.Gschneidner Jr., J. Phys.: Condens Matter, 18 (2006) 3937.

[54] Y. Mozharivskyj, A. O. Pecharsky, V. K. Pecharsky, G. J. Miller, K.A. Gschneidner Jr., Phys. Rev. B, 69 (2004) 144102.

[55] V. K. Pecharsky, A. O. Pecharsky, Y. Mozharivskyj, K. A. Gschneidner, Jr., and G. J. Miller, Phys. Rev. Lett., 91 (2003) 207205.

[56] C. Magen, L. Morellon, Z. Arnold, P. A. Algarabel, C. Ritter, M. R. Ibarra, J. Kamarad, A. O. Tsokol, K. A. Gschneidner Jr., V. K. Pecharsky, Phys. Rev. B, 74 (2006) 134427.

[57] N. Marcano, P. A. Algarabel, J. R. Fernandez, C. Magen, L. Morellon, N. K.Singh, D. L. Schlagel, K. A. Gschneidner, Jr., V. K. Pecharsky and M. R. Ibarra, Phys. Rev. B, 85 (2012) 024408.

[58] V. K. Pecharsky, K. A. Gschneidner Jr., J. Magn. Magn. Mater., 167 (1997) L179.

[59] E. Parthe, Acta Crystallogr., 13 (1960) 868.

[60] J. Arbuckle, E. Parthe, Acta Crystallogr., 15 (1962) 1205.

[61] N. C. Baezinger, J. J. Hegenbarth, Acta Crystallogr., 17 (1964) 620.

[62] I. Mayer, I. Shidlovsky, Inorg. Chem., 8 (1969) 1240.

[63] E. I. Gladyshevskii, Neorgan. Mat., 868 (1965) 702.

[64] G. H. Lander and P. J. Brown, Phil. Mag., 16 (1967) 521.

[65] J. K. Yakinthos, I. P. Semitelou, and E. Roudaut, Solid State Commun., 59 (1986) 227.

[66] I. P. Semitelou, J. K. Yakinthos, and E. Roudaut, J. Phys. Chem. Solid., 56 (1995) 891.

[67] J. Leciejewicz, B. Penc, et al., Acta Phys. Pol. A, 113 (2008) 1193.

[68] K. S. V. L. Narasimhan, H. Steinfink, and E. V. Ganapathy, J. Appl. Phys., 40 (1969) 51.

[69] K. H. J. Buschow and J. F. Fast, Phys. Status Solidi, 21 (1967) 593

[70] D. I. Tcherney, K. S. V. L. Narasimhan, and H. Steinfink, IEEE Trans. Magn., September (1969) 222.

[71] T. Tsutaoka, Y. Nishiume, T. Tokunaga, J. Mag. Mag. Mat., e421-e422 (2004) 272.

[72] S. K. Dhar, P. Manfrinetti, A. Palenzona, and M. Pani, J. Alloys Compd., 347 (2002) 1.

[73] S. M. Barmin, R. P. Krentsis, P. V. Gel'd, and V. G. Batalin, Fiz. Tverd. Tela, 21 (1979) 3174.

[74] Y. Mudryk, D. Paudyal, V. K. Pecharsky, and K. A. Gschneidner Jr., Phys. Rev. B, 85 (2012) 014116.

[75] T. Tsutaoka, A. Tanaka, Y. Narumi, M. Iwaki, K. Kindo, Physica B, 405 (2010) 180.

[76] J. Szade, G. Skorek, A. Winiarski, J . Cryst. Growth, 205 (1999) 289.

[77] J. S. Meyers, L. S. Chumbley et al., Scripta Mater., 47 (2002) 509.

[78] O. Ugurlu, L. S. Chumbley, T. A. Lograsso, D. L. Schlagel, Acta Mater., 53 (2005) 3525.

[79] O. Ugurlu, L. S. Chumbley, D. L. Schlagel, T. A. Lograsso, A. O. Tsokol, Scripta Mater., 53 (2005) 373.

[80] O. Ugurlu, L. S. Chumbley, D. L. Schlagel, T. A. Lograsso, Acta Mater., 54 (2006) 1211.

[81] M. Manekar et al., J Phys: Condens Matter, 18 (2006) 6017.

[82] L.S. Chumbley, O. Ugurlu, R.W. McCallum, K.W. Dennis, Y. Mudryk, K.A. Gschneidner Jr., V.K. Pecharsky, Acta Mater., 56 (2008) 527.

[83] O. Ugurlu, L. S. Chumbley, D. L. Schlagel, T. A. Lograsso, A. O. Pecharsky, 134th TMS (Minerals, Metals and Materials Society) Annual Meeting, Light Metals. 2005;p1181-1185.

[84] Z. Qian, L. S. Chumbley, S. Misra, G. J. Miller, V. K. Pecharsky, K. A. Gschneidner Jr., K. Ahn, A. S. Chernyshov, N. K. Singh, Acta Mater., 57 (2009) 3374.

[85] O. Ugurlu, L. S. Chumbley, C. R. Fisher, J. Mater. Res., 21 (2006)2669.

[86] H. Fu, X. Zu, T. Shen, Thermochim. Acta, 445 (2006) 53.

[87] J. D. Moore, K. Morrison, G. K. Perkins, D. L. Schlagel, T. A. Lograsso, K. A. Gschneidner Jr., V. K. Pecharsky, L. F. Cohen, Adv. Mater., 21 (2009) 3780.

[88] Y. Mudryk, V. K. Pecharsky, K. A. Gschneidner, Jr., Z. Anorg. Allg. Chem., 637(2011) 1.

CHAPTER 2. Effects of Mechanical Grinding and Low Temperature Annealing on Crystal Structure of Er_5Si_4

A paper to be submitted to Journal of Alloys and Compounds

Q. Cao, L. S. Chumbley, Y. Mudryk, M. Zou, V. K. Pecharsky, and K. A. Gschneidner Jr.

Abstract

The effect of mechanical grinding and subsequent low temperature annealing on the orthorhombic to monoclinic structural transition in the Er_5Si_4 compound was studied by X-ray powder diffraction using both a conventional laboratory Cu $K\alpha_1$ radiation and a high-energy synchrotron source. A reversible phase transition from the orthorhombic to monoclinic structure was observed as a result of the mechanical grinding. Low temperature annealing causes a transformation of the monoclinic phase back to the orthorhombic, presumably by relief of residual stress introduced during the grinding process.

Introduction

The rare-earth-based intermetallic compounds $R_5(Si_xGe_{1-x})_4$, where R are the lanthanides, is a family of magnetocaloric materials first studied by Smith et al. in 1966 [1]. Ever since the giant magnetocaloric effect was discovered in $Gd_5Si_2Ge_2$ in 1997 [2], this family has

captured the attention of researchers all over the world and has led to extensive studies on the magnetic properties and the microstructures of these intermetallic compounds. Smith et al. believed that both the R_5Si_4 silicides and R_5Ge_4 germanides crystallize with the Sm_5Ge_4 type orthorhombic structure [3]. However, Holtzberg et al. [4] noted that the crystal structures of R_5Si_4 and R_5Ge_4 were in fact different. The $R_5(Si_xGe_{1-x})_4$compounds are layered structures [3, 5] consisting of essentially equivalent sub-nanometer thick two-dimensional atomic slabs. The absence or presence of Si(Ge)-Si(Ge) covalent-like bonds between these slabs determine the crystal structure and the type of magnetic ordering of the compounds. Three main crystal structures in the R_5Si_4 and R_5Ge_4 alloys are: (1) the Sm_5Ge_4-type orthorhombic structure (Pnma) with weak inter-slab Si(Ge)-Si(Ge) bonds; (2) the $Gd_5Si_2Ge_2$-type monoclinic structure ($P112_1/a$) with alternating strongly and weakly interacting slabs since one half of the inter-slab bonds are present and the other half are broken; and (3) the Gd_5Si_4-type orthorhombic structure (Pnma) with all the inter-slab Si(Ge)-Si(Ge) bonds being short and relatively strong . The phase transformations between these structures can be induced by a number of triggers such as temperature, applied magnetic field, pressure and chemical composition, which in turn leads to a change in magnetic ordering of the $R_5(Si_xGe_{1-x})_4$ intermetallic compounds [5-13]. Many of these compounds display unusual coupling of magnetic and crystallographic structure transitions. For instance, magnetic ordering occurs simultaneously with the crystallographic change in $Gd_5Si_2Ge_2$ [13], ferromagnetic ordering accompanied by a crystal rearrangement can be triggered by a magnetic field in Gd_5Ge_4 [14], and a pressure-induced magneto-structural coupling is present in $Tb_5Si_2Ge_2$ [15]. Conversely, the compound Er_5Si_4 exhibits an interesting decoupling of the magnetic and structural transformations [16 -17]. The phase

transformation temperature in Er_5Si_4 is extremely sensitive to applied hydrostatic pressure as compared to other known 5:4 compounds [10]. In addition, its structural transition in the paramagnetic region weakly depends on the applied magnetic field, as observed in both polycrystalline [18] and single-crystalline samples [19]. For these reasons, Er_5Si_4 is an interesting compound to study.

The identification of crystal structures and the investigation of phase transitions in the $R_5(Si_xGe_{1-x})_4$compounds are often performed using X-ray powder diffraction techniques [14, 19-23] since it is well known that these analytical methods are capable of quick and accurate material characterization in such fields as metallurgy, mineralogy, forensic science, archeology, condensed matter physics, and the biological and pharmaceutical sciences. The most widespread use of powder diffraction is in the identification and characterization of crystalline solids. Through analysis of collected diffraction patterns, information such as the amount and crystal structure of phases present in a sample can be obtained. Relative concentrations of different phases also can be calculated from a comparison of peak intensities for the identified phases. Phase analysis may become difficult in the case of the $R_5(Si_xGe_{1-x})_4$compounds where the large degree of peak overlap exists between the various structures, and errors in reported phase percentages can easily occur. Therefore, all potential factors that may cause the discrepancies in the phase amounts calculation should be closely examined.

A series of experiments described in this article were designed to study how differences in sample preparation may affect the reported results of the X-ray diffraction studies of an Er_5Si_4 alloy. In this study the duration of grinding time used to produce samples for powder

diffraction was varied as well as the type of X-ray diffractometer used. The effect these differences have on determined phase concentrations is presented and discussed.

Experimental Details

An Er_5Si_4 alloy (Er_5Si_4 #1) was prepared by arc-melting stoichiometric amounts of Er (99.98 wt.%) and Si (99.9995 wt.%) on a water-cooled copper hearth under an argon atmosphere. The button was re-melted several times to ensure homogeneity. The microstructure of this alloy was examined using a JEOL 6060LV scanning electron microscope equipped with an X-ray energy dispersive spectrometer.

The arc-melted Er_5Si_4 button was sectioned and a piece weighing 1.566 g was ground into powder with an agate mortar and pestle in an argon-atmosphere glove box. The resultant powder was screened using a clean sieve having openings of 38μm, and approximately one quarter of the uniformly mixed powder was separated from the total amount and divided evenly into three parts suitable for conventional X-ray powder diffraction (XRD), synchrotron high resolution powder diffraction (HRPD), and particle size measurements. The remaining powder was then ground for an additional 20 minutes, after which one third was again separated and divided into equal portions for conventional XRD, HRPD and particle size measurements. This basic process was then repeated two more times, producing a series of samples. The only difference between these samples is the length of grinding time to which the particles had been subjected. A flow chart of the entire

procedure is shown in Figure 1. The particle sizes of all powders were measured using a MicroTrac S3500 particle analyzer employing light scattering technology.

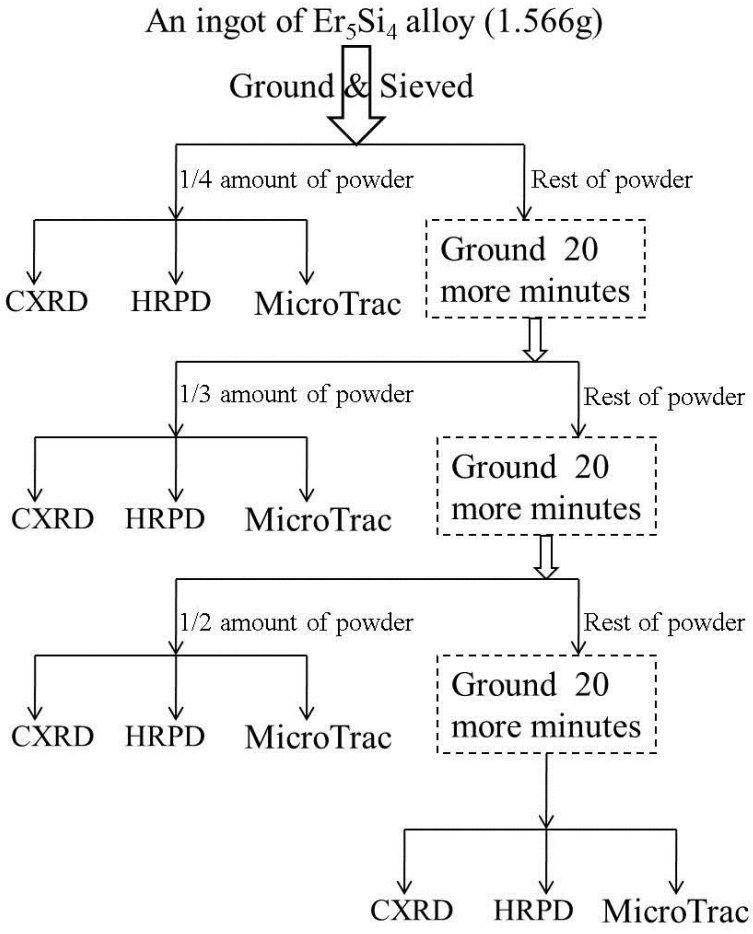

Figure 1. Flow chart showing powder sample preparation and handling for Er_5Si_4 #1.

Conventional X-ray powder diffraction (XRD) studies were carried out on a PANalytical X'Pert PRO diffractometer using monochromatic Cu $K\alpha_1$ radiation at ambient temperature. The Bragg-Brentano reflection geometry was used. The X-ray diffraction patterns covered a 2θ range 20°-120° with a step of 0.01675º. High resolution X-ray powder diffractions (HRPD) employing a synchrotron source were performed at Argonne National Laboratory

[24]. The mean operating wavelength for this source is 0.4138Å. Multiple point detectors were used for automatic data collection. The diffraction data were collected continuously from 0.5° to 50° with a scan speed of 0.01º /sec and spaced at 0.001º. The sample powders were coated on the inner walls of Kapton tubes that were rotated during the scan at a rate of ~ 5000 rpm. The collected diffraction data using both conventional laboratory Cu Kα radiation and a synchrotron source were quantitatively analyzed by the Rietveld method using LHPM RIETICA [25].

In order to study the effect of low temperature anneals on the XRD results of the ground powders, another Er_5Si_4 alloy, designated "Er_5Si_4 #2", was prepared in the same way as "Er_5Si_4 #1". A sample weighing ~ 1.5 g was separated from the "Er_5Si_4 #2" alloy and ground into powder in an argon-atmosphere glove box and screened with a sieve having openings of 38μm. A small amount of powder (named "38μm sieved") to be used as a control was extracted: one part was used for an initial XRD experiment while the rest was separated for anneals. The remaining powder was then ground for an additional 60 minutes (named "+60 min"). Again, a small part of the resultant powder was taken for conventional XRD, and the remainder was used for annealing experiments.

The annealing was performed as follows: the powders were wrapped in tantalum foil and sealed in a quartz tube which was evacuated and then filled with helium gas. Several pieces of pure yttrium metal were also inserted into the tube to act as oxygen getters. The sealed quartz tubes were annealed at 500˚C for 20 minutes and air cooled. The annealed powders were then examined with conventional XRD.

Experimental Results

Scanning Electron Microscopy

The microstructure of the first Er_5Si_4 alloy in the as-cast state is shown in Figure 2. The morphology of one random area of the polished and ion-etched sample surface imaged with secondary electrons (SE) is shown in Figure 2a, while the corresponding image using backscattered electrons (BSE) is shown in Figure 2b. The atomic number sensitivity of BSE imaging produces contrast that indicates the existence of four phases, namely, a black phase, two gray phases of different shades, and a series of thin linear features growing in specific directions that appear white. Combined with EDS analysis (Table 1), the black phase is identified as ErSi (i.e. the 1:1 phase), and the two gray phases (light-gray matrix marked "L" and dark-gray grain marked "D") have the same composition of Er_5Si_4 (i.e. the 5:4 phase). There are two possible reasons for the gray areas having the same composition but different contrast, both related to the complex crystallography of Er_5Si_4. As discussed in [26], the dark-grey grain may be exactly the same phase as the light-grey matrix, only possessing a slightly different orientation. Another possibility is that the observed contrast is due to the presence of the monoclinic 5:4 phase, which has a slightly different crystal structure from that of the orhtorhombic 5:4 matrix. This small difference could be sufficient to alter the coefficient of back scattering associated with each region due to the electron channeling effect [27], producing a slight contrast difference.

A reliable composition from the white linear features is difficult to obtain using EDS in SEM due to their narrow size. Spreading of the incident electron beam due to interactions

with the sample as predicted using Monte Carlo simulations [28] shows that any composition detected will actually be a combination of the matrix and the white features. However, based on previous research results [29, 30], we believe the linear features are Er_5Si_3, (i.e. the 5:3 plates).

Table 1. Compositions of phases observed in the Er_5Si_4 #1 sample. Experimental data are the averages of several sampled areas.

Element	Black phase (1:1)		Light-grey phase (5:4)		Dark-grey phase (5:4)	
	Theoretical at.%	Experimental at.%	Theoretical at.%	Experimental at.%	Theoretical at.%	Experimental at.%
Si	50.0	47.5	44.4	42.9	44.44	42.6
Er	50.0	52.5	55.6	57.1	55.56	57.4

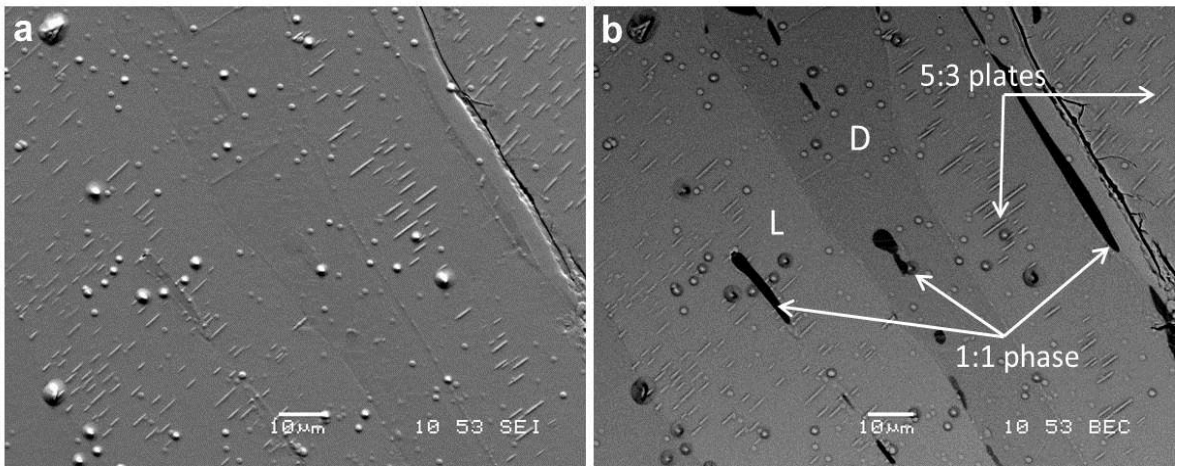

Figure 2. SEM images of sample Er_5Si_4 #1 obtained using (a) secondary and (b) backscattered electrons.

Powder Size Measurement using MicroTrac

It is logical to assume that extending the length of mechanical grinding time should result in a continuing decrease of average particle size. This was confirmed by the particle size

measurements, and the results showing the median particle size and standard deviation of each sample are listed in Table 2. Although the median sizes of the powders were measured, it is safe to suggest that the change of the median size reflects that of the average size, and they both have the same variation trend. As seen in Table 2, the median particle size steadily decreases from 11.9 μm to 3.02 μm as a function of grinding time. The distribution in powder sizes as denoted by the standard deviation of the measurements is also expected to decrease with increasing grinding time, and this was confirmed, dropping from a high of 11.79 μm to 6.64 μm.

Table 2. Powder size measurement results of Er_5Si_4 #1 as a function of grinding time.

Samples	Median Size (μm)	Standard Deviation (μm)
Er_5Si_4 -38μm	11.9	11.8
Er_5Si_4 +20	6.71	8.93
Er_5Si_4 +40	4.17	6.71
Er_5Si_4 +60	3.02	6.64

Conventional X-ray Powder Diffraction using Laboratory Radiation

The XRD patterns obtained using conventional laboratory Cu $K\alpha_1$ radiation of the four Er_5Si_4 powder samples that differ from one another in grinding time are shown in Figure 3. The data were collected from 20 to 120 degrees, but due to the low intensity of Bragg reflections and strong peak overlap at high Bragg angles, only data in the range 20º- 80º were used for Rietveld refinement. For convenience, the initial sieved powder is further designated "Er_5Si_4-38 μm" in this article, while the other three powder samples are named "Er_5Si_4 +20", "Er_5Si_4 +40" and "Er_5Si_4 +60" to denote that the grinding time was extended

by 20, 40 and 60 additional minutes. Figure 3 shows that as the grinding time increases, the measured diffraction intensity drops and the peak widths increase. This is expected because decreased grain size and microstrains introduced by the mechanical grinding broaden the Bragg peaks [31]. It is also well known that long-term mechanical grinding can transform crystalline material into amorphous material (for example, GdNiAl [32]).

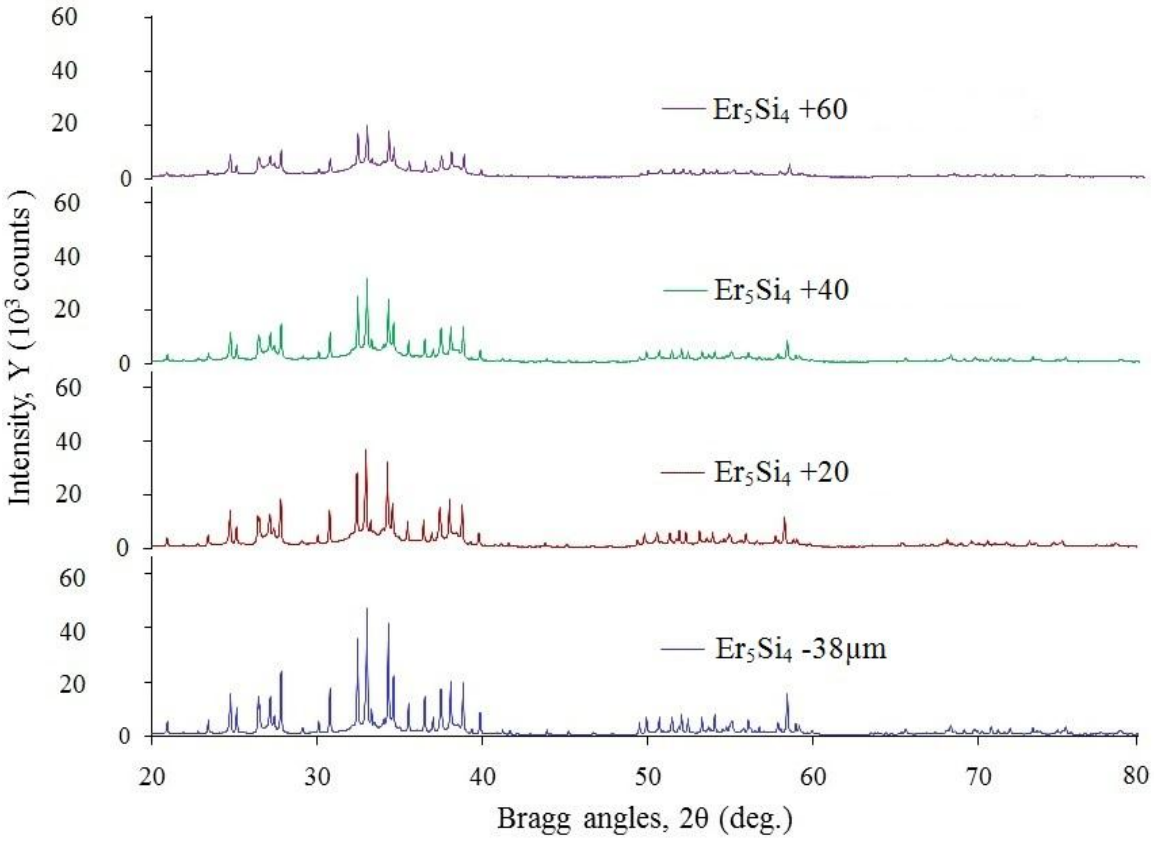

Figure 3. Comparison of observed X-ray powder diffraction patterns using Cu $K\alpha_1$ radiation at room temperature from four powder samples from Er_5Si_4 #1 which were ground for different time.

Rietveld refinement of the XRD patterns of the four powder samples indicates that there are three phases in Er_5Si_4, namely 5:4 orthorhombic phase (space group: Pnma), 5:4 monoclinic phase ($P112_1/a$), and 1:1 orthorhombic phase (Cmcm). The three rows of lines (tick marks)

below the measured X-ray diffraction pattern in Figure 4 show the locations of the calculated peaks for these phases. From top to bottom, the three sets of tick marks indicate the positions of the Bragg peaks for the orthorhombic 5:4 phase, monoclinic 5:4 phase, and 1:1 phase respectively.

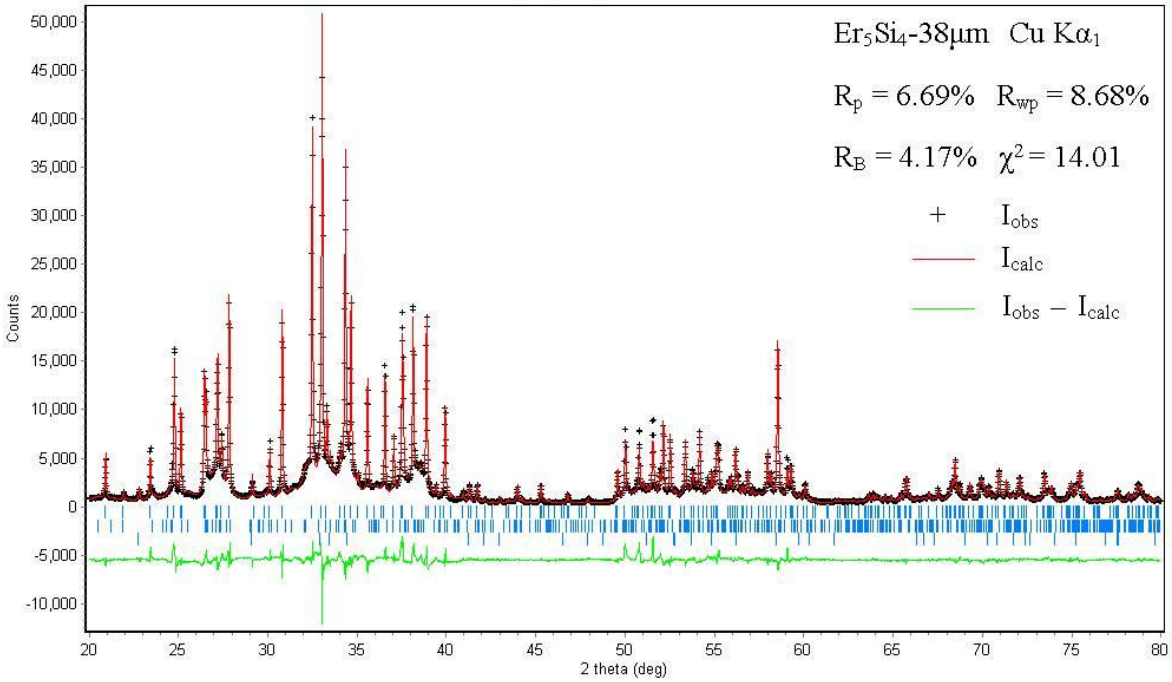

Figure 4. Rietveld refinement results of X-ray powder diffraction pattern of Er_5Si_4 -38µm (from Er_5Si_4 #1) collected using Cu $K\alpha_1$ radiation.

Comparing the XRD results with those obtained using SEM, no 5:3 phase was detected, which is expected given the difficulties in the detection of thin 5:3 plates in a 5:4 matrix reported in previous studies [26, 33]. Due to the extremely small concentration of the 5:3 phase (commonly less than 1 vol.%) and the strong overlap in Bragg peaks of 5:3 and 5:4 phases, the 5:3 phase is difficult to resolve using the conventional X-ray diffraction method. This is especially true for Cu Kα radiation because the energy of these x-rays nearly

coincides with the location of the L absorption edges of the lanthanides, causing strong fluorescence that results in a high background signal.

The concentrations of the three phases present in the four Er_5Si_4 powder samples as determined from Rietveld refinement are summarized in Table 3. As the grinding time is extended the volume percentage of the 5:4 monoclinic phase increases while the amount of the 5:4 orthorhombic phase decreases.

Table 3. Phase concentrations in Er_5Si_4 #1 obtained using conventional XRD employing Cu $K\alpha_1$ radiation. Numbers in parentheses are standard deviations.

Phases	Vol.% of different phases			
	Er_5Si_4 -38μm	Er_5Si_4 +20	Er_5Si_4 +40	Er_5Si_4 +60
Orth 5:4	57.3 (±1.2)	41.1 (±1.1)	39 (±1)	26.7 (±0.3)
Mono 5:4	40.9 (±0.5)	57.4 (±0.7)	59.6(±0.7)	72.2 (±0.7)
Orth 1:1	1.8(±0.1)	1.5 (±0.1)	1.3 (±0.1)	1.1 (±0.1)

High Resolution Powder Diffraction using Synchrotron Radiation

Diffraction patterns from the four Er_5Si_4 powder samples characterized using HRDP are compared in Figure 5. In this case the entire scan range covered 0.5º to 50º, however, only data in the range 4º-25º were used for the Rietveld refinement due to the possibility of large errors at low and high angles where data are collected with fewer detectors. Similar to the laboratory XRD experiments, the maximum intensity of peaks decreases and the width of the peaks increases as a function of grinding time. Figure 6 gives the diffraction patterns of "Er_5Si_4 -38μm" and "Er_5Si_4+60", with the positions of the Bragg peaks of orthorhombic 5:4 phase, monoclinic 5:4 phase, and 1:1 phase indicated with tick marks from top to bottom.

Detailed analysis shows that Bragg peaks of the 5:3 phases, seen in the SEM images, can be identified in the synchrotron data of the initial powder Er_5Si_4-38 μm". We attributed this to the higher resolution of the synchrotron diffraction system coupled with the better signal-to-noise ratio possible with the lower fluorescence that occurs when using higher energy X-rays. However, the 5:3 peaks are very weak due to their extremely low volume percentage (< 1 vol. %) and (in most cases) significant overlap with the Bragg peaks of orthorhombic 5:4 and monoclinic 5:4 phases.

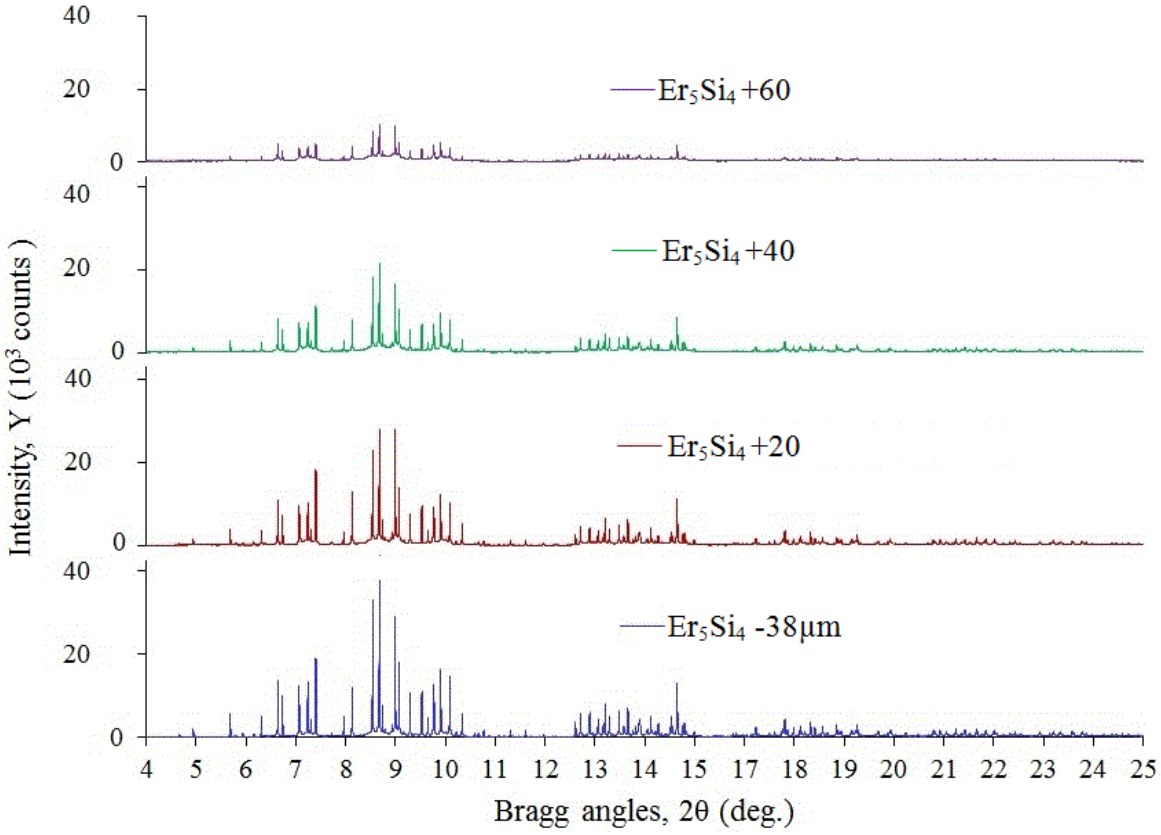

Figure 5. Comparison of high resolution powder diffraction patterns using synchrotron radiation at room temperature from four powder samples from Er_5Si_4 #1 that were ground for different times.

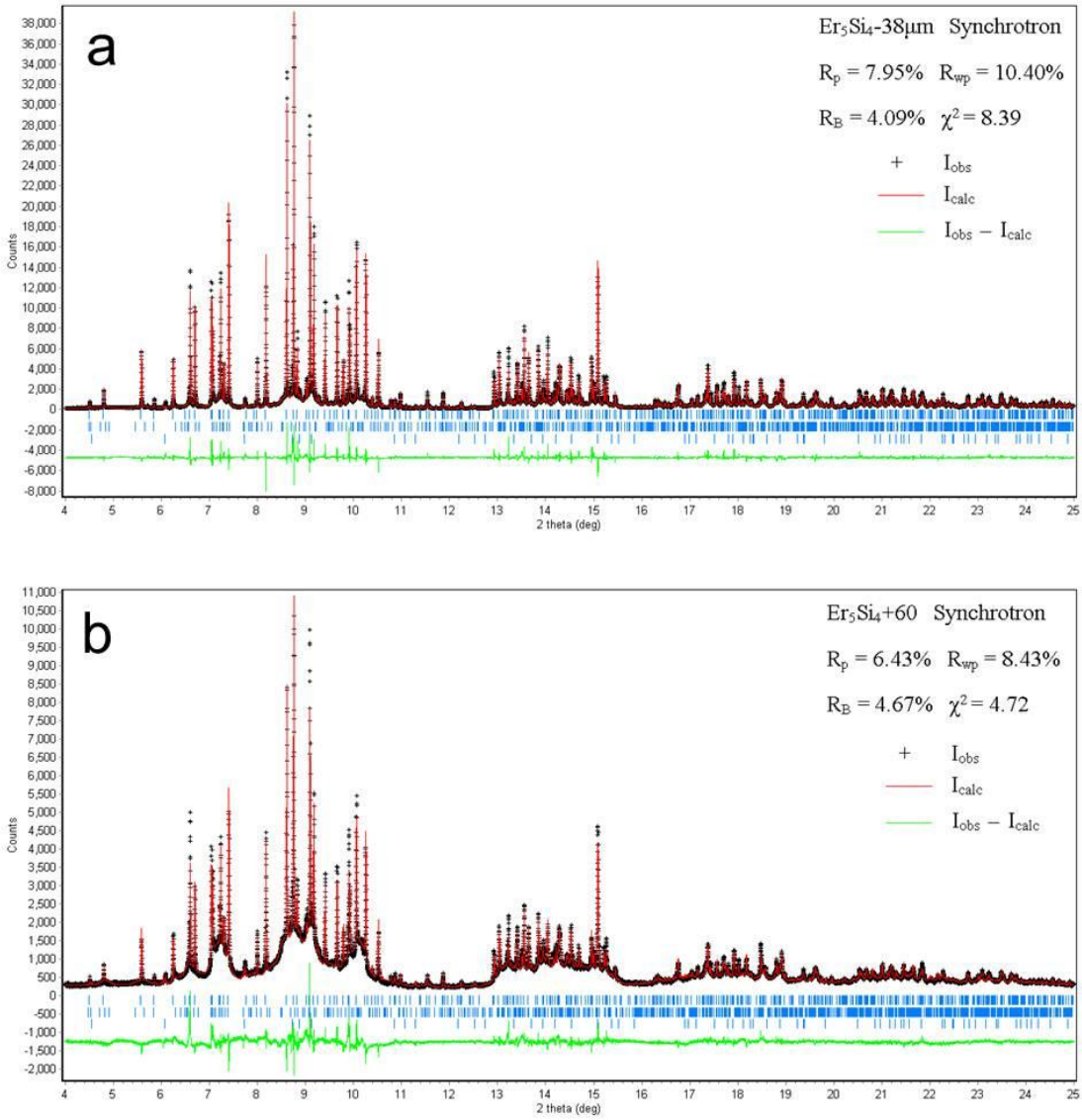

Figure 6. Rietveld refinement results of high resolution powder diffraction patterns of (a) Er_5Si_4 - 38μm and (b) Er_5Si_4+60 (from Er_5Si_4 #1) collected using synchrotron radiation.

These observations are consistent with the results of previous work on lutetium-doped erbium silicide $(Er_{0.9}Lu_{0.1})_5Si_4$ that was also studied by using synchrotron radiation [26]. Note that although visual observation of SEM images reveals the existence of a small amount of 5:3 phase, the Rietveld refinement was not able to determine any meaningful

quantity of this phase, thus tick marks denoting this phase were omitted from Figure 6. The concentrations of phases as determined from Rietveld refinement for the four Er_5Si_4 powder samples are listed in Table 4.

The values in Table 4 show the same trend indicating a shift from the orthorhombic 5:4 to the monoclinic 5:4 with longer grinding times as seen in Table 3. However, the absolute values are somewhat different. Another difference is that the amount of the 1:1phase as measured using synchrotron radiation appears to be more constant and does not display any dependence on the time of grinding.

Table 4. Phase concentrations in Er_5Si_4 #1 obtained using synchrotron radiation. Numbers in parentheses are standard deviations.

Phases	Vol.% of different phases			
	Er_5Si_4 -38μm	Er_5Si_4 +20	Er_5Si_4 +40	Er_5Si_4 +60
Orth 5:4	66.8 (±0.2)	56.1 (±0.2)	45.3 (±0.2)	27.8 (±0.1)
Mono 5:4	31.7 (±0.2)	42.2 (±0.2)	53.2 (±0.2)	70.9 (±0.3)
Orth 1:1	1.6 (±0.1)	1.7 (±0.1)	1.6 (±0.1)	1.3 (±0.1)

Low Temperature Annealing Experiments

XRD examinations of the two powder samples that differ in the amount of grinding time made from the "Er_5Si_4 #2" were carried out using laboratory Cu $K\alpha_1$ radiation. The observed XRD patterns of each powder sample before and after annealing are shown in Figure 7. For both samples, the width of the Bragg peaks is reduced after the powders were annealed; this can be seen clearly in the insets of Figure 7. The positions of the Bragg peaks for orthorhombic 5:4 phase, monoclinic 5:4 phase, and 1:1 phase are marked from top to bottom with three sets of bars. The calculated Bragg peak positions of the three phases are

nearly unchanged after the heat-treatment, therefore, in order to simplify the plots, only the peak positions calculated from the XRD data of the un-annealed powders are shown in the two insets. After annealing the intensity of the orthorhombic 5:4 peaks increases while the intensity of the monoclinic 5:4 peaks decreases and in some cases almost disappears. For example, it is obvious that five peaks of the monoclinic 5:4 phase, marked as (131), (230), $(1\bar{3}\ 2)$, $(1\bar{4}2)$ and (301), are no longer observed after the powders were annealed. By comparing the vertical axis of Figs. 7a and b, one can see that the measured diffraction intensity dropped as the grinding time increased, which is the same as what has been observed in Figs. 3 and 5.

The calculated concentration of phases present in the Er_5Si_4 powder samples changed considerably after the powders were annealed, and the values determined from Rietveld refinement are summarized in Table 5. It is instructive to compare these experimental results to those from Er_5Si_4 #1 (Table 3). Although the initial concentrations of phases are different since they came from two different arc-melted buttons, the effect of mechanical grinding on the relative phase concentrations is consistent. Namely, the concentration of the monoclinic 5:4 phase increased while that of the orthorhombic 5:4 phase decreased with the extending of the mechanical grinding time. The concentration of the monoclinic 5:4 phase more than doubled after grinding the powder for 60 more minutes. Additionally, it is apparent that regardless of the length of grinding time, the concentration of the monoclinic 5:4 phase drops while the amount of the orthorhombic 5:4 phase increases as a result of annealing at the relatively low temperature 500˚C. Taking the experimental and calculation

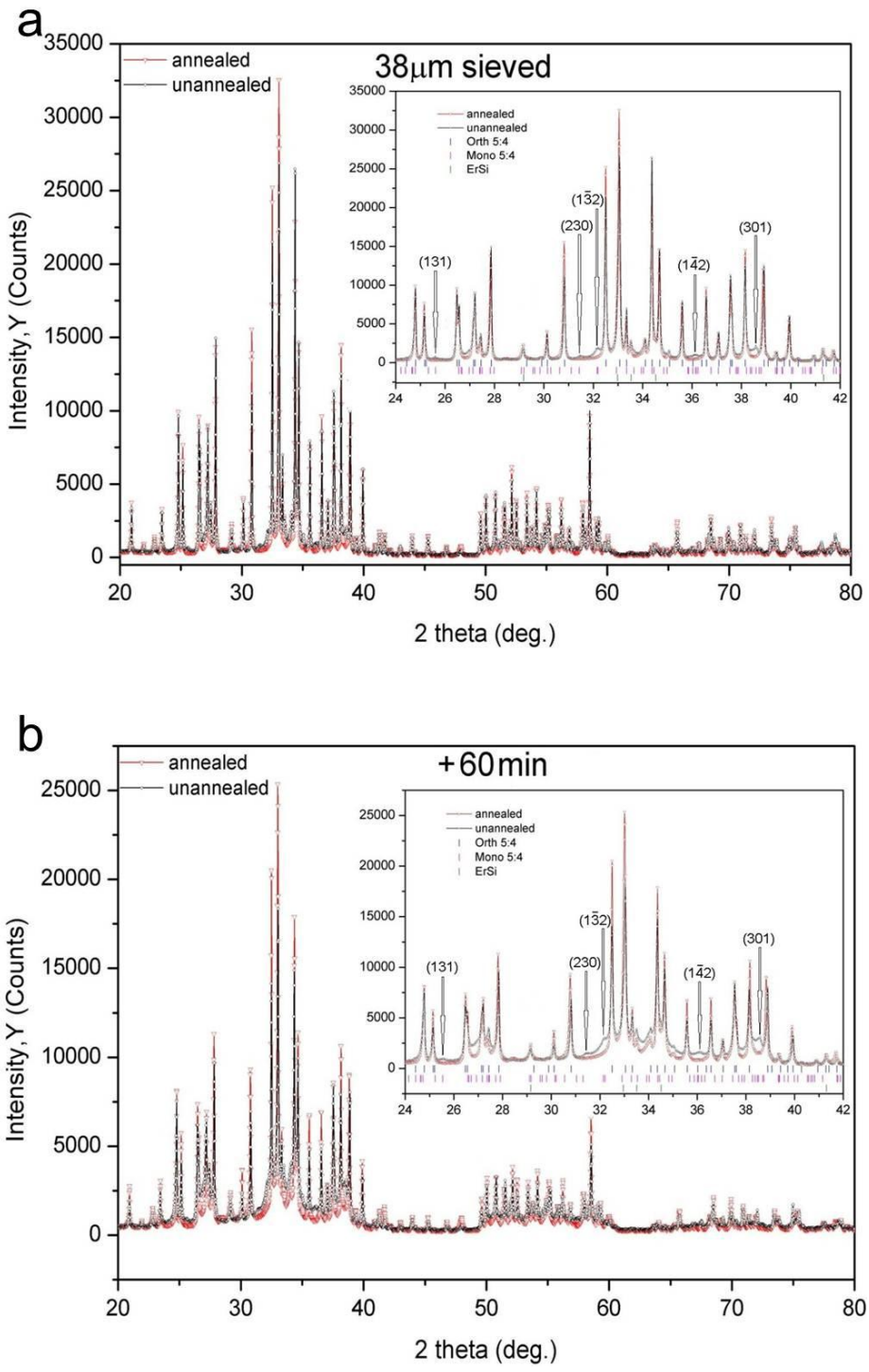

Figure 7. Comparison of observed XRD patterns of (a) "38μm sieved" powder sample and (b) " + 60min" powder sample collected before and after annealing (from Er_5Si_4 #2). The insets show an enlargement of the X-ray patterns between 24° and 42° 2θ.

Table 5. Phase concentrations in Er_5Si_4 #2 powder samples both before and after annealing (Cu Ka_1 radiation). Numbers in parentheses are standard deviations.

Powder samples	38μm sieved		+60min	
Powder treatment	unannealed	annealed	unannealed	annealed
R_p of the Rietveld Refinement	7.33	9.33	7.09	8.75
R_{wp} of the Rietveld Refinement	9.23	12.24	9.40	11.82
R_B of the Rietveld Refinement	4.37	4.97	3.71	4.06
χ^2 of the Rietveld Refinement	7.67	12.89	8.69	12.95
Vol.% of Orthorhombic 5:4	71.0 (±1.3)	88.3 (±2.1)	39.4 (±1.1)	64.2 (±1.8)
Vol.% of Monoclinic 5:4	25.5 (±0.4)	7.0 (±0.3)	58.3 (±0.8)	32.1 (±0.7)
Vol.% of Orthorhombic 1:1	3.5 (±0.1)	4.7 (±0.1)	2.3 (±0.1)	3.7 (±0.1)
Reduction in Vol.% of Mono 5:4 due to annealing	18.5		26.2	

errors into account, the concentration of the 1:1 phase can be regarded as constant and is not affected either by the mechanical grinding or the low-temperature annealing processes.

Discussion

Comparing the calculated phase concentrations listed in Table 3 and Table 4, the phase concentrations obtained from conventional XRD data (Table 3) differ from those obtained from synchrotron data (Table 4) for each of the four Er_5Si_4 powder samples, especially for sample "Er_5Si_4 +20" where the concentrations of monoclinic 5:4 and orthorhombic 5:4 calculated from conventional XRD data are much different (~ 15 %) from those calculated from synchrotron data. Additionally, the synchrotron results clearly show a higher percentage of the orthorhombic 5:4 in the "Er_5Si_4 -38μm" sample, while the amount of ErSi 1:1 is approximately the same. This difference may be due to the large number of peaks present in this system and the ever-present problem of peak overlap. The synchrotron data

provide more distinct peaks, allowing a better determination of the actual phase percentages present.

Despite the discrepancies described above, the trend seen in the conventional XRD data stills holds true for the HRPD. The calculated vol. % of the orthorhombic 5:4 decreases while that of the monoclinic 5:4 increases with increasing grinding time. The change is even more striking considering that the HRPD data started with apparently a higher amount of orthorhombic 5:4 than the conventional XRD data. The phase ratios in the powder sample that experienced the longest grinding time (i.e. sample "Er_5Si_4 +60") are approximately the same when measured using the two different techniques.

The four Er_5Si_4 powder samples used for XRD and HRPD are from the same ingot of the arc-melted button. SEM examination showed that the multiple phases are not absolutely uniformly distributed through the sample, the powders were extensively mixed before being divided into several parts. Thus, one is presented with the question as to why the length of grinding time has created such a divergence in the obtained results. The transition from orthorhombic 5:4 to monoclinic 5:4 is clear and significant.

The most logical explanation for such a shift is the hypothesis that mechanical grinding causes a phase transition from the orthorhombic 5:4 to the monoclinic 5:4. As described in [34], the $R_5(Si_xGe_{1-x})_4$ intermetallic compounds are composed of tightly bonded and nearly two-dimensional slabs. The interaction between the slabs, which can be asserted by the presence/absence of the interslab Si(Ge)-Si(Ge) bonds, easily varies as a function of an external thermodynamic stimuli. Research has shown that with an appropriate change of

temperature, hydrostatic pressure, and applied magnetic field, half of the Si(Ge)-Si(Ge) bonds may break through a reversible structural transition, causing a crystallographic change from one polymorphic structure to another, i.e., from orthorhombic to monoclinic or vice versa [5-7, 19, 34,]. For example, when a hydrostatic pressure was imposed on a polycrystalline Er_5Si_4 alloy [10] or a single-crystal Er_5Si_4 [11], the pressure was seen to drive the paramagnetic monoclinic structure to paramagnetic orthorhombic structure. In other words, the observed results at first sight appear to be in contradiction to the results seen in this study. However, it is important to realize that the force experienced by the Er_5Si_4 powder samples during mechanical grinding is fundamentally different from that exerted on the bulk Er_5Si_4 samples in studies [10] and [11], where the applied hydrostatic pressure acts with equal magnitude on the sample in all directions. The force exerted on the sample during mechanical grinding is almost entirely a shear force, not isotropic. Compared to the monoclinic 5:4 phase, the orthorhombic 5:4 phase has a lower unit cell volume and it is reasonable to promote the transition from monoclinic structure to orthorhombic phase by increasing the hydrostatic pressure exerted on the Er_5Si_4 alloy.

During mechanical grinding the material is subjected to shear stresses. When such stresses exceed the yield strength, fracture of the material occurs along atomic planes of maximum shear stress. Therefore, it is reasonable to expect that mechanical grinding will have a different effect on phase transitions occurring in an Er_5Si_4 alloy when compared to a hydrostatic application of pressure.

Given the amount of residual shear strain that can be introduced into the crystal structure of the Er_5Si_4 sample when exposed to long-term mechanical shearing forces, it may cause the

slabs to shift a small amount, breaking half of the Si(Ge)-Si(Ge) bonds and resulting in a transition from the orthorhombic 5:4 to the monoclinic 5:4. Thus a shear stress-induced phase transformation occurs. As grinding time increases, more orthorhombic phase transforms to the monoclinic phase, increasing the concentration of the monoclinic 5:4. Actually, stress-induced phase transformations are quite common in materials and are used in a wide number of metallic and ceramic systems, ranging from steels [35-37] to transformation-toughened zirconia [38, 39].

As can be seen in Figures 3, 5, 6, and 7, the width of Bragg peaks increases as the mechanical grinding time extends, which is expected. It is known that Bragg peak broadening is related to both the crystallite (grain) size and microstrain. The impact of the average crystallite size (τ) and microstrain (ε) on Bragg peak broadening (β, in radians) can be formulated as [31]:

$$\beta = \lambda / (\tau \cdot \cos\theta) \qquad (1)$$

and

$$\beta = k \cdot \varepsilon \cdot \tan\theta \qquad (2)$$

where λ is the wavelength, θ is the Bragg angle and k is a constant that depends on the presence of microstrain. In other words, peak broadening can be expected to occur due to decreased crystallite size and /or increased strain, and both of these conditions could be occurring in this study. With increasing grinding time the average powder size decreases, which can be derived from Table 2, and this trend is also expected to occur for τ, the average crystallite size. In addition, although it cannot be definitively proven, the mechanical grinding is expected to introduce microstrains, which also cause the peak

broadening β to increase as per Equation 2. The resultant increase of the Bragg peak broadening leads to more peak overlap between the monoclinic 5:4 and orthorhombic 5:4 phase, which causes the error in the calculated concentrations of phases to increase. The error introduced would be even larger for conventional X-ray diffraction, which has lower resolution compared to the synchrotron radiation. This tendency for greater error can be seen by comparing the standard deviations of the calculated phase concentrations listed in Tables 3 and 4. Although larger errors occur, the calculated concentrations of phases are still quite credible considering that both the monoclinic 5:4 and orthorhombic 5:4 phases have broader peaks. Further, Rietveld refinement is not based on the analysis of a few peaks, but all peaks are included. The standard deviations of the concentrations are less than 2 vol. % (see Tables 3, 4, 5), which reflects the accuracy of the calculated concentrations of phases.

Finally, while the exact values of the calculated phase concentrations may be slightly different from the actual concentrations in the samples due to the peak broadening effect noted above, the shear stress-induced phase transition is definitely occurring in Er_5Si_4. This conclusion is supported by a number of observations and deductions. Firstly, the observed change in phase concentrations is substantial and repeatable and therefore cannot be attributed solely to errors occurring during the phase analysis. Secondly, since the transformation between the orthorhombic 5:4 and monoclinic 5:4 does not require any change in chemical composition, no other phase percentages should be affected. This agrees with the fairly constant amount of the 1:1 phases in all experiments. Finally, the results of

the low temperature annealing of the ground powders also support the phase transition hypothesis.

Low-temperature annealing is a well-known method for releasing residual stress introduced during mechanical grinding. It is often used to reduce peak broadening due to the stress component and allows a better determination of structural parameters and actual phase compositions. The sharper Bragg peaks clearly seen in Figure 7 shows the residual stress has been significantly reduced. At the same time, the annealing caused the disappearance of some monoclinic 5:4 peaks and decreased the vol. % of the monoclinic 5:4 phase (Table 5). Thus, two effects, namely peak broadening and a stress-induced phase transition, are both revealed by the annealing process and can be distinguished from each other. The annealing study also shows that the stress-induced transition is not stable and is reversible once the residual stress is released.

In Table 5 it can be seen that after annealing the vol. % of the monoclinic phase in the "38μm sieved" powder sample dropped to ~ 7 vol. % from the original ~ 25.5 vol. %, tested in the as-ground state. Assuming it is impossible to completely drive the monoclinic structure back to the orthorhombic, simply because it may be difficult to relieve all stress in extremely fine powders, it is safe to conclude that the second arc-melted Er_5Si_4 alloy (Er_5Si_4 #2) initially had less than 7 vol.% of monoclinic 5:4 phase. Although SEM examination was not conducted on the ingot that separated from Er_5Si_4 #2 before it was subjected to grinding, observations of the entire surface of the remains of Er_5Si_4 #2 using SEM would tend to support this number as being a reasonable average value based on the quantitative analysis result of the sampled area.

Table 5 also shows that a greater drop in the vol. % of the monoclinic 5:4 phase is seen in the "+60 min" than for the "38μm sieved", although the annealing process for the two samples was the same. This is expected given that "+60 min" can be expected to have a higher degree of stress (and, therefore, higher amount of the monoclinic phase as confirmed by Table 5) due to the extended grinding time. Thus, a greater driving force exists for the reverse transformation once annealing begins, resulting in a more rapid drop in the amount of monoclinic phase.

At this time it is not clear whether extending the annealing time (or possibly increasing the annealing temperature) would have caused the amount of the monoclinic phase in the "+60 min" sample to drop to the same level noted in the "38μm sieved" sample. The question really becomes one of whether particle size plays a role in phase stability. It was seen that for the "38μm sieved" sample the material was not entirely orthorhombic after annealing. If the particle size has no effect on phase stability, then it might be possible to drive the reverse reaction from the monoclinic to orthorhombic back to essentially 100% of the as-arc-melted amount by either extending the annealing time or raising the temperature for the same time. However, if the particle size does affect the reverse reaction, it may be impossible to completely drive the reaction back to completion in particles where the size drops below a critical value. Experiments are underway to answer these questions.

Conclusions

The effect of mechanical grinding and subsequent heat treatment of ground powder on the concentrations of different phases present in erbium silicide (Er_5Si_4) was studied by X-ray powder diffraction experiments using both conventional laboratory Cu $K\alpha_1$ radiation and a high-energy synchrotron radiation source. The observed relative amounts of the orthorhombic and monoclinic phases depend on the grinding time and the X-ray diffraction technique used. A shear stress-induced phase transition from the orthorhombic 5:4 to the monoclinic 5:4 was seen occurring in the erbium silicide Er_5Si_4 as a result of a long-term mechanical grinding process. This phase transition is reversible, and the monoclinic phase will revert to the orthorhombic structure once the material is subjected to annealing at low temperatures. This result suggests that mechanical forces also have an important effect on the crystal structure of the rare-earth $R_5(Si_xGe_{1-x})_4$ intermetallic compounds, as do temperature, applied magnetic field, hydrostatic pressure and chemical composition. Given the similarity in structures of all the $R_5(Si_xGe_{1-x})_4$ family of alloys, it is possible that deformation-induced transitions occur in all of these materials.

Acknowledgments

This work was performed at Ames Laboratory under contract no.DE-AC02-07CH11358 with the US Department of Energy. This research was supported by the Office of Basic Energy Sciences, Materials Science Division of the US DOE. The high-resolution powder diffraction in this study was carried out at the 11-BM synchrotron beamline of APS/ANL.

Use of the Advanced Photon Source at Argonne National Laboratory was supported by the U. S. Department of Energy, Office of Science, Office of Basic Energy Sciences, under Contract No. DE-AC02-06CH11357. The authors wish to thank David Byrd and Joel Rieken for the particle size measurements, and Elizabeth Bertelson for the preparation of the second Er_5Si_4 sample.

References

[1] G. S. Smith, A. G. Tharp and Q. Johnson, Nature, 210 (1966) 1148.

[2] V. K. Pecharsky and K. A. Gschneidner Jr., Phys. Rev. Lett., 78 (1997) 4494.

[3] G. S. Smith, A. G. Tharp and Q. Johnson, Acta Crystallogr., 22 (1967) 940.

[4] F. Holtzberg, R. J. Gambino and T. R. McGuire, J. Phys. Chem. Solids, 28 (1967) 2283.

[5] V. K. Pecharsky and K. A. Gschneidner, Jr., Adv. Mater., 13(9) (2001) 683.

[6] A. O. Pecharsky, K. A. Gschneidner, Jr., V. K. Pecharsky, D. L. Schlagel and T. A. Lograsso，Phys. Rev. B, 70 (2004) 144419.

[7] C. Ritter1, C. Magen, L. Morellon, P. A. Algarabel, M. R. Ibarra, V. K. Pecharsky, A. O. Tsokol and K. A. Gschneidner Jr，J. Phys.: Condens. Matter, 18 (2006) 3937.

[8] L. Morellon, Z. Arnold, P. A. Algarabel, C. Magen, M. R. Ibarra and Y. Skorokhod, J. Phys.: Condens. Matter, 16 (2004) 1623.

[9] Y. Tseng, H. Ma, C. Yang, Y. Mudryk, V. K. Pecharsky, K. A. Gschneidner, Jr., N. M. Souza-Neto, and D. Haskel, Phys. Rev. B, 83 (2011)104419.

[10] C. Magen, L. Morellon, Z. Arnold, P. A. Algarabel, C. Ritter, M. R. Ibarra, J. Kamarad, A. O. Tsokol, K. A. Gschneidner, Jr., and V. K. Pecharsky, Phys. Rev. B, 74 (2006) 134427.

[11] N. Marcano, P. A. Algarabel, J. Rodroguez, C. Magen, L. Morellon, Niraj K. Singh, D. L. Schlagel, K. A. Gschneidner, Jr., V. K. Pecharsky and M. R. Ibarra, Phys. Rev. B, 85 (2012) 024408.

[12] C. Magen, Z. Arnold, L. Morellon, Y. Skorokhod, P. A. Algarabel, M. R. Ibarra, and J. Kamarad, Phys. Rev. Lett., 91 (2003) 207202.

[13] C. Magen, L. Morellon, P. A. Algarabel, M. R. Ibarra, Z. Arnold, J. Kamarad, T. A. Lograsso, D. L. Schlagel, V. K. Pecharsky, A. O. Tsokol, and K. A. Gschneidner Jr., Phys. Rev. B, 72 (2005) 024416.

[14] V. K. Pecharsky, A. P. Holm, K. A. Gschneidner, Jr., and R. Rink, Phys. Rev. Lett., 91 (2003) 197204.

[15] L. Morellon, Z. Arnold, C. Magen, C. Ritter, O. Prokhnenko, Y. Skorokhod, P. A. Algarabel, M. R. Ibarra, and J. Kamarad, Phys. Rev. Lett., 93, (2004) 137201.

[16] V. K. Pecharsky. A. O. Pecharsky, Y. Mozharivskyj, K.A. Gschneidner Jr., G.J.Miller, Phys Rev. Lett., 91 (2003) 207205.

[17] Y. Mozharivskyj, A.O. Pecharsky, V.K. Pecharsky, G.J.Miller, K.A. Gschneidner Jr., Phys Rev. B, 69 (2004) 144102.

[18] Ya. Mudryk, V.K. Pecharsky, and K.A. Gschneidner, Jr., Z. Anorg. Allg. Chem., 637 (2011) 1948.

[19] Ya. Mudryk, Niraj K. Singh, V.K. Pecharsky, D.L. Schlagel, T.A. Lograsso, and K.A. Gschneidner, Jr., Phys. Rev. B, 85 (2012) 094432.

[20] A. O. Pecharsky, K.A. Gschneidner Jr., V.K. Pecharsky, C.E. Schindler, J. Alloys Compd., 338 (2002) 126.

[21] A. P. Holm, V. K. Pecharsky, K. A. Gschneidner, Jr., R. Rink, M. N. Jirmanus, Rev. Sci. Instrum., 75 (2004) 1081.

[22] M. Zou, Y. Mudryk, V. K. Pecharsky, K. A. Gschneidner, Jr. D. L. Schlagel and T. A. Lograsso, Phys. Rev. B, 75 (2007) 024418.

[23] L. Morellon, J. Blasco, P. A. Algarabel, and M. R. Ibarra, Phys. Rev. B, 62 (2000)1022.

[24] Advanced Photon Source. Argonne (IL): Argonne National Laboratory (US). Available from: http://www.anl.gov/

[25] B. A. Hunter. RIETICA, a visual Rietveld program, Internationals union of crystallography commission on powder diffraction Newsletter No.20 (1998), http://www.rietica.org.

[26] Q. Cao, L. S. Chumbley, Ya. Mudryk et al., unpublished research. A paper entitled

"Phase Identification of Lutetium doped Er_5Si_4" has been submitted for publication.

[27] J. Goldstein, D. Newbury, D. Joy, C. Lyman, P. Echlin, E. Lifshin, L. Sawyer, J. Michael, Scanning Electron Microscopy and X-Ray Microanalysis, 3rd edition. Springer; 2007. (p247-256, Chapter 5)

[28] D. E. Newbury, D. C. Joy, P. Echlin, C. E.Fiori and J. I. Goldstein, Advanced Scanning Electron Microscopy and X-ray Microanalysis. New York: Plenum Press. 1986. (p.19-26. Chapter 1)

[29] O. Ugurlu, L. S. Chumbley et al., Scr. Mater., 53 (2005) 373.

[30] O. Ugurlu, L. S. Chumbley et al., J. Mater. Res., 21 (2006) 2669.

[31] V. K. Pecharsky and P. Y. Zavalij. Fundamentals of Powder Diffraction and Structural Characterization of Materials. Boston : Kluwer Academic Publishers. 2003. (p.172 Chapter 2).

[32] B. Chevalier1, J. L. Bobet, J. Sánchez Marcos, J. Rodriguez Fernandez and J. C. Gómez Sal, Appl. Phys. A, 80 (2005) 601.

[33] L. S. Chumbley, O. Ugurlu, R. W. McCallum, K. W. Dennis, Y. Mudryk, K.A. Gschneidner Jr., V. K. Pecharsky, Acta Mater., 56 (2008) 527.

[34] W. Choe, V. K. Pecharsky, A. O. Pecharsky, K. A. Gschneidner Jr., V. G. Young Jr., G. J. Miller., Phys. Rev. Lett., 84 (2000) 4617.

[35] A. O. Inegbenebor, R. D. Jones and Brian Ralph, J. Mater. Sci., 24 (1989) 3529.

[36] E. D. Cabanillas, E. P. Alvarez, A. Hey and R. C. Mercader, Hyperfine Interact., 66 (1991) 295.

[37] Y. Ivanisenko, W. Lojkowski and H. J. Fecht, Mater. Sci. Forum, 539-543 (2007) 4681.

[38] B. Budiansky and L. Truskinovsky, J. Mech. Phys. Solids, 41 (1993) 1445.

[39] S. Yuh, C. Chou, Mater. Lett., 52 (2002) 69.

CHAPTER 3. Electron Microscopy Studies of Lutetium Doped Erbium Silicide ($Er_{0.9}Lu_{0.1})_5Si_4$

A paper published in Materials Characterization 62 (2011) 737

Q. Cao and L. S. Chumbley

Abstract

Examination of bulk microstructures of lutetium doped erbium silicide $(Er_{0.9}Lu_{0.1})_5Si_4$ (space group: Pnma) using scanning and transmission electron microscopy (SEM, TEM) reveals the existence of thin plates of a hexagonal phase (space group: $P6_3/mcm$) where the stoichiometric ratio in moles between the rare earths and Si is 5 to 3, i.e. the 5:3 phase. The orientation relationship between the matrix and the plates was determined as $[010]_m \parallel [10\bar{1}0]_p$. This observation adds credence to the assumption that all linear features noted in alloys of the rare-earth intermetallic family $R_5(Si_xGe_{1-x})_4$ are of the stoichiometric ratio 5:3 and possess a common orientation relationship with the parent 5:4 alloys.

Introduction

Application of the magnetocaloric effect of magnetic materials is a promising technology that offers a potential for high energy efficiency in achieving large-scale refrigeration. The most promising alloys for such an application are found in the rare-earth based intermetallic

family $R_5(Si_xGe_{1-x})_4$ (where R is one of the lanthanide rare earths). Indeed, the unique combination of magnetic properties and structural transitions [1, 2] exhibited by many members of this family presents numerous opportunities in advanced energy transformation applications. Extensive studies have been performed on the magnetic properties and the application of this family of materials since the giant magnetocaloric effect was discovered in $Gd_5Si_2Ge_2$ in 1997 [3, 4]. Successful future implementation of these materials in novel devices depends on a fundamental understanding of the structure-property relationships that exist at all length scales. Thus, the study of the microstructure of the $R_5(Si_xGe_{1-x})_4$ family has also drawn a considerable amount of attention.

The earliest studies [5] reported a distinct linear feature visible on the surface of Gd_5Si_4, $Gd_5Si_2Ge_2$, and Gd_5Ge_4 alloys. Later work on the $R_5(Si_xGe_{1-x})_4$ family (hereafter referred to as 5:4) [6-8] showed the linear features were not a surface feature but a separate second phase existing throughout the bulk of the material. The initial microstructural studies indicated these linear features appear relatively independent of the initial crystal structure and composition of the parent matrix [8, 9] and exist in every alloy examined, including R = Gd [5-10], Tb, Dy, Er [8, 11] and Yb [12], Ho [12,13]. Further studies in the $Gd_5(Si_xGe_{1-x})_4$ system proved that these linear features are thin plates [7] and have a hexagonal crystal structure [7] and a stoichiometric composition of $Gd_5(Si_xGe_{1-x})_3$ [6,7] (hereafter referred to as 5:3). The orientation relationship between the 5:3 thin plates and the 5:4 matrix in the $Gd_5 Si_2Ge_2$ and Gd_5Ge_4 has also been determined to be approximately $[010]_m \parallel [10\bar{1}0]_p$ [14].

While considerable work has been carried out on characterization of the Gd-based 5:4

alloys [5-14], much less detailed work has been done on other systems. The similarities in crystal structure, microstructure, phase diagrams, atomic bonding, etc. have caused researchers to generally assume that the linear features seen in other $R_5(Si_xGe_{1-x})_4$ type alloys are also 5:3 phases, possessing the same orientation relationship and formation characteristics as those detailed for the Gd-based system. While this is a reasonable assumption, a complete characterization of an alloy in another 5:4 system has yet to be conducted to provide confidence in this assumption. Such a characterization is the focus of this study. Three main reasons were considered when selecting the sample of this study. Firstly, of the three crystal structures present in $R_5(Si_xGe_{1-x})_4$ systems, namely Gd_5Si_4-type orthorhombic structure (O(I), space group: Pnma, all bonds connected between layers), $Gd_5Si_2Ge_2$-type monoclinic structure (space group: $P112_1/a$, half of the bonds connected between layers) and Sm_5Ge_4-type orthorhombic structure (O(II), space group: Pnma, no bonds connected between layers) [15], previous conclusions about the orientation relationship between the 5:3 plates and the 5:4 matrix were obtained from the characterization of alloys possessing the second and third type of crystal structures. By choosing an alloy with the Gd_5Si_4-type orthorhombic structure for investigation, all three basic matrix structures will have been covered. Secondly, all previously examined $R_5(Si_xGe_{1-x})_4$ alloys have involved alloys containing a single rare-earth with substitutions made to vary the Si/Ge ratio. This examination is the first to investigate what effects result to the orientation relationship between the plates and the matrix if substitutions occur in the rare-earth metal content. Finally, the majority of work has been done on the $Gd_5(Si_xGe_{1-x})_4$ system. By choosing a different rare-earth-based 5:4 system the validity of the assumptions that have been made thus far can be strengthened. Accordingly, an $(Er_{0.9}Lu_{0.1})_5Si_4$ alloy was

chosen as the object of this study.

Experimental Details

An $(Er_{0.9}Lu_{0.1})_5Si_4$ alloy was prepared by arc-melting high- purity Er, Lu, and Si mixed in appropriate amounts corresponding to the stoichiometric ratio 4.5:0.5:4 under argon atmosphere. The button was weighed after being re-melted several times and was found to have lost ~0.6 wt.% as compared to the total initial amounts of pure Er, Lu and Si. SEM characterization of the ion-etched sample was carried out using a JEOL 6060LV scanning electron microscope equipped with an X-ray energy dispersive spectrometer. Samples for transmission electron microscope (TEM) studies were mechanically ground, dimpled and ion-milled to electron transparency. An FEI Tecnai G^2 F20 transmission electron microscope equipped with EDS and STEM mode was used for composition studies and high-resolution electron microscopy. For electron diffraction studies a Philips CM30 TEM operated at 300kv was used since it was easier to tilt the sample and possessed a smaller selective area diffraction aperture.

Experimental Results

SEM and bright field TEM images of the $(Er_{0.9}Lu_{0.1})_5Si_4$ sample are shown in Figure 1. Contrast produced in the SEM image using backscattered electrons (BSE) (Fig. 1a) shows the existence of three phases, the gray matrix assumed to be the 5:4 phase, thin white linear

features growing in specific directions and a small amount of a dark phase. EDS analysis indicates the composition of the dark phase is $(Er_{0.9}Lu_{0.1})Si$, i.e. the 1:1 phase. The white linear features are presumably 5:3 plates, although they are too small to obtain reliable composition data using EDS in SEM. The thin plates can be seen easily using TEM bright field (BF) imaging, Figure1b and c. The thicknesses of the plates are on the order of tens of nanometers. Selected area diffraction (SAD) was performed in order to confirm that the thin plates are a 5:3 hexagonal phase with characteristics and orientation relationship analogous to those in the Gd-based system. Figure 2 shows SAD patterns taken from the matrix only (Figure 2a) and when the aperture was positioned to overlap both matrix and plates (Figure 2b). The two separate diffraction patterns are shown as indexed in Figure 2b, with the matrix lattice being delineated by solid lines, while dashed lines are used for the plates. Although slight differences in measured lattice parameters exist due to the substitution of Lu into the lattice, the pattern can be indexed as having the electron beam oriented parallel to the [010] and $[10\bar{\mathbf{1}}\mathbf{0}]$ zone axes of orthorhombic matrix Er_5Si_4 and hexagonal Er_5Si_3 plates, respectively. Thus, the orientation of the thin plates satisfies the relation $[010]_m \parallel [10\bar{\mathbf{1}}\mathbf{0}]_p$, which is the same orientation relationship reported between the plates and matrix in $Gd_5Si_2Ge_2$ and Gd_5Ge_4 [14].

A high-resolution TEM image of one thin plate is shown in Figure 3a with a small indexed SAD pattern inset in the top-left corner. According to the indexed SAD pattern, the angle between the $(\bar{1}2\bar{1}0)_p$ planes and $(00\bar{1})_m$ planes is 7º; this rotation can be easily seen in the higher magnification view of Figure 3b between the lattice fringes of the two phases. The rotation angle of 7º is consistent with the results reported for $Gd_5Si_2Ge_2$ and Gd_5Ge_4 in [14].

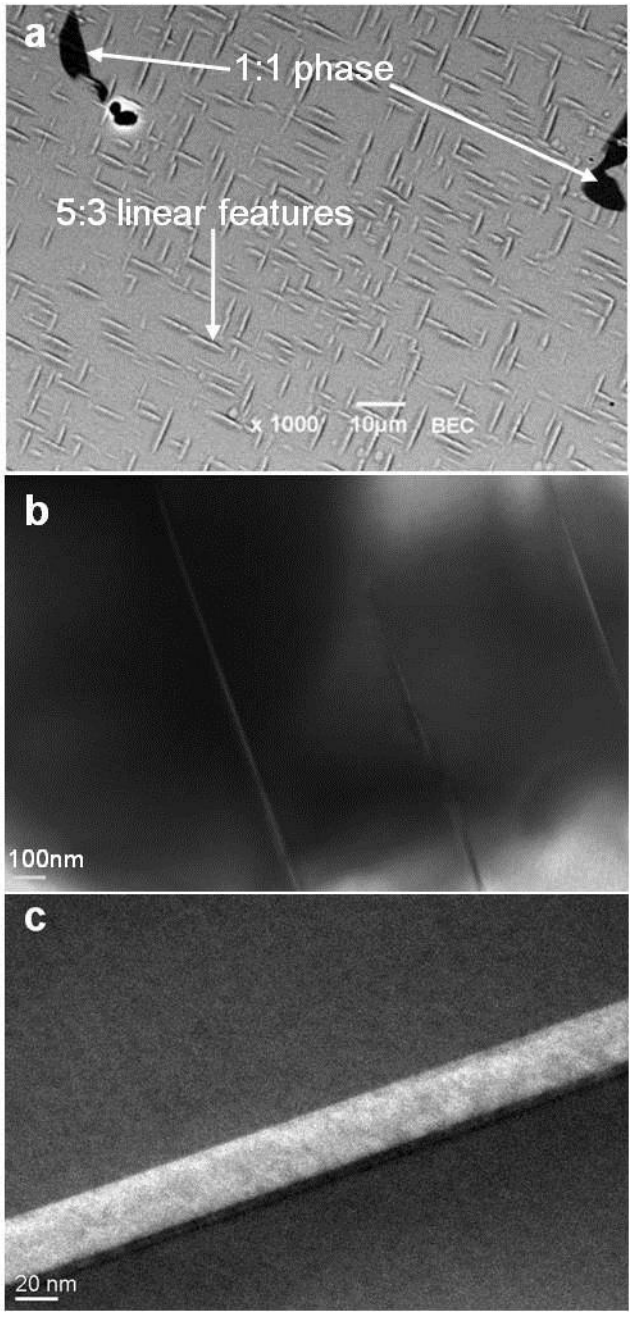

Figure 1. SEM and TEM images of $(Er_{0.9}Lu_{0.1})_5Si_4$ (a) BSE image, (b) BF image of three parallel thin plates, (c) one thin plate at higher magnification.

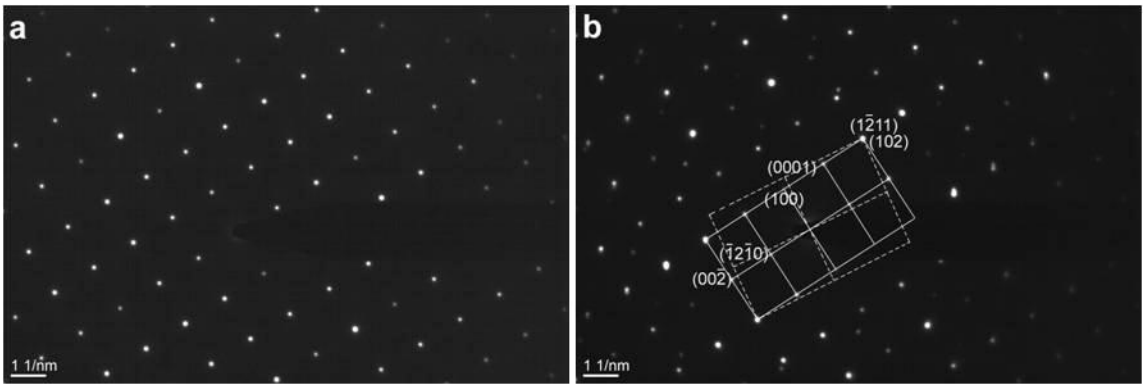

Figure 2. SAD pattern taken from (a) matrix only and (b) matrix including a thin plate. Indexing shows the matrix as solid lines, plates as dashed lines.

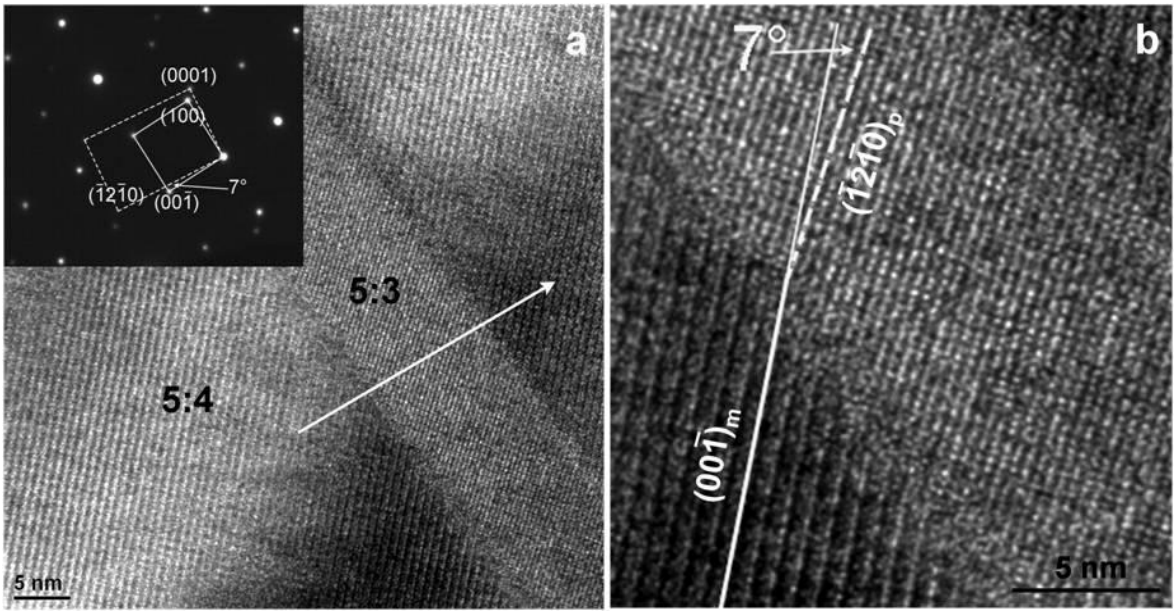

Figure 3. (a) High resolution TEM image of one thin plate with an indexed SAD pattern (inset). Solid lines: matrix; dashed lines: plate. (b) Enlarged interface image between 5:4 matrix and 5:3 plate showing 7° rotation between $(\bar{1}2\bar{1}0)_p$ and $(00\bar{1})_m$ planes.

The average interval between the lattice fringes of the matrix was measured to be 7.55Å, which is very close to the d-spacing of $(00\bar{1})_m$ planes (7.59 Å) obtained from the indexing of the SAD pattern. For the plate, the average interval is 4.16 Å, also nearly equivalent to

the d- spacing of $(\bar{1}2\bar{1}0)_p$ planes (4.15 Å) calculated from the SAD pattern. Images such as these prove conclusively that the plates are not twin structures and are exactly analogous to the 5:3 structures studied in $Gd_5Si_2Ge_2$ and Gd_5Ge_4 [14]. Final confirmation comes in the results of an EDS scan taken across the thin plate shown in Figure3a. The results (Figure 4) reveal the total atomic percentage of the rare-earth (Er + Lu) in the thin plate is ~ 62 at.%, which is close to the theoretical value 62.5 at.% of 5:3 phase. The total atomic percentage of Er and Lu in the matrix is about 56 at.%, which is also consistent with the theoretical value 55.5 at.% of 5:4 phase. It is interesting that the Lu appears to be distributed fairly equally between the two phases (Figure 4b).

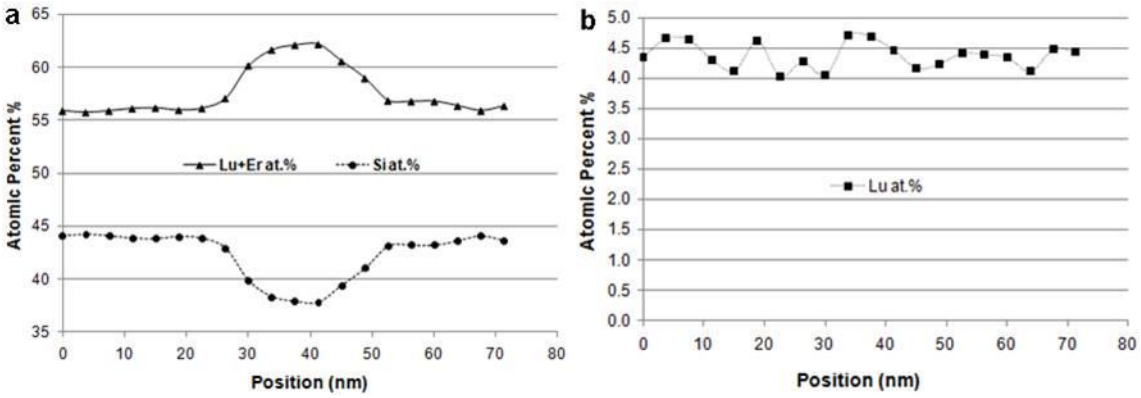

Figure 4. EDS line scans showing compositions in at.% taken across the thin plate in Fig.3a (arrow indicates the scan direction). (a) Difference in (Er+Lu) and Si compositions between matrix and plate. (b) Lu variation.

Discussion

There is only a small composition difference between the 5:4 matrix and the 5:3 plates and TEM images show that the actual thickness of the plates is fairly small, being always in the

range of several nanometers to hundreds of nanometers. When taken together these facts imply that the process that results in phase transformation from 5:4 to 5:3 can be accomplished through "short range" atom transport [16]. Comparing the 5:3 thin plates found in the $(Er_{0.9}Lu_{0.1})_5Si_4$ sample with those observed in other systems [7,10-14] it appears the plates produced in single crystal samples [7,11,13,14] prepared using a tri-arc method [17] are much thicker than those observed in polycrystalline samples [10,12] made by an arc-melting method. The reason for this may be attributed to the difference in cooling rate between these two techniques of crystal preparation. For the tri-arc pulling method, there are a series of copper baffles and a small amount of alcohol present inside the pulling rod (3/8 inch in diameter, 17 inch long) to which the single crystal is attached. The alcohol removes heat from the system by evaporating at the hot end of the rod, condenses at the cold end of the rod, then runs back down to the hot end to start the process over again. An external set of fans blows air to remove heat from the rod and condense the alcohol. While effective this system is still relatively inefficient at heat removal when compared to an arc-melting arrangement. In arc-melting the melted button (~ 1 cm in diameter, ~ 0.3 cm in thickness) is solidified on a copper hearth (12 inches in diameter), which is cooled by chilled flowing water. Thus, a huge heat sink exists for heat removal, and heat is extracted by direct conduction through the copper. Although no data were taken to measure the cooling rate of these two techniques, it is reasonable to assume that the tri-arc pulling method removes heat from the system relatively slowly, much more slowly than in the arc-melting technique. The more rapid cooling rate of the melt in arc-melting can be expected to produce a finer microstructure in the solidified melt. As suggested in [14], the formation mechanism of 5:3 thin plates is best described as displacive-diffusional where the diffusion

process is a short-range shuffling of atoms that occurs at high temperatures. The faster the cooling rate of the melt, the shorter the time that sufficient atomic mobility exists at high temperatures for atoms to shuffle and form the 5:3 structure.

Indexing the SAD patterns indicates the orientation relationship existing between the 5:3 plates and the 5:4 matrix in the $(Er_{0.9}Lu_{0.1})_5Si_4$ sample (Gd_5Si_4-type orthorhombic (I)) is the same as that in $Gd_5Si_2Ge_2$ (monoclinic) and Gd_5Ge_4(Sm_5Ge_4-type orthorhombic (II)) reported in [14]. The rotation angle between the $(\bar{1}2\bar{1}0)_p$ planes and the $(00\bar{1})_m$ planes is 7º (Figure 3) which also is in agreement with what was observed in $Gd_5Si_2Ge_2$ and Gd_5Ge_4 [14]. Therefore, the previously assumed orientation relationship $[010]_m \parallel [10\bar{1}0]_p$ is indeed true, and the hypothesis is strengthened that a similar relationship exists for any compounds with Gd_5Si_4-type orthorhomic (I), $Gd_5Si_2Ge_2$-type monoclinic, or Sm_5Ge_4-type orthorhombic (II) structure in the $R_5(Si_xGe_{1-x})_4$ family that contain 5:3 plates.

The BF images of 5:3 thin plates in $(Er_{0.9}Lu_{0.1})_5Si_4$ (Figure1b,1c) reveal the thickness of the plates varies from 10nm to 30nm, much thinner than they appear in the SEM image (Figure1a). This is in agreement with previous studies [9], which suggested that the thickness of the plates observed using SEM is artificially thickened due to the effect of ion-etching, resulting in an over-estimation of the volume percentage of 5:3 phase.

The d-spacings of the $(00\bar{1})$ planes of the orthorhombic 5:4 matrix and the $(\bar{1}2\bar{1}0)$ planes of the hexagonal 5:3 plates, obtained from SAD pattern and HRTEM image, are compared in Table 1. The d-spacings obtained by measuring the HRTEM image are expected to have higher degree of error associated with them due to the manner by which there are obtained,

i.e. measurement from an image from a specific location in the sample rather than an average over a large region of the sample. While the lattice parameters and d-spacings obtained from selected area electron diffraction (SAD) are more accurate since the values are averaged over a relatively larger volume, overall the data are consistent with each other with the degree of difference being well inside the relative errors of the techniques used.

Table 1. The comparison of d-spacing of $(00\bar{1})_m$ and $(\bar{1}2\bar{1}0)_p$ planes obtained from HRTEM and SAD.

	d-spacing (Å) obtained from following two methods	
d-spacing	SAD	HRTEM
$d(00\bar{1})_m$	7.59	7.55
$d(\bar{1}2\bar{1}0)_p$	4.15	4.16

It should be noted that the arc-melted sample used in this study and in the previous studies [14] dealing with the orientation relationship between the plates and the matrix were as-cast samples, not heat treated after solidification. While several studies have involved heat-treated samples [6,13] the morphology of the plates remains unchanged from what is seen in the as-cast samples. Recent experiments suggest that extended heat treatments at extremely high temperatures can result in dissolution of the plates [13]. However, even in that instance no significant change in morphology of the plates was seen other than the obvious dissolution taking place. Therefore, it can be assumed that the orientation relationship between the plates and the matrix in heat-treated samples is unchanged from what existed when the plates initially preciptated from the matrix upon solidification, and remains constant as long as the plates persist.

Finally, formation of 5:3 plates would require an excess of silicon to be present if the ideal 5:4 starting composition had been maintained. However, the ~ 0.6 wt. % weight loss seen after melting indicates a small amount of the initial constituents evaporated and was pumped out of the arc-melting chamber. With Si being more volatile than Er and Lu, it is possible it was lost at a higher rate than the rare earths. More likely is that a large part of the excess of silicon entered the observed 1:1 phase. Previous synchrotron high resolution powder diffraction studies of this sample [18] have shown that the volume percentages of the 5:3 plates and the 1:1 phase are comparable, 0.60 % for 5:3 plates and 0.49 % for 1:1 phase.

Conclusions

(1) Combining the results obtained using SEM and TEM, it is clear that the linear features in the $(Er_{0.9}Lu_{0.1})_5Si_4$ sample are hexagonal 5:3 phases.

(2) The thickness of 5:3 plates in 5:4 alloys prepared by the tri-arc pulling method is greater than those prepared by the arc-melting method. The higher cooling rate of the arc-melting technique allows less time for significant diffusion to cause thickening , yet the plates are still extensive in the other two directions. These observations support the validity of a displacive-diffusional formation mechanism of the 5:3 plates as proposed in [14].

(3) TEM studies of the $(Er_{0.9}Lu_{0.1})_5Si_4$ sample indicate the orientation relationship between the 5:3 plates and the matrix is $[010]_m \parallel [10\bar{1}0]_p$, which is the same as that in other reported

$Gd_5(Si_xGe_{1-x})_4$ alloys. This adds credence to the assumption that this orientation relationship exists in any compounds with Gd_5Si_4-type orthorhomic (I), $Gd_5Si_2Ge_2$-type monoclinic, or Sm_5Ge_4-type orthorhombic (II) structures in the $R_5(Si_xGe_{1-x})_4$ family that contain 5:3 plates.

Acknowledgments

This work was performed at Ames Laboratory under contract no.DE-AC02-07CH11358 with the US Department of Energy. This research was supported by the Office of Basic Energy Sciences, Materials Science Division of the US DOE. The authors wish to thank N.K. Singh for preparing the arc-melted materials used in this study and also V.K. Pecharsky and K.A. Gschneidner Jr. for their support for this study.

References

[1] V. K. Pecharsky, K. A. Gschneidner Jr., Adv. Mater., 13 (2001) 683.

[2] A. O. Pecharsky, K.A. Gschneidner Jr., V. K. Pecharsky, C. E. Schindler, J. Alloy. Compd., 338 (2002) 126.

[3] V. K. Pecharsky, K. A. Gschneidner Jr., Phys. Rev. Lett., 78 (1997) 4494.

[4] V. K. Pecharsky, K. A. Gschneidner Jr., Appl. Phys. Lett., 70 (1997) 3299.

[5] J. Szade, G. Skorek, A. Winiarski, J. Cryst. Growth, 205 (1999) 289.

[6] J. S. Meyers, L. S. Chumbley, F. Laabs, A. O. Pecharsky, Scripta Mate., 47 (2002) 509.

[7] O. Ugurlu, L. S. Chumbley, D. L. Schlagel, T. A. Lograsso, A. O. Tsokol, Acta Mater. 53 (2005) 3525.

[8] O. Ugurlu, L.S. Chumbley, D. L. Schlagel, T. A. Lograsso, A. O. Tsokol, Scripta Mater.,

53 (2005) 373.

[9] L. S. Chumbley, O. Ugurlu, R. W. McCallum, K. W. Dennis, Y. Mudryk, K. A. Gschneidner Jr., V. K. Pecharsky, Acta Mater., 56 (2008) 527.

[10] H. Fu, Y. Chen, T. Zhang, M. Tu, J. Chin. R E. Soc.(in Chinese) 23(2005)409.

[11] O. Ugurlu, L. S. Chumbley, D. L. Schlagel, T. A. Lograsso, A. O. Pecharsky, 134th TMS (Minerals, Metals and Materials Society) Annual Meeting, Light Metals. 2005; 1181-1185.

[12] Z. Qian, L. S. Chumbley, S. Misra, G. Miller, V. K. Pecharsky, K. A. Gschneidner Jr., K. Ahn, A. S. Chernyshov, N. K. Singh, Acta Mater., 57 (2009) 3374.

[13] Q. Cao, L. S. Chumbley, Z. Qian, Intermetallics. 18 (2010) 1021.

[14] O. Ugurlu, L. S. Chumbley, D. S. Schlagel, T. A. Lograsso, Acta Mater., 54 (2006) 1211.

[15] V. K. Pecharsky, K. A. Gschneidner Jr., J. Alloy. Compd., 260 (1997) 98.

[16] S. Banerjee, Mater. Sci. Forum, 1 (1984) 239.

[17] D. L. Schlagel, T. A. Lograsso, A. O. Pecharsky, J. A. Sampaio. 134th TMS (Minerals, Metals and Materials Society) Annual Meeting, Light Metals. 2005;1177-1180.

[18] Q. Cao, L. S. Chumbley et al., Unpublished research. A paper entitled “Phase Identification of Lutetium Doped Erbium Silicide $(Er_{0.9}Lu_{0.1})_5Si_4$” has been submitted for publication.

CHAPTER 4. Thermal Stability of $RE_5(Si_xGe_{1-x})_3$ Plates in $RE_5(Si_xGe_{1-x})_4$ alloys, where RE = Gd and Ho

A paper published in Intermetallics 18 (2010) 1021

Q. Cao, L. S. Chumbley, and Z. Qian

Abstract

The stability of $RE_5(Si_xGe_{1-x})_3$ plates was studied through electron microscopy examination of as-cast and annealed Gd_5Ge_4 single-crystal samples. Thermal annealing of samples at 1200˚C showed instability of the plates and a sluggish dissolution into the matrix. Scanning electron microscopy of $Ho_5(Si_{0.8}Ge_{0.2})_4$ samples that had undergone laser surface melting indicated that the resulting rapid cooling of the melt pool suppressed precipitation of the characteristic 5:3 thin plates.

Introduction

The possibility of producing devices that utilize the magnetocaloric effect as an alternate technology for refrigeration, rather than the common gas compression / expansion method, has long been of interest. Cooling slightly below room temperature (~ 250 K – 290 K) is of particular interest because of the potential impact on energy savings and environmental

concerns. Materials with large magnetocaloric effects are desirable as they have improved energy efficiency. The family of $RE_5(Si_xGe_{1-x})_4$ intermetallic compounds where RE is one of the lanthanide rare earths is such a material, especially the $Gd_5(Si_xGe_{1-x})_4$ system, which possesses not only a giant magnetocaloric effect [1,2], but also colossal magnetostriction [3], and giant magnetoresistance [4].

Extensive research on the magnetic properties of $RE_5(Si_xGe_{1-x})_4$ (hereafter referred to as "5: 4" compounds), has resulted in the microstructures of this 5:4 system capturing the attention of researchers [5-11,14,15]. The earliest studies [5] reported the existence of linear features visible on the surface of Gd_5Si_4, $Gd_5Si_2Ge_2$, and Gd_5Ge_4 samples. Later work [6-8] showed the linear features were not a surface feature but a separate second phase existing throughout the bulk of the material, with a stoichiometric composition of $Gd_5(Si_xGe_{1-x})_3$ (hereafter referred to as "5: 3" compounds). This phase forms as thin plates, oriented in specific crystallographic directions [7-9]. The plates possess a high aspect ratio, extending tens (and often hundreds) of microns in two directions but with a thickness usually on the order of 100 nm. Interestingly, the presence of 5:3 thin plates has been confirmed in essentially every alloy examined in the $RE_5(Si_xGe_{1-x})_4$ family including RE = Gd, Tb, Dy, Er [8,10] and Yb, Ho [11]. The precipitation of 5:3 plates appears relatively independent of the initial crystal structure and composition of the parent matrix [8, 9].

Given the promise of the 5:4 alloys, the effect of 5:3 plates on their magnetic properties is of considerable interest. Moore et al. [12] studied the magnetic phase transition of $Gd_5Si_2Ge_2$ by using local scanning Hall probe imaging and found that 5:3 plates act as "seeds" for the nucleation and growth of ferromagnetic clusters in the paramagnetic matrix.

The practical implication of this observation is that by controlling the presence of 5:3 plates it may be possible to lower both the critical fields needed for the appearance of the giant magnetocaloric effect and the amount of hysteresis in the system. In another study Pecharsky et al. [13] compared the magnetocaloric effect of as-cast and heat-treated $Gd_5Si_2Ge_2$ samples. Experimental results showed that heat treatment at 1570 K for 1h leads to phase purification and homogenization of the as-cast sample, which produces a considerable enhancement of the magnetocaloric effect. However, this study did not involve any observation of the samples, so it is unknown what effect the heat treatment may have had on the microstructure and presence of the 5:3 plates.

The majority of studies concerning 5:3 plates have been based on as-cast materials. Ugurlu et al. [14] investigated the persistence of the 5:3 plates in $Gd_5Si_2Ge_2$ under thermal cycling and concluded that the 5:3 plates are stable in the temperature range -70˚C to 850˚C. Somewhat surprising was that alloy compositions specifically chosen in an attempt to avoid 5:3 formation still possessed 5:3 plates whenever the 5:4 phase was present, pointing to an unusual stability of the 5:3 plates within a 5:4 matrix. However, that study was limited in scope with an emphasis on cycling of the temperature, rather than on long-term stability at higher temperatures. The stability of the microstructure of $RE_5(Si_xGe_{1-x})_4$ compounds, particularly as regards the 5:3 thin plates, when annealed at higher temperatures for longer periods of time has not been reported until now, which is the purpose of this article.

The thermal stability of the 5:3 plates has been investigated in a Gd_5Ge_4 single-crystal sample by annealing the sample at 1200˚C for a total of 24 hours. The morphology of the 5:3 plates in the as-cast state, after 12 hours and after 24 hours of annealing was compared.

In addition, the effect of rapid cooling on the formation of the 5:3 plates in $Ho_5(Si_{0.8}Ge_{0.2})_4$ sample was also investigated and is discussed in this article.

Experimental Details

A Gd_5Ge_4 single crystal was obtained from the Materials Preparation Center of the Ames Laboratory [16]. Appropriate quantities of Gd (metals basis, 99.99996%) and Ge (99.999% pure) were cleaned and arc melted several times to ensure homogeneity under an argon atmosphere. The resulting button was used as the charge material to produce a single crystal by a tri-arc crystal pulling method [17] . Polycrystal $Ho_5(Si_{0.8}Ge_{0.2})_4$ was produced by arc-melting Ho (99.97 wt.% pure), Si (99.99 wt.% pure), and Ge (99.99 wt.% pure) under an argon atmosphere. Approximately 1 wt.% excess of holmium was added to offset evaporation. Within the sensitivity of the x-ray diffraction technique, both samples appeared to be single-phase alloys.

The as-cast Gd_5Ge_4 single-crystal sample was sectioned into two parts. One piece was used to prepare a thin foil for TEM characterization in the as-cast state while the second was used to study the effect of heat treatment on the microstructure and stability of the 5:3 plates. SEM examination was first performed for the as-cast sample after the surface was polished and ion-etched, then the sample was sealed in a quartz ampoule and annealed at 1200˚C. The sample was wrapped with a Ta foil to separate it from the quartz. To minimize oxidation of the sample during annealing the quartz was evacuated and filled with a protective argon gas to a pressure of 0.18bar, and a piece of pure Gd metal also was sealed

in the ampoule to act as a getter. After 12 hours of annealing, the sample was quenched in an ice-water mixture. A thin oxidized layer on the surface was removed and the sample was examined using SEM.

In order to study the change of the morphology of the 5:3 plates with the heat treatment time, the same sample was again sealed as described above and annealed at the same temperature for another 12 hours. Before the second twelve-hour period of annealing, several segments of 5:3 plates were marked using Vicker's hardness indentations to ensure that the location of exactly the same plates observed after 12 hours of annealing could be identified after the 24 hour anneal. The sample was quenched again after the second twelve-hour anneal, and SEM images were obtained after a series of ion-etching and polishing cycles, each cycle resulting in the removal of ~ 7 μm of material. The annealed sample was thinned for TEM characterization by dimpling and ion-milling to a thin foil.

The as-cast $Ho_5(Si_{0.8}Ge_{0.2})_4$ sample was polished and ion-etched and examined with SEM to establish an initial microstructure. To produce a rapidly solidified structure, a Nd : YAG laser was run across the surface of the sample using the following operational parameters: pulse width (FWHM) < 100 nanoseconds; wavelength λ = 1064 nanometers; average power = 0.4watts; DC current = 23 amperes ; Ar flow = 50 cubic feet per hour; scan rate = $1mm.sec^{-1}$. After laser melting, the surface of the sample was again examined using SEM, and the results were compared to the initial condition to investigate the effect of rapid cooling on the formation of 5:3 plates.

SEM characterization was carried out using a JEOL 6060LV scanning electron microscope equipped with an X-ray energy dispersive spectrometer. Samples for TEM studies were examined using an FEI Tecnai G^2 F20 transmission electron microscope, also equipped with an X-ray energy dispersive spectrometer.

Experimental Results

Scanning Electron Microscopy

Scanning electron microscopy (SEM) images of the Gd_5Ge_4 single crystal in the as-cast state and annealed state are shown in Figure 1. Long, thin plates of 5:3 are present initially in a fairly high density. After annealing at 1200˚C for 12 and 24 hours, the overall number and length of plates appears to decrease dramatically. What were identified to be plates at low magnification appeared less certain at higher magnifications, as closer observation revealed that the thin white line associated with 5:3 [7] was absent from many of the rough surface produced by polishing and etching, Figure 1d.

Since the higher Gd at.% present in the 5:3 plates as opposed to the surrounding matrix make them more subject to oxidation, it was suspected that the observed features seen after the 24 hour anneal were artifacts due possibly to oxidation and / or polishing. This hypothesis raised the possibility that the decrease seen in 5:3 plates was not due to dissolution of the plates at all, but merely the result of surface oxidation effects, as a thin oxide layer was present after each anneal despite being sealed in quartz under a protective

Ar atmosphere. In order to eliminate this possibility, efforts were made to mark the location of several thin plates in the Gd_5Ge_4 single crystal sample so they could be positively identified and their morphology monitored. The detailed comparison of the morphology of

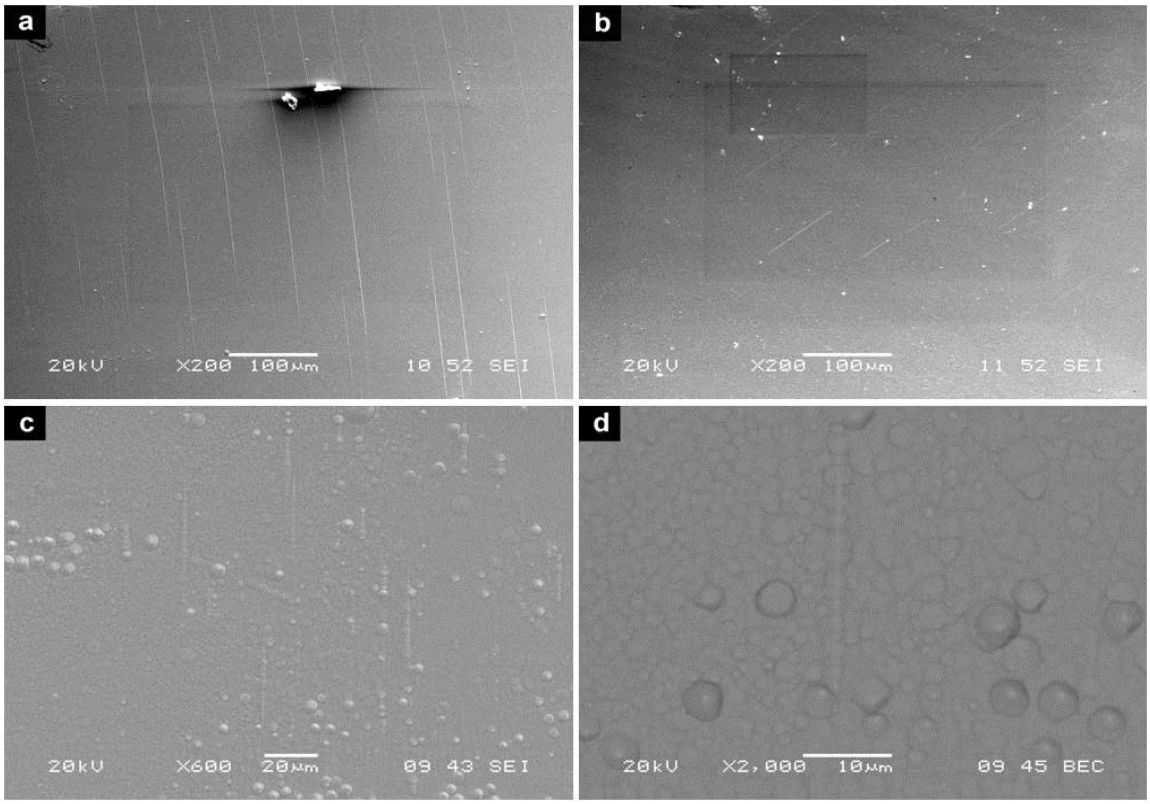

Figure 1. SEM images of Gd_5Ge_4 in the a) as-cast, b) after a 12 hour anneal at 1200˚C, and c)after a 24 hour anneal at 1200˚C. d) High magnification of the "plates" shown in c).

one of the marked 5:3 thin plates is shown in Figure 2. After 12 hours of annealing a 5:3 thin plate that was still present was marked by placing two diamond pyramid hardness marks on either end, Figure 2a. The plate selected was initially ~ 45 µm in length. The sample was then polished to ensure that the plate did extend into the depth of the sample, and was not merely a surface effect left from the initial 12 hour anneal. A layer of material ~7µm in depth was removed by polishing without changing the appearance of the plate,

giving confidence that the marked feature was indeed a plate of 5:3 that extended into the sample presumably to a depth commensurate with the observed length.

The sample was then annealed for an additional 12 hours and again viewed using SEM. The location of the 5:3 plates were quickly identified by means of the diamond pyramid marks and, considering the specific plate under discussion, initially it appeared as if the 5:3 phase was still present after the second twelve-hour anneal, Figure 2b. A series of polishing and ion-etching steps were then performed sequentially on the annealed sample to confirm the appearence of the marked 5:3 plates, as was done after the 12 hour anneal. After the first polishing step the plates were no longer visible, Figure 2c. This suggested one of two possibilities: 1) the plates visible in the as-annealed oxidized surface were simply the oxide surface remains of plates that had gone into solution, or 2) the plate surfaces had oxidized to a certain extent and the unoxidized portion of the plate might still be further below the surface. Additional polishing and etching steps were carried out, with new hardness marks added at the positions of the old ones before they were completely removed by each polishing and etching step to gaurantee the same region of interest was examined. This process was continued until ~35 μm of material was removed from the surface, however, no evidence for a 5:3 plate was ever seen, Figure 2d.

Transmission Electron Microscopy

Samples from the as-cast and 24 hour annealed material were also examined using transmission electron microscopy (TEM), Figure 3. TEM observation of the as-cast material showed the plates have very straight, distinct bundaries with the matrix, as discussed in [7,

9]. Energy Dispersive Spectroscopy (EDS) revealed the average composition of the plates to be around 67.3 at.% Gd vs. 60.3 at.% Gd for the matrix, Figure 3c. The 7% difference is consistent with the theoretical difference of Gd at. % between Gd_5Ge_3 and Gd_5Ge_4 (62.5 at.% Gd in Gd_5Ge_3 vs. 55.55 at.%Gd in Gd_5Ge_4). The systematic increase in the amount of rare earth occurs due to the formation of a thin rare-earth rich oxide film on the surface of the sample, one of the many difficulties that must be dealt with when identifying these plates [6,8].

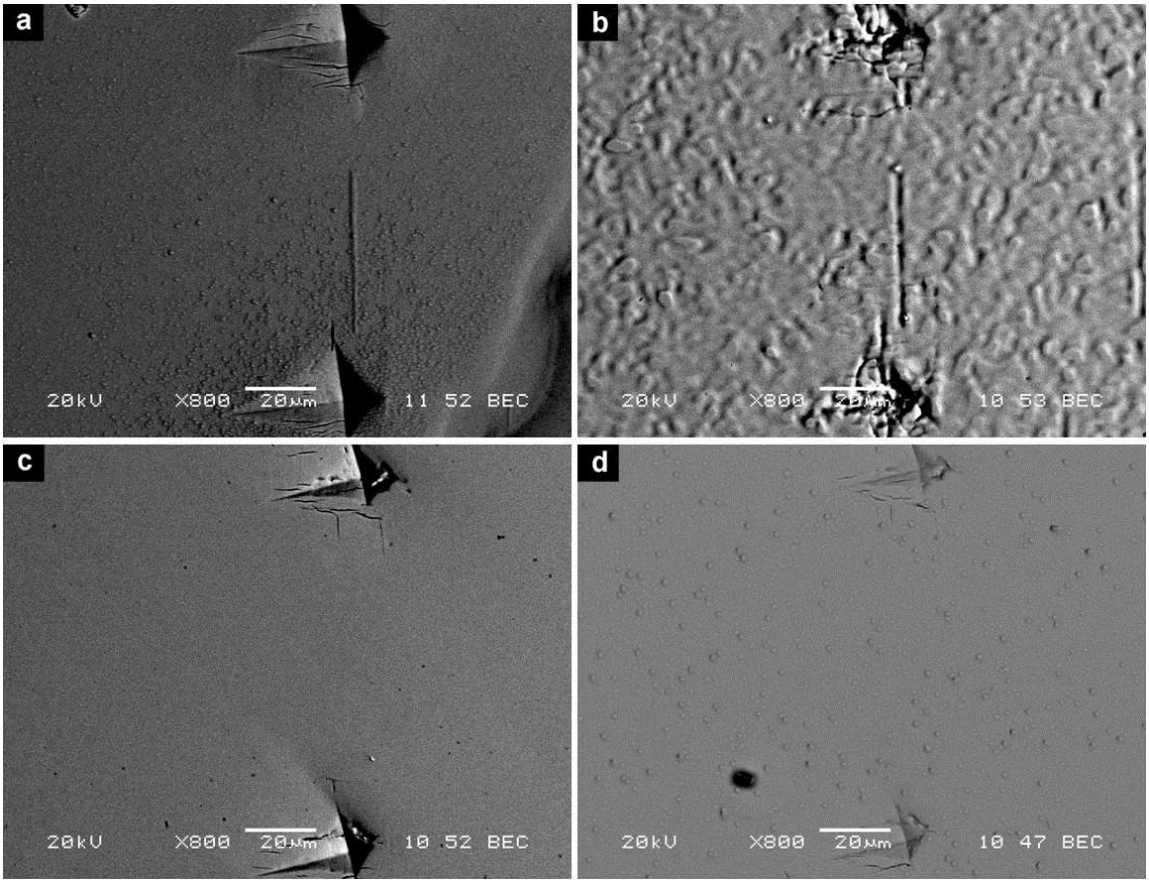

Figure 2. SEM images comparison of a marked thin plate. a) Initial ion-etched image after 12 hours of annealing. b) Initial image after an additional 12 hours of annealing at 1200˚C. c) View after polishing and ion-etching; the thin plate has disappeared. d) After several polishing / etching steps; no trace of the former plate is seen.

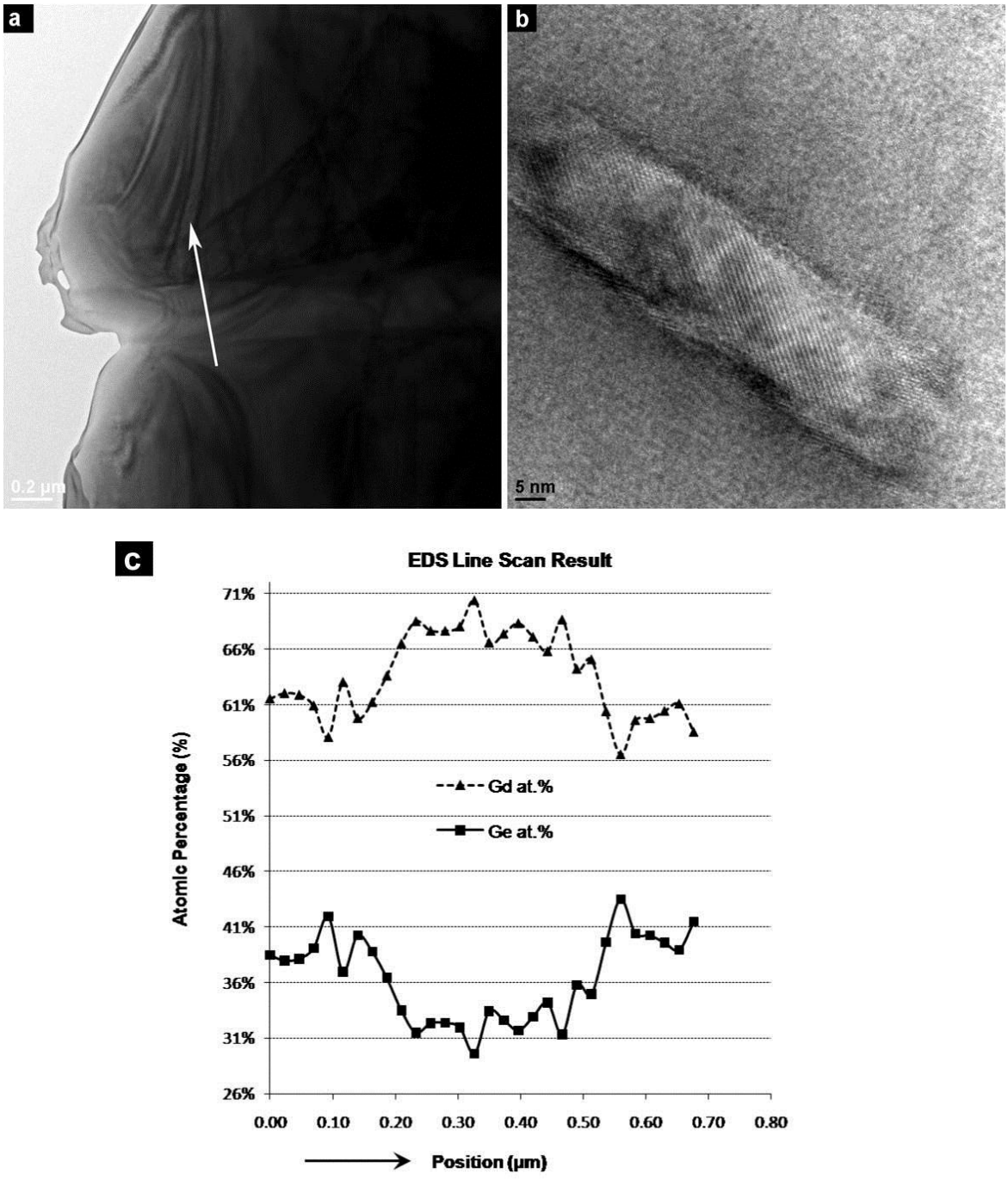

Figure 3. Transmission electron microscopy (TEM) images of Gd_5Ge_4 single crystal a) as-cast and b) after 24hours of annealing at 1200˚C. c) EDS line scan across the thin plate in (a) along the indicated direction.

A TEM image of a 5:3 plate after the 24 hour anneal is shown in Figure 3b. When comparing this image to that of Figure 3a, the length of the thin plates is seen to decrease dramatically after annealing, in agreement with the comparison result of SEM images (Figure 1). In addition to the change in the length of the thin plates, the TEM images reveal the width of the plates in the annealed sample is on the order of tens of nanometers, much more narrow than those in the as-cast sample, which are around hundreds of nanometers. Furthermore, the distinctive sharp boundaries at the sides of the plates have altered and the two ends of the thin plate in Figure 3b are not defined clearly, which reflects a gradual transition from 5:3 phase to 5:4 phase.

Rapid cooling

The precipitation of 5:3 within a 5:4 matrix has always been of interest due to the speed at which the reaction must occur [7,8]. Given that diffusion is required in order for the 5:3 plates to form, it was hypothesized that increasing the cooling rate at high temperatures upon cooling from the melt might prevent diffusion from occurring, leading to suppression of the precipitation of 5:3. Although the exact melting points of Si-Ho-Ge based 5:3 and 5:4 phases are not known , the melting points of 5: 3 and 5:4 phases in the Ho-Si binary system [18] and the Ho-Ge binary system [19] typically are very high (2120 K - 2220 K). Therefore, a high temperature process followed by a rapid cooling was desired. Laser surface melting, in which the material's surface is melted by a scanning laser beam, is a means of producing a refined or meta-stable microstructure in localized areas on a component due to the rapid cooling of the melt. Cooling rates during laser surface treatment

are on the order of 10^3 K·s^{-1} to 10^{11} K·s^{-1} [20]. While rapid cooling is often used to produce metastable structures, in this study the melting and subsequent rapid cooling of the laser surface was used to attempt to produce the thermodynamically stable structure.

A $Ho_5(Si_{0.8}Ge_{0.2})_4$ sample was used for the rapid cooling study. Figure 4 shows SEM images of a selected region with a high density of 5:3 plates both before and after laser surface melting. The laser surface melted region appears as a band that results from re-solidification of the melted material in the middle of Figure 4b. Comparison of the SEM images reveals that the 5:3 plates originally located in the fusion zone are now absent, although numerous cracks are observed.

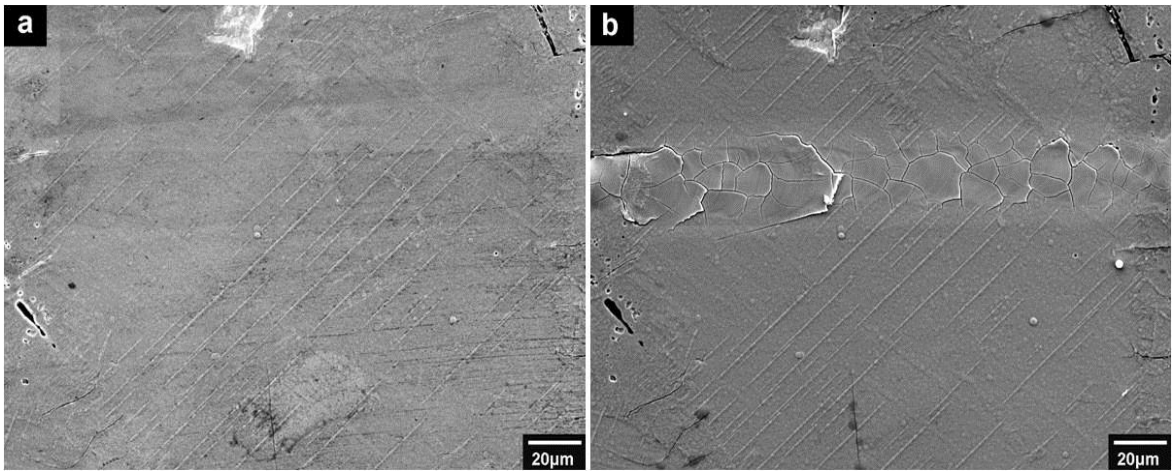

Figure 4. Scanning electron microscopy (SEM) images of a selected region on the surface of $Ho_5(Si_{0.8}Ge_{0.2})$ sample before and after laser surface melting, a) before laser surface melting, b) after laser surface melting with a band-shaped zone left in the middle of this region.

Discussion

Gd_5Ge_4 Material

According to the discussion in [7], and in agreement with the observed SEM and TEM images of the as-cast material, the initial size of the 5:3 plates in the Gd_5Ge_4 sample is on the order of 200 - 300 microns in extent in the plane of the sheet and 0.3 - 0.5 microns in thickness. Given these dimensions the extent of the marked 5:3 plates embedded into the 5:4 matrix after the 12 hour anneal could be expected to be much deeper than 7 μm, at least on average. Therefore, the possibility that the marked thin plates were completely removed during the initial polishing steps is extremely low. If the disappearance of the marked 5:3 plates on the surface was mainly caused by oxidization, the affected depth also should be fairly low since EDS analysis of the matrix as well as optical inspection indicated the oxidized layer was completely removed during the first polishing / etching sequence. After the marked 5:3 plates disappeared, no evidence of any phase was found in the position where the marked plate once existed. Therefore, a phase transformation of 5:3 back to 5:4 is the only possible reason for the disappearance of the marked thin plates. This is consistent with the TEM images, which also suggest a dissolution of 5:3 back into the matrix.

The actual temperature of the transition is still uncertain, as if whether a high temperature phase field actually exists as suggested [7,8]. Given the fairly sluggish rate at which the plates dissolve even at 1200˚C, it is probable that extremely long-term anneals would be necessary at lower temperatures to produce 5:3 plate dissolution.

$Ho_5(Si_{0.8}Ge_{0.2})_4$ Material

As the laser passed across the surface of the $Ho_5(Si_{0.8}Ge_{0.2})_4$ sample, the temperature of the regions heated by the laser rose promptly and reached the melting points of the 5:3 plates and 5:4 matrix. The plates and matrix melted rapidly, then the melt cooled very quickly. During the rapid cooling, the 5:3 plates didn't form, which means the rapid cooling suppressed the precipitation of the 5:3 plates. The cooling rates of techniques previously used to form 5:4 material (such as levitated melting [5], induction melting [6,11], and arc-melting [7, 8,10,15]) are far slower than that of laser melting, providing the time necessary for the diffusion required in order for the 5:3 plates to form.

The cracking observed in the laser-melted zones presumably is caused by stress concentration in these regions during the melting and re-solidification process. As the laser beam passed across the surface of the sample, the materials in the fusion zones (FZ) melted and subsequently re-solidified, and the regions in the heat-affected zones (HAZ) initially expanded and then contracted upon cooling. Stresses were introduced across the interface due to the unequal expansion and contraction of the HAZ and FZ, and these stresses were released by forming cracks.

Conclusions

Detailed SEM and TEM examination and comparison between the as-cast and annealed Gd_5Ge_4 single crystal have shown the thermal instability of Gd_5Ge_3 thin plates during long

term annealing above 1200˚C. The phase transformation of 5:3 to 5:4 phase occurs fairly sluggishly, being incomplete even after 24 hours annealing. However, it is reasonable to deduce that extending the annealing time and increasing the annealing temperature will lead to a thorough disapperance of the 5:3 thin plates. Laser surface melting performed on the surface of the $Ho_5(Si_{0.8}Ge_{0.2})_4$ sample shows that rapid cooling will suppress the precipitation of 5:3 plates in this alloy system, and it is assumed that similar results would be obtained for other rare-earth 5:4 alloys.

Acknowledgments

This work was performed at Ames Laboratory under contract no.DE-AC02-07CH11358 with the US Department of Energy. This research was supported by the Office of Basic Energy Sciences, Materials Science Division of the US DOE. The authors wish to thank D.L.Schlagel for preparing the single crystals used in this study and also P. A. Molian and his students for their help providing lasers for the rapid cooling experiments.

Reference

[1] V. K. Percharsky, K. A. Gschneidner Jr., Phys. Rev. Lett., 78 (1997) 4494.

[2] A. Giguere, M. Foldeaki, B. R. Gopal, R. Chahine, T. K. Bose, A. Frydman, J. A. Barclay, Phys. Rev. Lett., 83 (1999) 2262.

[3] L. Morellon, J. Blasco, P. A. Algarabel, M. R. Ibarral, Phys. Rev. B, 62 (2000) 1022.

[4] E. M. Levin, V. K. Percharsky, K. A. Gschneidner Jr., P. Tomlinson, J. Magn. Magn. Mater., 210 (2000) 181.

[5] J. Szade, G. Skorek, A. Winiarski, J. Cryst. Growth, 205 (1999) 289.

[6] J. S. Meyers, L. S. Chumbley, F. Laabs, A. O. Pecharsky. Scrip. Mater., 47 (2002) 509.

[7] O. Ugurlu, L. S. Chumbley, D. L. Schlagel, T. A. Lograsso, Acta Mater., 53 (2005) 3525.

[8] O. Ugurlu, L. S. Chumbley, D. L. Schlagel, T. A. Lograsso, A. O. Tsokol, Scrip. Mater., 53 (2005) 373.

[9] L. S. Chumbley, O. Ugurlu, R. W. McCallum, K. W. Dennis, Y. Mudryk, K. A. Gschneidner Jr., V. K. Percharsky, Acta Mater., 56 (2008) 527.

[10] O. Ugurlu, L. S. Chumbley, D. L. Schlagel, T. A. Lograsso, A. O. Pecharsky, 134th TMS (Minerals, Metals and Materials Society) Annual Meeting, Light Metals. 2005;1181-1185.

[11] Z. Qian, L. S. Chumbley, S. Misra, G. Miller, V. K. Pecharsky, K. A. Gschneidner Jr., K. Ahn, A. S. Chernyshov, N. K. Singh, Acta Mater., 57 (2009) 3374.

[12] J. D. Moore, K. Morrison, G. K. Perkins, D. L. Schlagel, T. A. Lograsso, K. A. Gschneidner Jr., V. K. Percharsky, L. F. Cohen, Adv. Mater., 21 (2009) 3780.

[13] A. O. Pecharsky, K. A. Gschneidner Jr., V. K. Pecharsky, J. Appl. Phys., 93 (2003) 4722.

[14] O. Ugurlu, L. S. Chumbley, C. R. Fisher, J. Mater. Res., 21 (2006) 2669.

[15] H. Fu, Y. Chen, M. Tu, T. Zhang, Acta Mater., 53 (2005) 2377.

[16] Materials Preparation Center, Ames Laboratory of US DOE, Ames, IA, USA. See: http://www.mpc.ameslab.gov.

[17] D. L. Schlagel, T. A. Lograsso, A. O. Pecharsky, J. A. Sampaio, 134th TMS (Minerals, Metals and Materials Society) Annual Meeting, Light Metals. 2005;1177-1180.

[18] V. N. Eremenko, V. E. Listovnichii, S. P. Luzan, Y. I. Buyanov, P. S. Martsenyuk, J. Alloy. Compd., 219 (1995) 181.

[19] T. B. Massalski, J. L. Murray, L. H. Bennett, H. Baker, Binary Alloy Phase Diagrams, Vol 2. Ohio: American Society for Metals; 1987.

[20] J. C. Ion, Laser Processing of Engineering Materials: principles, procedure and industrial application. Amsterdam ; Boston: Elsevier/Butterworth-Heinemann; 2005.

CHAPTER 5. Characterization of Precipitated Second Phase Plates in a Gd_5Ge_3 Alloy

A paper to be submitted to Acta Materialia

Q. Cao and L. S. Chumbley

Abstract

The bulk microstructure of the compound Gd_5Ge_3 was examined using scanning and transmission electron microscopy and optical microscopy. SEM examination revealed a series of linear features present in the Gd_5Ge_3 matrix. Optical microscopy observation suggested that the linear features are actually thin plates. TEM observation including electron diffraction and energy dispersive spectroscopy revealed the thin plates possess an orthorhombic structure and a stoichiometric composition of Gd_5Ge_4. The orientation relationship between the matrix and the precipitate thin plates was determined to be $[10\bar{1}0]\ (1\bar{2}11)_m \parallel [010]\ (10\bar{2}\,)_p$.

Introduction

The rare-earth intermetallic compound $R_5(Si_xGe_{1-x})_4$ (R = lanthanides) is an important family when considering magnetic properties. The crystal structure of $R_5(Si_xGe_{1-x})_4$ is somewhat complex consisting of “slabs” or atoms bonded together differently in relation to

the Si/Ge ratio and the specific rare-earth element R. There are four main structures: the Sm_5Ge_4-type orthorhombic structure (Pnma) with no inter-slab Si(Ge)-Si(Ge) bonds; the $Gd_5Si_2Ge_2$-type monoclinic structure ($P112_1/a$) with half of the inter-slab bonds connected; the Gd_5Si_4-type orthorhombic structure (Pnma) with all inter-slab Si(Ge)-Si(Ge) bonds connected; and the Zr_5Si_4 tetragonal structure ($P4_12_12$) [1-3]. Due to their extreme magnetic properties, the structures, phase transformations, and thermodynamic properties of various $R_5(Si_xGe_{1-x})_4$ alloys including Ce [4], Sm [5], Gd[6], Ho [7], Er [8] and Yb [9] have been systematically studied by several research groups. Extensive research on the magnetic properties of $R_5(Si_xGe_{1-x})_4$ has resulted in the microstructures of these systems (referred to as "5:4") being closely examined. A number of studies [10-19] have reported the ubiquitous presence of thin plates of $R_5(Si_xGe_{1-x})_3$ (referred to as "5:3") with the matrix of 5:4 compounds. The structure and orientation of these plates has been determined [14-15].

The $R_5(Si_xGe_{1-x})_3$ family of intermetallic compounds, where R = lanthanides, is another family of magnetic materials with rich physical properties. As seen from the existing binary phase diagrams of R-T (R = lanthanides, T = Si, Ge), most of lanthanides possess a 5:3 compound, including Sm [20], Gd [21, 22], Ho [23], Er [24], and Yb [25,26]. In the majority of cases the 5:4 and 5:3 are adjacent line compounds. Compounds in the 5:3 family crystallize in the Mn_5Si_3-type hexagonal $D8_8$ structure [27] with the space group $P6_3/mcm$ [28-30]. The hexagonal symmetry of this particular crystallographic structure makes these materials a good matrix for modifications through chemical means, as the structure is very open and contains long channels into which alloying atoms may reside.

This allows a wide array of compounds to be synthesized that can be expected to exhibit rich physical and chemical properties.

The magnetic structure and properties of the $R_5(Si_xGe_{1-x})_3$ intermetallic compounds were explored soon after the identification of their crystal structure. The rare earth atoms of the 5:3 compounds are situated in two independent atomic positions, 4d and 6g. The atoms in site 4d account for the antiferromagnetic state of the compounds, while the atoms in site 6g account for the ferromagnetic properties [27]. Measurements of magnetization and magnetic susceptibility of a Nd_5Ge_3 single crystal indicated an irreversible magnetic-field-induced antiferromagnetic to ferromagnetic transition takes place along the c-axis below 26K [31]. Similar to the $R_5(Si_xGe_{1-x})_4$ compounds, the magnetic and structural transitions are also coupled for some of the $R_5(Si_xGe_{1-x})_3$ compounds. The coincidence between the Neel temperature and the temperature of the structural transition in Gd_5Ge_3 has been confirmed by Mudryk et al [32], and a large magnetostrictive effect was observed in Gd_5Ge_3 and Nd_5Ge_3 [33].

Although there is an increasing interest in the magnetic structure and properties of the $R_5(Si_xGe_{1-x})_3$ intermetallic compounds [31-37], no microstructure study of this 5:3 family has ever been performed so far. This article presents results concerning characterization of the microstructure of a Gd_5Ge_3 alloy.

Experimental Details

A single crystal of Gd_5Ge_3 was prepared from high purity starting material using a tri-arc crystal pulling method and then oriented to its major crystallographic directions using back-reflection Laue XRD and 2θ scans. The oriented slices were made by cutting the crystal with spark erosion. The two sides of one oriented slice were mechanically polished and viewed and examined using an optical microscope and the analysis software Axiovision. The bulk microstructures of the single crystal were examined using scanning electron microscopy (SEM) and transmission electron microscopy (TEM).

A polycrystalline sample of Gd_5Ge_3 was prepared by arc-melting the high purity elemental components Gd (99.996 wt.%) and Ge (99.999 wt.%) in an argon atmosphere at the 5:3 stoichiometric ratio. The arc-melted button was flipped and re-melted six times to ensure homogeneity. The resultant sample button appeared to be single-phase alloy within the sensitivity of the conventional Cu-Kα X-ray powder diffraction (XRD) equipment used for initial examination.

The surface of the polycrystalline sample was mechanically polished and sequentially both ion-etched and chemically etched with a mixture of 1vol. % of perchloric acid and 99 vol.% of methanol. The morphology of the sample surface was examined and monitored using SEM after each surface treatment process. The alloy was also sectioned and examined using TEM.

All SEM characterizations in this study were carried out using a JEOL 6060LV scanning electron microscope equipped with an X-ray energy dispersive spectrometer (EDS).

Samples for TEM studies were mechanically ground, dimpled and ion-milled to electron transparency. An FEI Tecnai G^2 F20 transmission electron microscope equipped with an X-ray energy dispersive spectrometer (EDS) was used for all bright-field (BF) images, crystal structure and lattice parameters determination, and compositional line scans in this study.

Experimental Results

Optical Microscopy

The observation results of the as-polished single crystalline Gd_5Ge_3 slice using optical microscope are shown in Figure 1, which shows there are numerous linear features present in the sample. Fig.1a was taken from the front surface of the slice while Fig.1b was taken from the corresponding position on the back surface of the slice. The patterns of linear features on both sides of the slice are mirror images of one another, possessing essentially the same angles, distances, and intervals between linear features. From this observation we can deduce that the two patterns are cross-sections of the same set of plate-like features, having a thickness at least equal to the thickness of the slice (~ 275 μm) where the intersections of the plates appear as narrow lines on both surfaces of the sample. The fixed 59° angle that exists between the plates suggests that the plates are oriented in specific directions within the matrix.

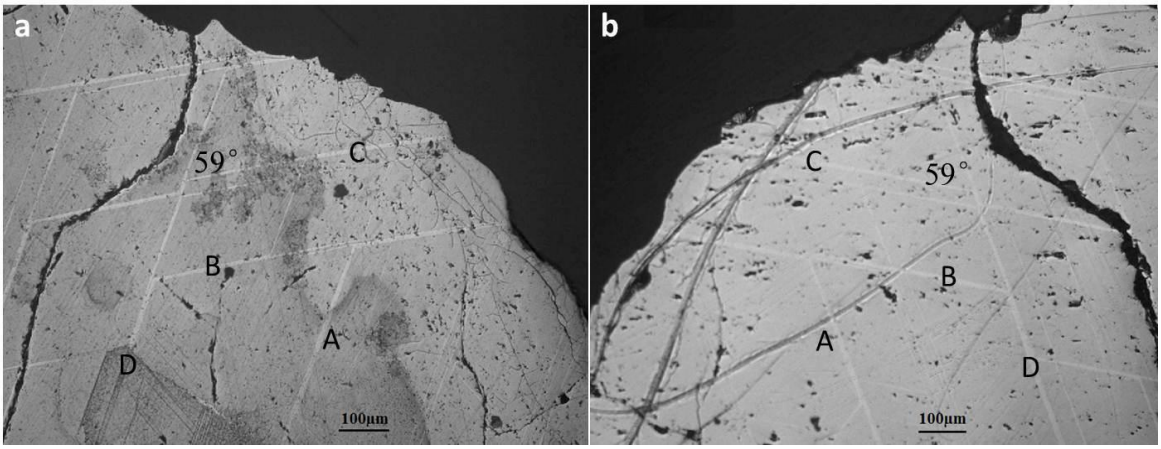

Figure 1. Optical microscope images of the single crystal Gd_5Ge_3 slice taken from a) front surface and b) back surface. The positions of four plates marked as A, B, C, and D appear mirrored in the two images.

Scanning Electron Microscopy

Scanning electron microscopy (SEM) images of the same area in the polycrystalline Gd_5Ge_3 sample in the as-polished, ion-milled and chemically etched states are shown in Fig. 2. It can be seen from the SEM images that contrary to the XRD results, the Gd_5Ge_3 alloy is not actually phase pure. The presence of a second phase, forming as a series of thin plates, is clearly seen in both secondary (SE) and backscattered (BSE) electron images (Figs.2a, 2b). The Z contrast information provided by the BSE image indicates the plates have a lower percentage of the heavy component Gd than the matrix since they appear as dark lines relative to the grey Gd_5Ge_3 matrix.

The morphology of the second phase shown in Figs. 2a and b was monitored after ion-milling (Fig. 2c) and chemical etching (Fig. 2d). The bombardment of argon ions during the ion-milling process results in a grooving of the polished surface in the positions where the

plates was originally located. After chemical etching, the same pattern as shown in Figs. 2a, 2b and 2c re-appears (Fig. 2d), with some additional plates now being evident.

Five thin plates lying in five different directions and sequentially numbered as "P_1", "P_2", "P_3", "P_4", and "P_5" in Fig. 2d were chosen as representatives for determining the relative composition of the secondary phase using EDS. The results obtained in comparison to each other and the matrix are summarized in Table 1. Note that the size of the thin plates are below 1 micron, so beam spreading will cause the actual composition determination to be somewhat inaccurate. The results revealed the average composition of the plates to be approximately 57.7 at.% Gd, 42.3 at.% Ge vs. 64.1 at.% Gd, 35.9 at.% Ge for the matrix. Thus, the second phase composition as measured by EDS using SEM tends toward that of the intermetallic 5:4 phase, which ideally is 55.6 at.% Gd and 44.4 at.% Ge. The width of a large number of plates was measured on the chemically etched sample (Fig. 2d). The average was found to be 320nm with values ranging from 95 nm to 460 nm.

Scanning electron microscopy (SEM) images of the single crystal Gd_5Ge_3 sample in the as-polished state are shown in Fig. 3. Fewer variants of plates are seen in this image as compared to the polycrystalline sample and the size of the plates is somewhat larger, ranging from 1μm to 12μm with an average of 5μm. The compositions of the matrix and five plates, numbered as "P_6", "P_7", "P_8", "P_9", and "P_{10}" in Fig. 3b, were measured using EDS, and are also summarized in Table 1. The EDS results show the average composition of the plates to be around 54.6 at.% Gd and 45.4 at.% Ge, which is consistent with the theoretical values of the Gd_5Ge_4 phase. Due to the much larger size of the plates compared to those existed in the polycrystalline Gd_5Ge_3 sample, it can be expected that beam

spreading effects are less detrimental to accurate quantitative determination and the plates are in fact the 5:4 intermetallic.

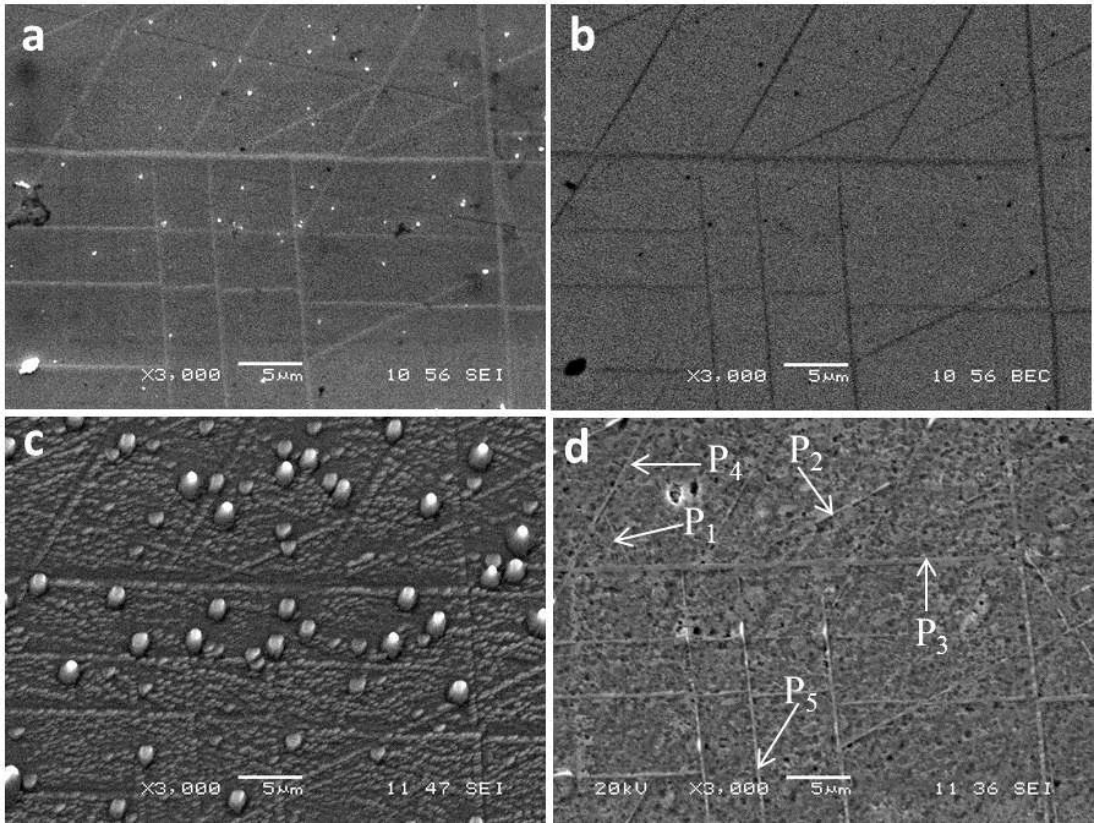

Figure 2. SEM images of the same area in the polycrystalline Gd_5Ge_3 sample in the as-polished state using a) secondary electron and b) backscattered electron; c) after ion-milling; d) after chemically etching.

Table 1: Compositions of ten linear features and matrix obtained from polycrystalline and single crystalline Gd_5Ge_3 samples.

Polycrystal	P_1	P_2	P_3	P_4	P_5	Matrix
Gd at.%	57.9	58.1	57.3	57.8	57.6	64.1
Ge at.%	42.1	41.9	42.7	42.2	42.4	35.9
Single crystal	P_6	P_7	P_8	P_9	P_{10}	Matrix
Gd at.%	54.8	54.6	54.6	54.3	54.6	61.6
Ge at.%	45.2	45.4	45.4	45.7	45.4	38.4

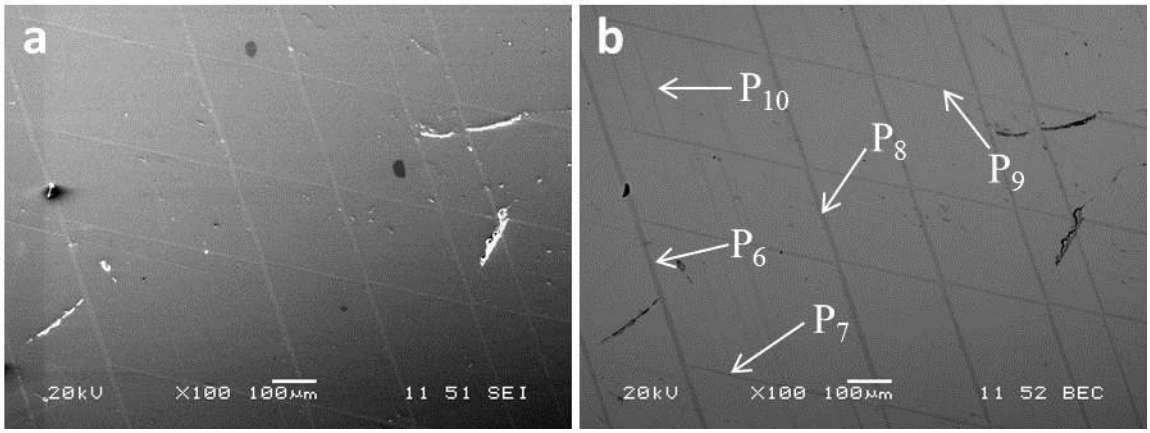

Figure 3. SEM images of the same area in the single crystal Gd_5Ge_3 sample in the as-polished state using a) secondary electron contrast and b) backscattered electron contrast.

Transmission Electron Microscopy

TEM studies of the material confirmed that the thin plates seen optically and in SEM observations are a second phase. A bright field image of the second phase in the polycrystalline Gd_5Ge_3 alloy is shown in Fig.4a. The large amount of bend contours present in the phase suggests a high degree of strain exists within it. The width of the phase is measured as ~ 300 nm. An EDS line scan across the phase (Fig. 4b) revealed that the average composition is about 60.3 at.% Gd, 39.7 at.% Ge with the matrix being about 67.6 at.% Gd, 32.4 at.% Ge. Thus, the composition agrees with the earlier SEM results which indicated that the plates are depleted in the rare earth with respect to the matrix and possess a composition tending toward the 5:4 intermetallic.

Selected area diffraction (SAD) patterns of the plates were also obtained and one example is shown as an inset in Fig. 4. The patterns can be indexed as being orthorhombic and

correlate well to those expected from the intermetallic Gd_5Ge_4. The obtained lattice parameters are summarized in Table 2.

Table 2: Lattice Parameter comparison between 5:4 plates in Gd_5Ge_3 and 5:4 matrix in Gd_5Ge_4.

	a(Å)	b(Å)	c(Å)
Gd_5Ge_4 matrix	7.52	15.23	7.76
Plates in Gd_5Ge_3	7.58	15.18	7.72

In order to determine the crystallographic orientation relationship between the 5:4 plates and the matrix, several different zone axes directions were taken where the selective area aperture was positioned to overlap both matrix and plates. Three indexed diffraction patterns are shown in Fig. 5, with the 5:3 matrix lattice being outlined by solid lines while dotted lines are used for the 5:4 plates. From these SAD patterns, the stereographic projections describing the crystallographic orientation relationship between the matrix and

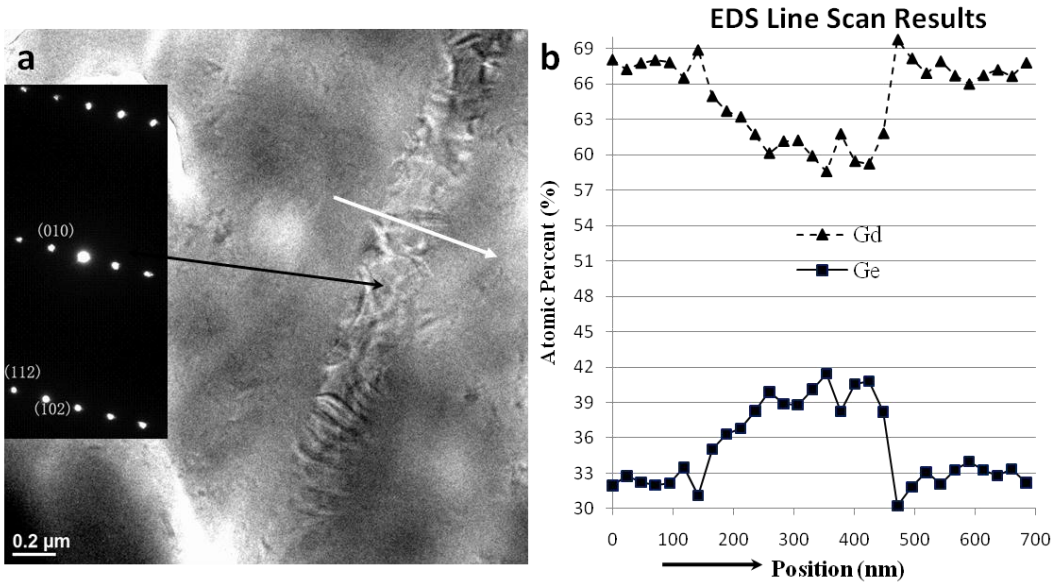

Figure 4. a) Bright Field (BF) image of one 5:4 plate in polycrystalline Gd_5Ge_3 alloy, b) EDS line scan across the thin plate in (a) along the line indicated by the white arrow.

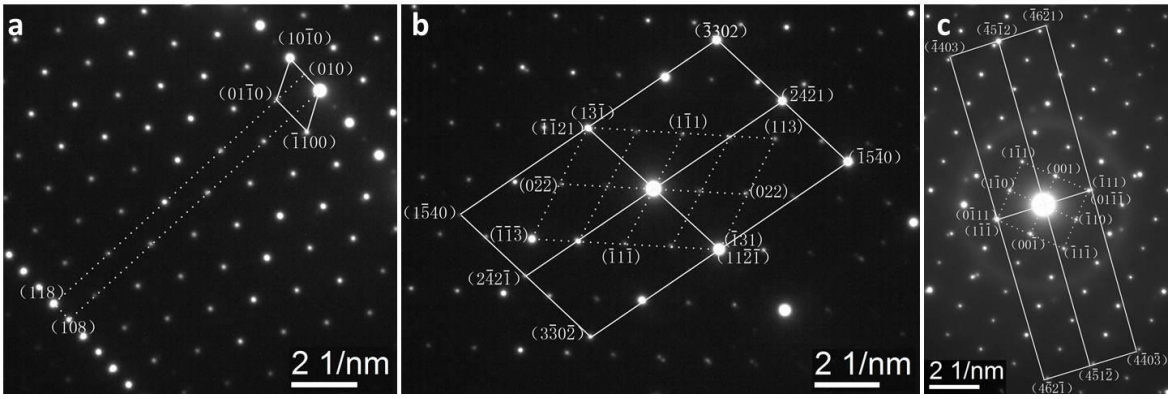

Figure 5. Mixed diffraction patterns of 5:4 plates and 5:3 matrix in the Gd_5Ge_3 single crystal. a) $B_1 = [0001]_m \parallel [80\bar{1}]_p$; b) $B_2 = [3\bar{1}\bar{2}6]_m \approx\parallel [21\bar{1}]_p$; c) $B_3 = [10\ 1\ \overline{11}\ 12] \approx\parallel [110]_p$.

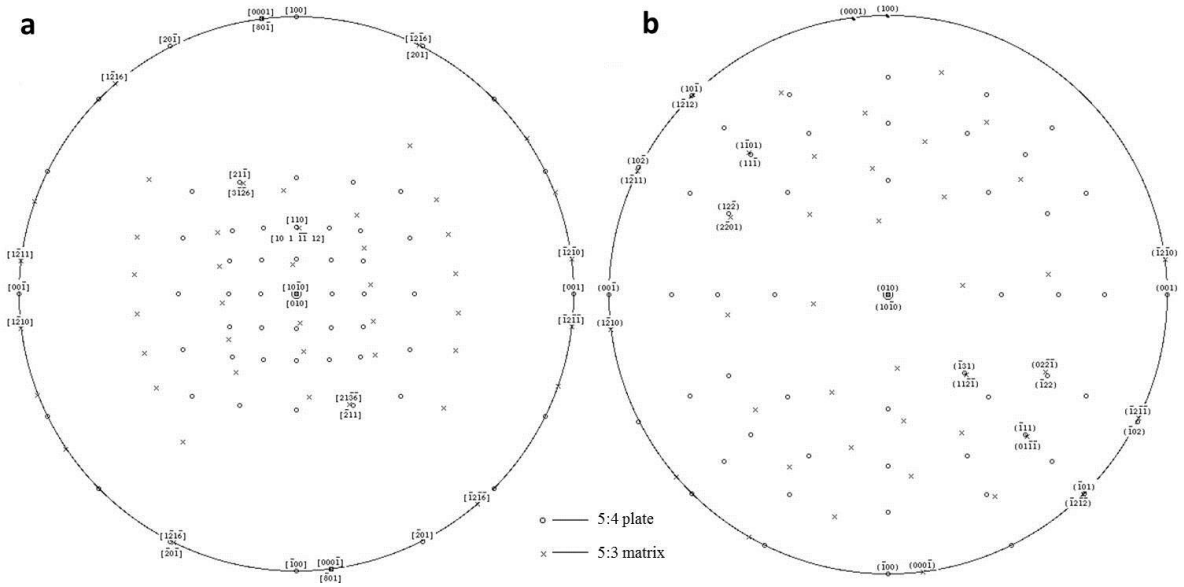

Figure 6. Stereographic projections for a) directions and b) planes plotted according to diffraction patterns shown in Fig. 5.

the plates could be developed and the results are shown in Fig. 6 (Fig. 6a, directions; Fig. 6b, planes). According to Fig.5a, the diffracting conditions are such that the electron beam is parallel to $[0001]_m \parallel [80\bar{1}]_p$, while Fig. 5b shows the $[3\bar{1}\bar{2}6]$ zone axis of the matrix is approximately parallel to the $[21\bar{1}]$ zone axis of the 5:4 plates. The actual angle between

these two zone axes is approximately one degree which can be obtained from the stereographic projection in Fig.6a. Figure 5c reveals that the zone axis of the matrix with high index [10 1 $\overline{11}$ 12] is approximately parallel to the low index zone axis [110] of the 5:4 phase. Figure 6 shows the angle between them is less than one degree.

Discussion

The morphology of the linear features observed in Gd_5Ge_3 (Figs. 1, 2 and 3) shows fairly conclusively that the features in the 5:3 matrix are in fact thin plates and are comparable to the linear features first noted as being present in 5:4 compounds [10] and subsequently identified as thin plates of 5:3 [11-18]. Using SEM, the 5:3 plates appear in the 5:4 compounds as white lines due to their higher rare earth content (Refer to Fig. 2 of Ref. [12], Fig. 2 of Ref. [14], Fig. 1 of Ref. [15], Figs. 6 and 7 of Ref. [16], and Fig. 2 of Ref. [18]). In the present study of Gd_5Ge_3 the visible lines appear dark in the grey matrix when being imaged with backscattered electrons (Fig. 2b and Fig. 3b), indicating a reduced rare earth content. Thus, BSE imaging alone would suggest the plates in the Gd_5Ge_3 compound are in fact the 5:4 compound. This tentative identification is supported by the composition results obtained from quantitative EDS in the SEM. While the measured compositions are not stoichiometrically exact, this is expected since the incident beam in the SEM is slightly larger than the thickness of the 5:4 phase in the polycrystalline sample. Given the size of the beam interaction volume at the voltages used the actual measurement consists of sampling

both the linear features and the surrounding 5:3 matrix. Consequently, the experimental results of the Gd at.% of the linear features is higher than the stoichiometric value. Comparing the plates in Fig.2 with those in Fig. 3, the size of the precipitated plates in the single crystalline Gd_5Ge_3 is much larger than those present in the polycrystalline Gd_5Ge_3, presumably due to the differences in cooling between the two sample preparation techniques as discussed in [38]. The larger size of the 5:4 plates in the single crystal (see in Table 1) results in a more accurate composition determination and are in a good agreement with the theoretical values.

The identification of the plates in the polycrystalline Gd_5Ge_3 as 5:4 phases is strengthened by the TEM observations. The EDS line scan in the TEM study revealed that the Gd at.% of the plates in Gd_5Ge_3 sample is ~ 60.3% which is in excellent agreement with measurements from bulk Gd_5Ge_4 samples [17]. Similarly, the Gd at.% of the matrix in Gd_5Ge_3 sample, measured as ~ 67.6%, is consistent with the values obtained from 5:3 plates in Gd_5Ge_4 samples [17]. Although the results are not exactly equivalent to the expected stoichiometric literature values, reasons for the discrepancies have been identified and discussed previously [11, 13, 17].

More conclusive than compositional measurements are the electron diffraction results where SAD analysis (Table 2) revealed the second phase has an orthorhombic structure and possesses lattice parameters close to those of Gd_5Ge_4. Based on such overwhelming experimental evidence from optical, scanning and transmission microscopy, there is no doubt that the linear features observed in the Gd_5Ge_3 alloy are 5:4 plates.

While ion-etching seems to enhance imaging of 5:3 plates in a 5:4 matrix [14, 18, 19] just the opposite appears true for 5:4 plates in a 5:3 matrix. This is logical since enhancement of 5:3 plates in a 5:4 matrix occurs due to the softer material (i.e. the 5:4 matrix) being milled away at a high rate than the plates. The harder 5:3 plates become exposed due to the milling and protrude above the 5:4 matrix, standing on the apexes of ridges and appearing in the form of thin white lines. This disparity in milling rates works to obscure the 5:4 plates in the 5:3 compounds where in this instance a thin, shallow channel marking the trace where the plate intersects the surface is all that results due to the milling process.

Chemically etching the surface of the polycrystalline Gd_5Ge_3 sample after ion-milling was much more effective at exposing the presence of the 5:4 plates. Given the reactivity of rare earths, it is possible that the higher atomic percentage of Gd in the 5:3 phase results in the 5:3 matrix being etched faster than the 5:4 plates, making the 5:4 plates easily seen once again. This allows plates such as the one marked as "P_1" in Fig. 2d to be seen after etching where it was not visible in the as-polished state. Another possible explanation for this is that the distribution of plates in the bulk of the sample as a function of depth results in certain plates appearing more prominent as material is etched away.

Finally, in 5:4 compounds a single set of 5:3 plates with variants in two equivalent crystallographic directions is reported in [10-14, 16, 18] while parallel plates laying along only one direction were reported in [17, 18]. Reference [14] hypothesized that a structural relationship must exist between the parent matrix and the plates in order for such widespread growth on specific directions to occur in these 5:4 intermetallic compounds, and this assumed orientation relationship was subsequently determined in [15]. Given this

data, a specific orientation relationship should also exist for the observed 5:4 plates in 5:3 matrix of this study.

From the combined stereographic projections for 5:4 plates in a 5:3 matrix (Fig. 6), the orientation relationship $[10\bar{1}0]\,(1\bar{2}11)_m \parallel [010]\,(10\bar{2}\,)_p$ is deduced, which is exactly the same orientation relationship between the 5:3 plates and 5:4 matrix reported in previous studies [15, 38]. Therefore, it seems that the crystalgraphic orientation relationship between the 5:3 and 5:4 phase is fixed, that is $[10\bar{1}0]\,(1\bar{2}11)_{5:3} \parallel [010]\,(10\bar{2}\,)_{5:4}$, no matter which phase precipitates as thin plates from the other phase.

The difference between 5:4 growing in 5:3 as opposed to 5:3 growing in 5:4 relates to the number of variants that should be expected to appear. When the parent phase is orthorhombic or monoclinic, the determined crystallographic relationship says growth of the hexagonal 5:3 phase occurs along an invariant line, which can be associated with a two-fold axis [15]. Thus, growth is equally favorable in two different direction, resulting in the appearance of two distinct variants [15]. However, if the parent matrix is hexagonal and the precipitate is orthorhombic, the two invariant line growth directions now can occur on any of three distinct $<10\bar{1}0>$ - type directions that exists in the six-fold hexagonal lattice. Thus, instead of two variants being seen, six crystallographically equivalent variants are possible. This results in the large number of varants seen in a single grain of the polycrystalline sample imaged in Fig. 2d.

It is interesting that a unique relationship seems to exist between 5:3 and 5:4 compounds within the $R_5(Si_xGe_{1-x})_4$ / $R_5(Si_xGe_{1-x})_3$ families of compounds, with neither compound

existing entirely by itself. As noted in [16] the material seems to go to extraordinary lengths to possess both structures simultaneously, even when concerted attempts are made to avoid precipitate formation. Further study is needed to determine exactly what factors are involved in producing this unique relationship.

Conclusions

Studies employing optical, scanning and transmission electron microscopies have shown that arc-melted Gd_5Ge_3 is not single phase as indicated by XRD results but contains a separate second phase that exists throughout the bulk of the material in the form of thin plates. Using a combination of electron diffraction and EDS the plates are identified as having an orthorhombic structure and a composition approaching that of stoichiometric 5:4. A crystallographic orientation relationship between the 5:4 plates and the 5:3 matrix is elucidated to be $[10\bar{1}0]\,(1\bar{2}11)_m \parallel [010]\,(10\bar{2}\,)_p$, which is the same relationship that results when second phase 5:3 plates precipitate from a 5:4 matrix. The difference in this case is that growth of the precipitate in a hexagonal matrix results in six variants of plates being observed, rather than the two variants seen when growth occurs with the orthorhombic phase being the matrix.

Acknowledgments

This work was performed at Ames Laboratory under contract no. DE-AC02-07CH11358

with the US Department of Energy. This research was supported by the Office of Basic Energy Sciences, Materials Science Division of the US DOE. The authors wish to thank Yaroslav Mudryk and D. L. Schlagel for preparing the arc-melted alloys and the single crystals used in this study and are always grateful to V. Pecharsky and K. Gschneidner for their assistance and advice.

References

[1] V. K. Pecharsky, K. A. Gschneidner Jr., 13 (2001) 683.
[2] K. A. Gschneidner Jr., V. K. Pecharsky, J. Alloy. Compd., 303-304 (2000) 214.
[3] V. K. Pecharsky, K. A. Gschneidner, Jr., Pure Appl. Chem., 79(2007) 1383.
[4] H. Zhang, Ya. Mudryk, Q. Cao et al., J. Appl. Phys., 107 (2010) 013909.
[5] K. Ahn, V. K. Pecharsky et al., Phys. Rev. B, 76 (2007) 014415.
[6] A.O. Pecharsky, K. A. Gschneidner, Jr. et al., J. Alloy. Compd., 338 (2002)126-135.
[7] A. M. Pereira, J. B. Sousa et al., Phys. Rev. B, 77 (2008) 134404.
[8] A.O. Pecharsky, K. A. Gschneidner, Jr. et al., Phys. Rev. B, 70 (2004) 144419.
[9] K.Ahn, A. O. Tsokol et al., Phys. Rev. B, 72 (2005) 054404.
[10] J. Szade J, G. Skorek et al., J .Cryst. Growth, 205 (1999) 289-293.
[11] J. S Meyers, L. S. Chumbley et al., Scrip. Mater., 47(2002) 509-514.
[12] O.Ugurlu, L. S. Chumbley et al., 134th TMS (Minerals, Metals and Materials Society) Annual Meeting. Light Metals. (2005) 1181.
[13] O. Ugurlu, L. S. Chumbley et al., Scrip Mater., 53 (2005) 373.
[14] O. Ugurlu, L. S. Chumbley et al., Acta Mater., 53(2005) 3525.
[15] O. Ugurlu, L. S. Chumbley et al., Acta Mater., 54 (2006) 1211.
[16] O. Ugurlu, L. S. Chumbley et al., J. Mater. Res., 21(2006) 2669.
[17] Q. Cao, L. S. Chumbley, Z. Qian, Intermetallics, 18 (2010) 1021.
[18] Z. Qian, L. S. Chumbley et al., Acta Mater., 57 (2009) 3374.

[19] L. S. Chumbley, O. Ugurlu et al., Acta Mater., 56 (2008) 527.

[20] A. B. Gokhale and G. J. Abbaschian, Bull. Alloy Phase Diagrams, 9(5) (1988) 582.

[21] H. Okamoto, J. Phase Equilib. Diffus., 30 (2) (2009) 213.

[22] H. Okamoto, J. Phase Equilib. Diffus., 33 (2) (2012) 163.

[23] H. Okamoto, J. Phase Equilib., 17(4) (1996) 370.

[24] H. Okamoto, J. Phase Equilib., 18 (4) (1997) 403.

[25]A. Palenzonaa, P. Manfrinettia , S. Bruttib, G. Balduccib, J. Alloy. Compd., 348 (2003) 100. [26] M. Pania , A. Palenzona, J. Alloy. Compd., 360 (2003) 151.

[27] K. S. V. L. Narasimhan, H. Steinfink, and E. V. Ganapathy, J. Appl. Phys., 40 (1969) 51.

[28] E. Parthe, Acta Crystallogr., 13 (1960) 868.

[29] J. Arbuckle, E. Parthe, Acta Crystallogr., 15 (1962) 1205.

[30] N. C. Baezinger, J. J. Hegenbarth, Acta Crystallogr., 17 (1964) 620.

[31] T. Tsutaoka, A. Tanaka et al., Physica B, 405 (2010) 180.

[32] Y. Mudryk, D. Paudyal, V. K. Pecharsky, and K. A. Gschneidner Jr., Phys. Rev. B, 85 (2012) 014116.

[33] M. Doerr, M. Rotter, A. Devishvili et al., J. Phys.: Conf. Ser., 150 (2009) 042025.

[34] I. P. Semitelou, J. K. Yakinthos et al., J. Phys. Chem. Solids, 56 (1995) 891.

[35] F. Canepa, S. Cirafici et al., J.Alloy. Compd., L1-L4 (2002) 335.

[36]T. Tsutaoka, Y. Nishiume et al., J. Magn. Magn. Mater., e421-e422 (2004) 272.

[37] Y. Narumi, Y. Tanaka et al., J. Phys. Soc. Jpn., 77 (2008) 053711.

[38] Q. Cao, L. S. Chumbley. Mater. Charact., 62 (2011) 737.

CHAPTER 6. Concluding Remarks

Conclusions

This thesis has investigated the microstructure of several $R_5(Si_xGe_{1-x})_4$ and $R_5(Si_xGe_{1-x})_3$ alloys, where R = rare earth, in order to better understand the phases present, how those phases develop and grow, and the factors that determine phase formation. The following conclusions can be drawn:

1. A series of x-ray powder diffraction experiments using conventional Cu $K\alpha_1$ radiation and synchrotron source performed on Er_5Si_4 alloy powder revealed that the arc-melted Er_5Si_4 alloy was not pure Gd_5Si_4-type orthorhombic phase, but contained several impurity phases. These were identified as monoclinic Er_5Si_4 (space group: $P112_1/a$), orthorhombic ErSi (space group: Cmcm), and hexagonal Er_5Si_3 (space group: $P6_3/mcm$). Calculated phase concentrations using the Rietveld method showed that the amount of monoclinic 5:4 increased with increasing mechanical grinding time of the powder sample, while the concentration of orthorhombic 5:4 decreased. Other impurity amounts stayed relatively constant. This indicates a stress-induced phase transformation occurs during mechanical grinding. It is deduced that shear stress caused by the mechanical grinding break the interslab Si-Si bonds and drive the original orthorhombic structure to the monoclinic structure. This result would suggest that mechanical forces also have an important effect on the crystal structure of the rare-earth intermetallic compounds $R_5(Si_xGe_{1-x})_4$ just as temperature, applied magnetic field, pressure and chemical composition. The low

temperature annealing experiments designed to test the stability of the stress-induced phase transformation showed this crystal structure transition is reversible. Due to the release of the residual shear stress caused by the grinding, the monoclinic 5:4 phase will transfer back to the orthorhombic 5:4 phase upon annealing at low temperature (500˚C).

2. A comprehensive electron microscopy study of the lutetium doped erbium silicide $(Er_{0.9}Lu_{0.1})_5Si_4$ (O(I) structure) showed that although its unit cell volume slightly shrinks when compared to that of the un-doped compound Er_5Si_4 due to the Lu substitution (see Appendix), a similar bulk microstructure to that of the Er_5Si_4 is still observed, that is, the matrix of the $(Er_{0.9}Lu_{0.1})_5Si_4$ alloy still possesses linear features. The results of the EDS in TEM indicated that these linear features are actually lutetium doped 5:3 plates, which means that lutetium substitution takes place not only in the 5:4 matrix but also in the precipitate 5:3 plates. The crystal structure of the thin plates is hexagonal, the orientation relationship between the plates and the matrix is determined as being $[010]_m \parallel [10\bar{1}0]_p$, and the SAD patterns demostrated that the diffraction patterns of the plates are rotated ~ 7° relative to the matrix's pattern. All these observations are all consistent with what has been reported for the Gd_5Ge_4 (O(II) structure) and $Gd_5Si_2Ge_2$ (M strucutre) compounds [1]. Thus, the assumption that all the linear features present in any $R_5(Si_xGe_{1-x})_4$ compound are hexagonal 5:3 thin plates possessing the same orientation relationship with respect to the 5:4 matrix has been strongly supported.

3. The thermal stability of $R_5(Si_xGe_{1-x})_3$ plates was studied through electron microscopy examination of an as-cast and annealed Gd_5Ge_4 single crystal. The 5:3 thin plates became unstable and gradually vanished after the sample was annealed at very high temperatures

(1200˚C) for an extended period of time (> 24hrs). No new phase formed in the position where the disappeared plates ever existed, indicating a sluggish dissolution of 5:3 plates into the 5:4 matrix. Although the phase transition from 5:3 to 5:4 phase occurs fairly slowly, being incomplete even after 24 hours of annealing, a thorough disapperance of the 5:3 plates can still be reasonably expected by increasing the annealing temperature and extending the annealing time. The effect of rapid cooling processing was studied by comparing the morphology of a $Ho_5(Si_{0.8}Ge_{0.2})_4$ sample before and after the surface underwent laser surface melting. The 5:3 plates originally located in the fusion zone before melting vanished, although they were still present on either side of the melt pool, which indicated that the melting and resulting rapid cooling of the melt pool suppressed the precipitation of the 5:3 thin plates. In addition, 5:3 thin plates observed in polycrystalline $R_5(Si_xGe_{1-x})_4$ samples produced using an arc-melting method are always much thinner than those that exist in single crystal $R_5(Si_xGe_{1-x})_4$ samples prepared using tri-arc pulling method [2]. This is believed due to the difference in cooling rate between these two crystal preparation techniques. These observations, when considered as a whole, tend to support the the validity of the displacive-diffusional formation mechanism of the 5:3 thin plates first suggested by Ogurlu et al. [1] where the diffusion process is a short-range shuffling of atoms that occurs at high temperatures. The faster the cooling rate of the melt, the shorter the time available for the diffusion required in order for the 5:3 plates to form and the thinner the resultant 5:3 plates. If one ranks the above three techniques in order of cooling rate, the cooling rate of the laser surface melting is extremely fast, effectively eliminating the time necessary for diffusion to occur and suppressing the transformation. The cooling rate of the tri-arc pulling method is the slowest, and in this case the precipitate 5:3 plates are

the thickest, on the order of hundreds of nanometers. The cooling rate of the arc-melting method is between these two extremes with the thickness of the formed 5:3 thin plates ranging from several to tens of nanometers.

4. Studies of polycrystalline and monocrystalline Gd_5Ge_3 samples employing optical, scanning and transmission electron microscopies have shown that this material contains a separate second phase that exists throughout the bulk of the material in the form of thin plates. This second phase appears analogous to the thin plates seen in the 5:4 rare earth compound families, being extremely thin but of large extent, and a combination of electron diffraction and EDS techniques identified the plates as being an orthorhombic Gd_5Ge_4 compound. The crystallographic orientation relationship between the 5:4 plates and the 5:3 matrix was determined to be $[10\bar{1}0]\,(1\bar{2}11)_m \parallel [010]\,(10\bar{2}\,)_p$, which is the same as exists when second phase 5:3 plates precipitate from a 5:4 matrix. These results point to a unique relationship that exists between 5:4 and 5:3 compounds where both can lower their free energy of formation by existing together, and one phase always precipitating in the form of platelets within the other.

Recommendation for Future Work

1. Through the study of the effect of mechanical grinding on the phase transition in Er_5Si_4 alloy, it was found that the shear stress induced during the mechanical grinding led to a crystal structure transition from orthorhombic to monoclinic in Er_5Si_4. It would be interesting to see if this transformation could be controlled in some predictable manner.

Given the similarity in structures of all the $R_5(Si_xGe_{1-x})_4$ family of alloys, it is possible that deformation induced transitions occur in all of these materials. Further work is necessary to confirm this.

2. The experiments on thermal stability of the 5:3 plates in the 5:4 matrix indicate the plates are thermal unstable at above 1200˚C, and the laser surface melting related experiment shows that rapid cooling will suppress the precipitation of 5:3 plates. These results suggest that the thin plates form at a very high temperature and are cooling rate dependent. However, the specific transformation temperature at which the plates form is still unknown? Therefore, experiments to determine the temperature at which the formation of 5:3 plates occurs upon cooling could be done in the future. Since high resolution powder diffraction (HRPD) using the synchrotron source at Argonne National Lab can detect the 5:3 plates at a low volume concentration (see Appendix), it may be possible to monitor phase formation in-situ during cooling from the melt. A controlled furnace which can heat to a very high temperature (>1200˚C), such as a laser-heated aerodynamic levitation furnace [3], coupled with an in-situ high resolution synchrotron radiation source would be necessary for this study. These experiments could allow the mechanism of formation to be determined, leading to better structure control.

3. The relationship that exists between Gd_5Ge_4 and Gd_5Ge_3 compounds is unusual and exciting given the widespread appearance of plates of one phase within the other. A natural question that arises is, is this type of microstructural feature prevalent in other $R_5(Si_xGe_{1-x})_3$ compounds? What role do the thin plates serve as in the process of the magnetic ordering of the 5:3 matrix? Why do 5:3 and 5:4 compounds co-exist so pervasively? There must be

some fundamental scientific principle that explains why these observed microstructures are so prevalent that has yet to be determined. Studies aimed to answer this question involving computational methods coupled with scientific experiments would be of considerable interest.

3. Studies of the microstructure of $R_5(Si_xGe_{1-x})_4$ system reveal that besides the 5:3 linear features, there are two more different types of features existing in the matrix of these 5:4 compounds, referred to as "microscopic twins" (microtwins), and "macroscopic twins" (macrotwins). These two features were first observed by Meyers [4] (see Figure 1), and later seen by other researchers [5-7]. A relatively clear understanding of the nature and crystallography of the microtwins has been provided by Meyer [4,8], but the effect of this feature on the magnetic properties of the 5:4 compounds, as what has been done for the 5:3 plates [9], has never been reported. In addition, little or no work on the macrotwins has yet been conducted. Systematic studies of these two types of microstructural features remain to be done.

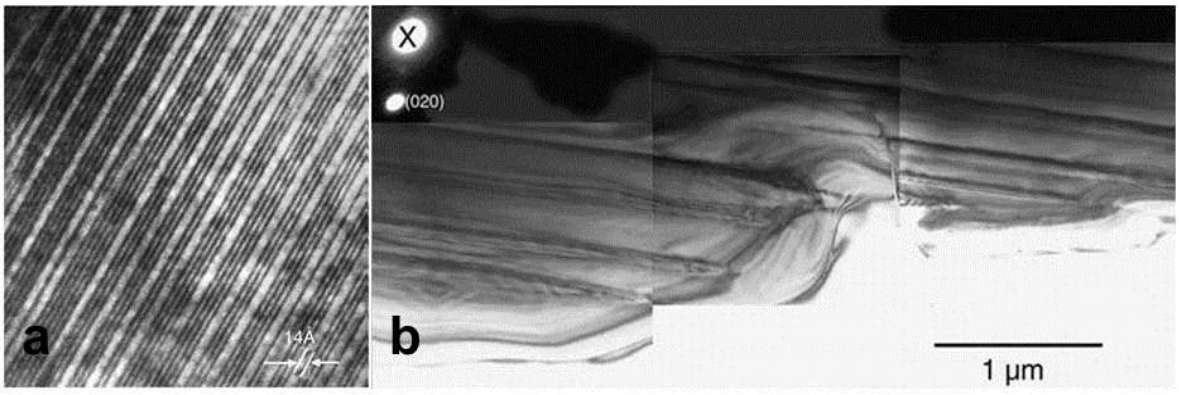

Figure 1. (a) HRTEM image of "microtwins", (b) BF image of "macrotwins in $Gd_5Si_2Ge_2$. (Ref. [2])

References

[1] O. Ugurlu, L. S. Chumbbley, D. L. Schlagel, T. A. Lograsso, Acta Mater., 54 (2006) 1211.

[2] D. L. Schlagel, T. A. Lograsso, A. O. Pecharsky, J.A. Sampaio, 134th TMS (Minerals, Metals and Materials Society) Annual Meeting, Light Metals. 2005; 1177-1180.

[3] J. J. Wall, R. Weber, J. Kim, P. K. Liaw, H. Choo, Mater. Sci. Eng. A, 445-446 (2007) 219.

[4] J. S. Meyers, L. S. Chumbley, F. Laabs, A. O. Pecharsky, Acta Mater., 51(1) (2003) 61.

[5] H. Fu, Y. Chen, T. Zhang, M. Tu, J Rare Earths, 23(4)(2005) 409.

[6] O. Ugurlu, L. S. Chumbley, C. R. Fisher, J. Mater. Res., 21(2006)2669-2674.

[7] Z. W. Du, A. S. Liu, B. L. Shao, Z. Y. Zhang et al., Mater. Charact., 59(2008) 1241.

[8] J. S. Meyers, Scott Chumbley, Wonyoung Choe, and Gordon J. Miller, Phys. Rev. B, 66 (2002) 012106.

[9] J. D. Moore, K. Morrison, G. K. Perkins, D. L. Schlagel, T. A. Lograsso, K. A. Gschneidner Jr., V. K. Pecharsky, L. F. Cohen, Adv. Mater., 21 (2009) 3780.

APPENDIX. Phase Identification in Lutetium Doped Er5Si4

A paper submitted to Materials Characterization

Q. Cao, L. S. Chumbley, Y. Mudryk, M. Zou, N. K. Singh, V. K. Pecharsky,

and K. A. Gschneidner Jr

Abstract

Phase identification in lutetium doped erbium silicide $(Er_{0.9}Lu_{0.1})_5Si_4$ (i.e 5:4) has been carried out using X-ray powder diffraction techniques employing both conventional laboratory Cu Kα radiation and a synchrotron source. Analysis of the results shows that the use of the synchrotron source allows detection of the hexagonal 5:3 phase, which is always seen and reported as thin elongated platelets in electron microscopic studies but typically goes undetected when using conventional X-ray powder diffraction methods due to the low concentration of the 5:3 impurity. In addition to the 5:3 phase, the $(Er_{0.9}Lu_{0.1})_5Si_4$ sample studied contains two other impurity phases besides the orthorhombic 5:4 matrix, namely, the monoclinic 5:4 phase, and the orthorhombic 1:1 phase. The results of these experiments show the difficulty of detecting the 5:3 impurity using conventional powder diffraction techniques.

Introduction

The magnetic properties, crystal structures, and microstructures of the rare-earth based intermetallic compounds $R_5(Si_xGe_{1-x})_4$ (5:4 hereafter), where R is a lanthanide metal, have attracted intense attention and been studied extensively over the last 15 years [1, 2] due to an unusual combination of giant magnetocaloric [3-5], colossal magnetostrictive [6,7] and giant magnetoresistive [8-10] properties in this family of materials. These 5:4 compounds all exhibit a strong coupling of magnetic and crystallographic sublattices [11, 12] except Er_5Si_4 where the structural transition and the magnetic ordering are extremely decoupled by nearly 190K [13,14]. This makes Er_5Si_4 a unique member of the 5:4 compounds and worthy of further investigation.

The crystallographic and magnetic structures of 5:4 compounds are controlled by the number of covalent-like Si/Ge-Si/Ge interslab bonds, which can be manipulated by temperature [11, 15], magnetic field [16, 17] and pressure[18 - 21]. Pressure application can include externally applied pressure (like hydrostatic pressure) and / or internal chemical pressure caused either by replacing the rare earth atoms of larger atomic radii with the rare earths of smaller atomic radii [22] or by replacing Ge with Si [18, 23]. The application of hydrostatic pressure on the Er_5Si_4 causes a rapid decrease in the temperature associated with the structural transition from the orthorhombic Gd_5Si_4-type to the monoclinic $Gd_5Si_2Ge_2$-type at a rate of dT_t/dP = -30 K/kbar [21]. However, the effect of chemical pressure on the structural transition has not been investigated for Er_5Si_4. Thus, lutetium doped erbium silicide $(Er_{0.9}Lu_{0.1})_5Si_4$ was chosen to explore this effect. Investigations on the structural transition and magnetic properties of this complex 5:4 compounds are currently underway

and will be reported when completed. Some initial results on the microstructure of the $(Er_{0.9}Lu_{0.1})_5Si_4$ have been published [24]. The electron microscope studies of $(Er_{0.9}Lu_{0.1})_5Si_4$ [24] revealed the presence of thin plates, a microstructural feature that appears in every $R_5(Si_xGe_{1-x})_4$ alloy studied to date [25-32] with composition corresponding to an $R_5(Si_xGe_{1-x})_3$ stoichiometry (referred to as the 5:3 phase). EDS results in the TEM [24] indicated that the 5:3 plates contained lutetium. The partial replacement of Er by Lu didn't alter the orientation relationship between the 5:3 plates and the 5:4 matrix, which is still the same as is seen in other reported $R_5(Si_xGe_{1-x})_4$ alloys [33].

The $R_5(Si_xGe_{1-x})_3$ compounds crystallize in the hexagonal Mn_5Si_3-type structure with space group $P6_3/mcm$ [34-36]. These compounds have a ferromagnetic (FM) ordering for rare earth atoms situated in the crystallographic 6g sites, and an antiferromagnetic (AFM) ordering in the 4d sites [37]. It is logic that the total ferromagnetism of a ferromagnetic phase will attenuate when an antiferromagnetic or nonmagnetic phase or a phase with lower ferromagnetism precipitates as a second phase in it. Only a phase with higher ferromagnetism could enhance the total ferromagnetism in a certain temperature range depending on the Curie temperatures of both phases. Regardless into which case the 5:3 plates will fall when compare to the corresponding 5:4 phase, the effect of the existence of 5:3 plates on the magnetic properties of the 5:4 matrix can be ignored if the vol.% of the precipitated 5:3 phase is low (e.g., less than 3 vol.% as reported in [38]).

Recent scanning Hall probe microscopy studies in the $Gd_5Si_2Ge_2$ [39] revealed that the 5:3 phases do play a role in that the precipitated platelets act as nucleation sites for magnetic transitions within the 5: 4 matrix. This suggests that if one can control the number and

distribution of the 5:3 plates, the unique magnetic properties of the parent matrix can be enhanced. Although it has been hypothesized that they form immediately after solidification via a diffusional – displacive reaction [33], the exact conditions and temperatures at which these platelets form remain unknown since the extremely high melting points (near or above 2000 K) of $R_5(Si_xGe_{1-x})_4$ compounds make it difficult to study phase transformations in these systems at high temperatures.

The apparently large volume concentration of the 5:3 plates within the 5:4 matrix has also created a certain amount of confusion. Early papers [40, 41] suggested that since powder diffraction experiments showed no evidence of any second phase, including 5:3, the thin plates that appeared to be present in large quantities must be a manifestation of a peculiar twin structure. However, subsequent studies employing both scanning and transmission electron microscopy (SEM, TEM) have shown that artifacts associated with sample preparation may give a false impression of the large overall volume of the 5:3 phase, the true values usually being anywhere from 1 to 3 vol.% [38]. The detection of such low amounts is difficult if not impossible in conventional X-ray powder diffraction (XRD) experiments, especially using Cu Kα radiation, due to the low signal-to-noise ratio that arises from a strong fluorescence of Gd and other lanthanides, whose absorption L-edges are close to the energy of Cu Kα radiation [42]. Other difficulties in the detection of the 5:3 plates have been discussed in a previous study [38].

One possible method for studying high temperature phase transformations in systems where the amount of material formed is small is by use of synchrotron radiation coupled with a temperature controlled environment that allows the sample to be heated to high

temperatures. A synchrotron radiation source provides many advantages when collecting powder diffraction data [43]. Among those are 1) the shorter wavelength of the synchrotron X-ray beam provides more accurate structural information by facilitating examination of a larger volume of reciprocal space; 2) the ability to easily adjust the wavelength of the incident beam eliminates the fluorescence problems; and 3) the extremely high flux and nearly non-divergent incident beam provides high resolution powder diffraction (HRPD) capability that allows a level of sensitivity and detail often impossible with a laboratory instrument. Bragg peaks can be more clearly resolved, which is essential for correct Rietveld refinement, and the high sensitivity enables the detection of weak peaks over a low background.

The purpose of this paper is to discuss the feasibility of using bulk diffraction techniques to determine the existence of the 5:3 platelets. Given their significance as nucleation sites for magnetic transitions, any study that would attempt to control their size, volume percentage, and distribution requires a more reliable bulk analysis method than is possible using conventional microscopy techniques. In this paper we report the results of X-ray powder diffraction experiments carried out using both the conventional sealed X-ray tube with copper anode and the Advanced Photon Source (APS) at Argonne National Laboratory to examine the phases and structures present in the lutetium doped Er_5Si_4. The results obtained suggest that synchrotron radiation is suitable for the study of minor impurities observed in $R_5(Si_xGe_{1-x})_4$ compounds.

Experimental Details

A polycrystalline $(Er_{0.9}Lu_{0.1})_5Si_4$ alloy was prepared by arc-melting of constituent elements weighed in stoichiometric proportions in a high-purity argon gas atmosphere. The phase purity was initially examined using conventional X-ray powder diffraction (XRD) performed at room temperature on a PANalytical X'Pert PRO diffractometer employing monochromatic Cu $K\alpha_1$ radiation. The diffraction pattern was collected between 20º and 80º 2θ with a step of 0.01675º. The microstructure of the sample was examined using a JEOL 6060LV scanning electron microscope (SEM) equipped with an X-ray energy dispersive spectrometer (EDS). For a more accurate phase identification in the $(Er_{0.9}Lu_{0.1})_5Si_4$ sample, a high resolution powder diffraction (HRPD) using the Advanced Photon Source (APS) at Argonne National Laboratory was carried out at the 11-BM synchrotron beamline.

Detailed sample preparation and handling procedures for HRPD are provided on the APS website [44]. The high-resolution powder diffraction experiment uses transmission geometry for data collection. Given the high X-ray absorption of the lanthanides, sample powders did not fully fill the Kapton tubes typically used for the experiments but were coated on the inner walls of the tubes with a thin layer of vacuum grease in order to increase the intensity of the diffracted beam.

High resolution diffraction data were collected at ambient temperature with a standard data collection protocol used for automatic data collection. Instrument parameters include: 30 KeV operating energy (mean wavelength: 0.4123Å); a continuous scan covering a 2θ range

from 0.5° to 50° with a scan speed of 0.01 degree/sec; data points spaced at 0.001 degrees with multiple point detectors used for data collection; a rotation rate of the Kapton sample tube was ~ 5000 rpm during the scan. Quantitative phase analysis and crystal structure refinements of different phases present in the $(Er_{0.9}Lu_{0.1})_5Si_4$ sample were performed by the Rietveld method using RIETICA LHPM [45].

Experimental Results

Scanning Electron Microscopy

SEM images of the $(Er_{0.9}Lu_{0.1})_5Si_4$ sample in the as-polished and ion-etched states are shown in Figure 1. Contrast produced in the SEM images using backscattered electrons (BSE) of the as-polished (Fig. 1a) and ion-etched samples (Figs. 1b, 1c) shows the coexistence of several phases. Three phases are seen clearly in Fig.1a and 1b while it seems that there are a total of four phases in Fig. 1c, namely linear features, a black phase, and two gray phases of different shades. The thin white linear features seen in the as-polished sample (Fig. 1a) become more visible after the sample is ion-etched (Fig. 1b). Previous transmission electron microscopy studies [24] have shown that these features are hexagonal 5:3 plates. The compositions obtained from other phases are shown in Table 1. EDS analysis of these phases shows there is no statistical difference in the composition of the light-grey and dark-grey phases in Fig. 1c (areas marked “1” and “2”, respectively); they both have compositions consistent with the 5:4 phases.

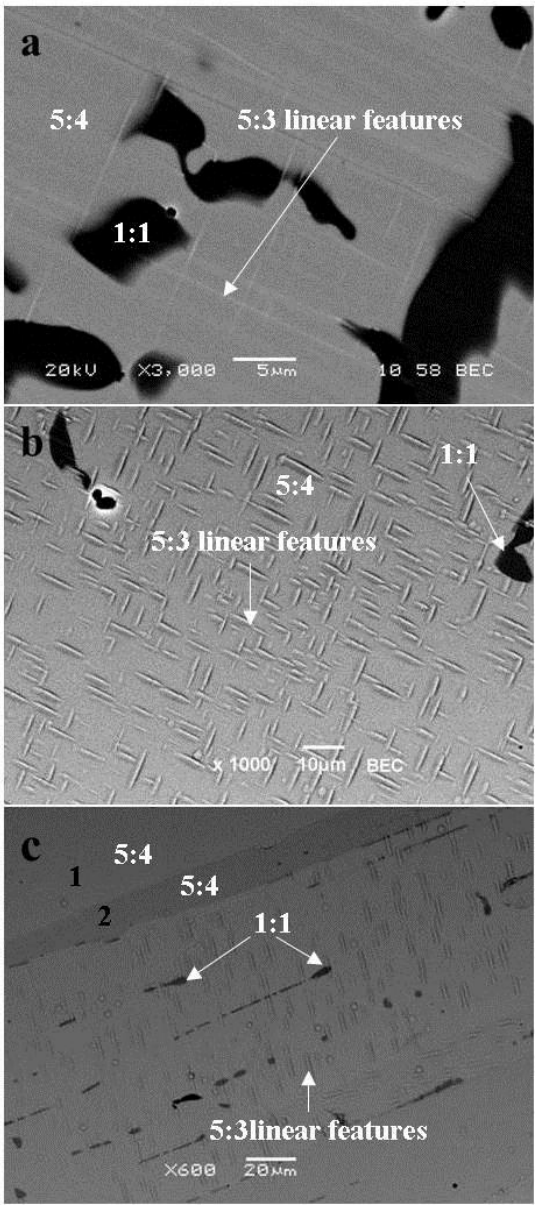

Figure 1. SEM images of $(Er_{0.9}Lu_{0.1})_5Si_4$ on (a) as-polished sample and (b), (c) ion-etched sample.

The dark phase (see Table 1) is Lutetium doped 1:1. Although the total average concentration of the rare-earths Er and Lu is 53.2 at.%, which is slightly higher than the 50 at.% expected from the idealized stoichiometry, this error is consistent with typical systematic errors from measuring a mixture of high (Er and Lu) and low (Si) atomic number elements. Note that the total average concentration of Er and Lu in the 5:4 matrix is

58.2 at.%, which is also slightly higher than the theoretical value of 55.5 at.%, yet the difference in the rare-earth composition between the 1:1 and 5:4 phases is fairly consistent at ~ 5 at.%.

Table 1. Compositions of phases observed in the $(Er_{0.9}Lu_{0.1})_5Si_4$ sample. All the experimental data are the averages of several areas with the same contrast.

	Black phase (1:1)		Light-grey phase (5:4)		Dark-grey phase (5:4)	
Element	Theoretical	Experimental	Theoretical	Experimental	Theoretical	Experimental
	at.%	at.%	at.%	at.%	at.%	at.%
Si	50	46.85	44.44	41.76	44.44	41.29
Er	45	47.68	50	51.35	50	52
Lu	5	5.47	5.56	6.89	5.56	6.71

X-ray Powder Diffraction using Laboratory and Synchrotron Radiation

The XRD pattern of the $(Er_{0.9}Lu_{0.1})_5Si_4$ alloy using laboratory Cu $K\alpha_1$ radiation is shown in Figure 2. The lattice parameters and phase concentrations determined using Rietveld refinement are listed in Table 2. In Fig. 2, three sets of vertical tick marks shown below the diffraction pattern correspond to the calculated locations of the Bragg peaks of the main 5:4 orthorhombic phase (space group Pnma), which is seen as the light grey phase in Fig. 1c, and the two impurity phases: the 5:4 monoclinic phase (space group $P112_1/a$) and the 1:1 orthorhombic phase (space group Cmcm), which are seen as the dark grey and black phases, respectively, in Fig.1c. No Bragg peaks of the hexagonal 5:3 phase could be resolved.

Table 2. Lattice parameters and phase concentrations in the $(Er_{0.9}Lu_{0.1})_5Si_4$ alloy, obtained from the Rietveld refinement of Cu $K\alpha_1$ radiation data.

Phase	Space group	Lattice Parameters (Å)			γ(°)	Vol.%
		a	b	c		
Orthorhombic 5:4	Pnma	7.2781(1)	14.3515(2)	7.5874(1)	90	87.97
Monoclinic 5:4	$P112_1/a$	7.3679(4)	14.383(1)	7.5272(5)	93.05	11.14
Orthorhombic 1:1	Cmcm	4.199(1)	10.376(3)	3.789(8)	90	0.89

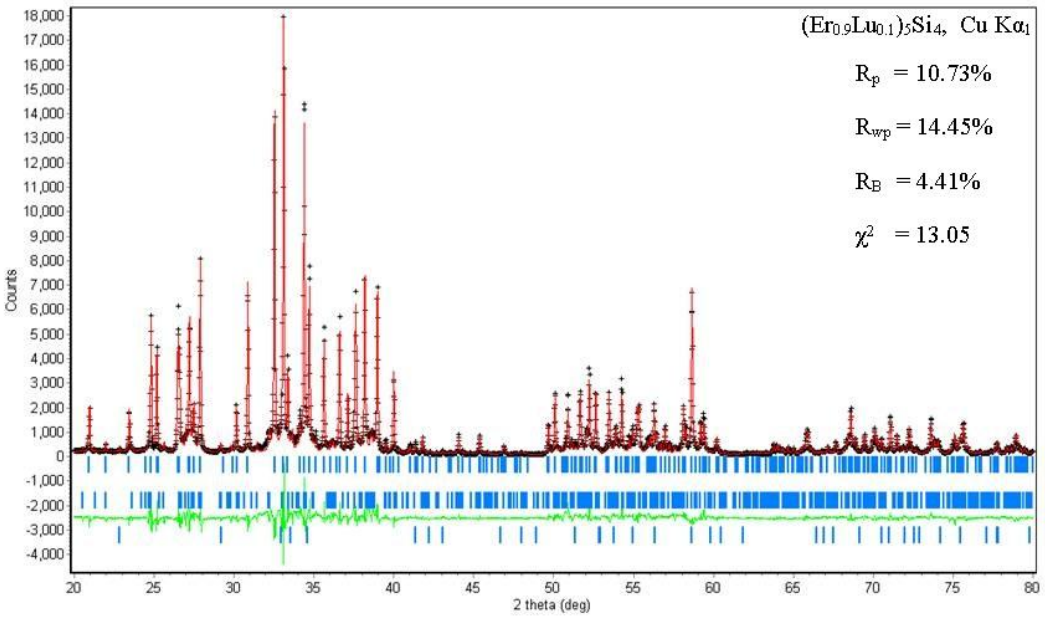

Figure 2. X-ray powder diffraction pattern of $(Er_{0.9}Lu_{0.1})_5Si_4$ at room temperature collected by using Cu $K\alpha_1$ radiation.

The results obtained using the 11-BM synchrotron beamline of APS/ANL are shown in Fig. 3 and Table 3. The scan range covers 0.5 to 50 degrees, but due to the possibility of large errors at high and low Bragg angles, where the data are collected with fewer detectors, only the data from 2.5º to 30º were used for the Rietveld refinement. Bragg peaks of the 5:3 phase are present in this set of data, although they are weak due to the extremely low

volume percentage of this impurity. Another difficulty is that most Bragg peaks from 5:3 overlap with those of the orthorhombic 5:4 matrix and the monoclinic 5:4 phase; only a few peaks exclusively belong to the 5:3 phase are separated enough to be clearly discernible. Two weak peaks showing the highest degree of separation are enlarged and shown in Fig. 3b. Even in these cases it is clear that significant overlap still exists. Tick marks are provided below the diffraction pattern from four different possible phases. The upper set of tick marks indicates the positions of the Bragg peaks of the orthorhombic 5:4 phase, the two middle ones are for the 1:1 and 5:3 phases respectively, and the lowest one is for the monoclinic 5:4 phase. According to Tables 2 and 3, the lattice parameters of the orthorhombic 5:4 and hexagonal 5:3 are smaller than those reported in the literature for pure Er_5Si_4 [46, 47] and Er_5Si_3 [48]. This is consistent with the smaller metallic radius of Lu (1.7349 Å) relative to Er (1.7566 Å) when Lu is substituted for Er in Er_5Si_4 and Er_5Si_3 lattices [49].

Table 3. Lattice parameters and phase concentrations in the $(Er_{0.9}Lu_{0.1})_5Si_4$ alloy, obtained from the Rietveld refinement of synchrotron radiation data.

Phase	Space group	Lattice Parameters (Å)			γ(°)	Vol.%
		a	b	c		
Orthorhombic 5:4	Pnma	7.2783(1)	14.3519(1)	7.5878(1)	90	90.95%
Monoclinic 5:4	$P112_1/a$	7.356(3)	14.412(6)	7.514(3)	92.94	7.96%
Orthorhombic 1:1	Cmcm	4.1894(9)	10.399(3)	3.7825(7)	90	0.49%
Hexagonal 5:3	$P6_3/mcm$	8.299(2)	8.299(2)	6.164(2)	120	0.60%

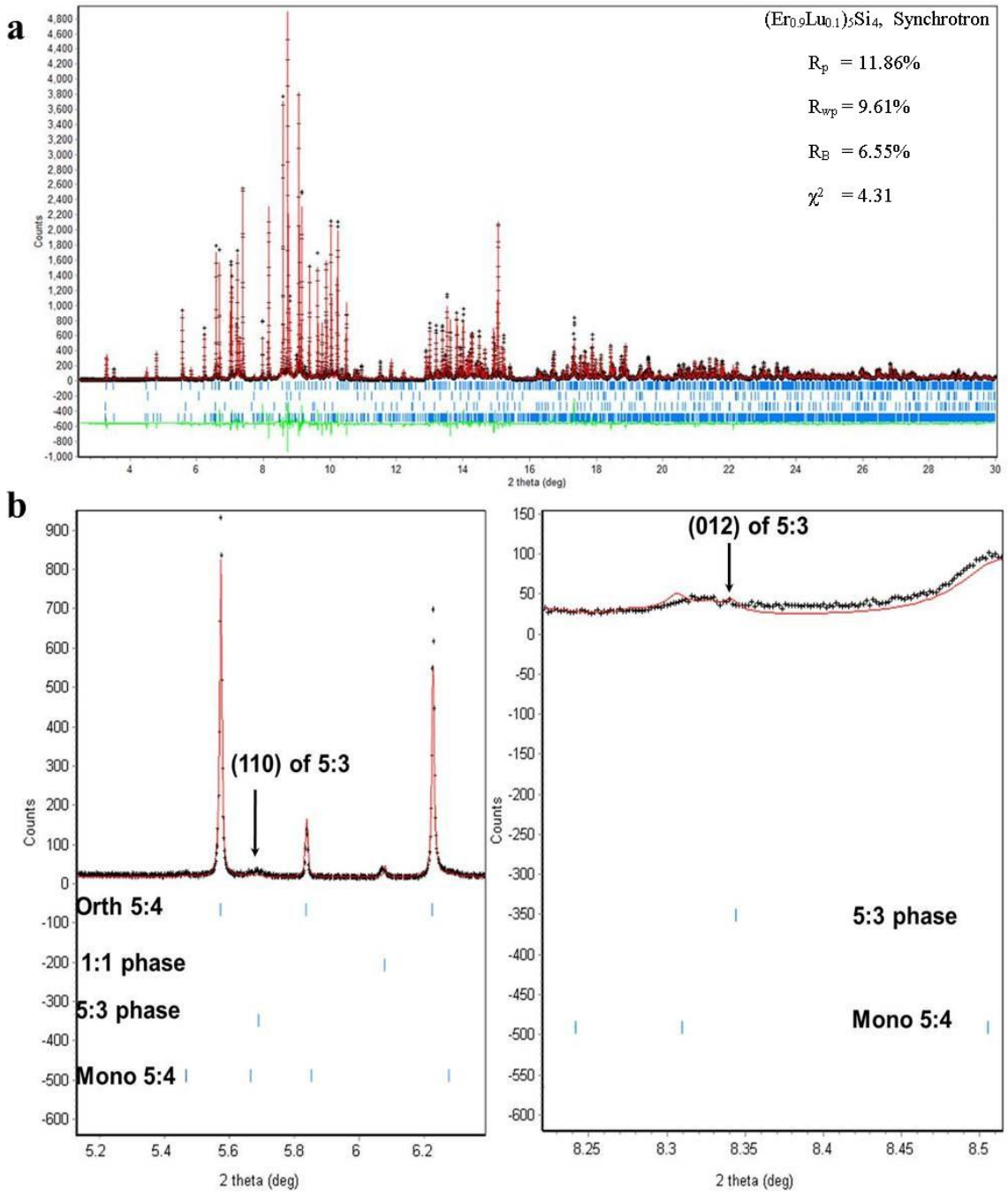

Figure 3. a) High resolution powder diffraction pattern of $(Er_{0.9}Lu_{0.1})_5Si_4$ at room temperature collected by using synchrotron radiation. b) Enlarged view of the location of hexagonal 5:3 phase peaks.

Discussion

Previous studies have confirmed that the width of 5:3 plates observed in SEM images is artificially inflated due to sample preparation artifacts, resulting in an overestimation of the amount present when using simple observation [38]. This explains why the 5:3 phase is undetectable (Fig. 2) using laboratory X-ray radiation and the intensities of the Bragg peaks that belong to this phase are still weak (Fig. 3) even when using synchrotron radiation source, yet the sample appears to contain a larger concentration of the 5:3 phase in the SEM images. As discussed in [38], samples that appear to contain a large amount of 5:3 (up to ~ 10 vol.%) may in fact have less than 1 volume percent.

Rietveld analysis of the conventional XRD results shows a larger amount of the 1:1 phase present in the sample than that of the 5:3 phase since the former was detected and the latter was not. However, a similar analysis using the synchrotron data indicates that the volume concentrations of the two impurity phases are nearly equivalent, with both being less than 1%. This difference is mainly due to the difference in absorption of Er and Lu for the Cu $K\alpha_1$ radiation as opposed to the synchrotron radiation. The linear absorption coefficients of bulk 5:3 and 1:1 phase for the Cu $K\alpha_1$ and synchrotron radiation can be calculated on the basis of the following equation [42]:

$$\mu = \rho_m \sum_{i=1}^{n} w_i \left(\frac{\mu}{\rho}\right)_i$$

where w_i is the weight fraction of the constituent in the compound, $(\mu/\rho)_i$ is elemental mass attenuation coefficient (which can be obtained from the NIST data-base [50]), and ρ_m is the

density of the compound, which can be calculated from the dimensions of the unit cell listed in Table 3. The results are compared in Table 4. Although the data in Table 4 are linear absorption coefficients in bulk materials, they give us a reasonable estimate of the difference in absorption coefficients in powder samples assuming that other variables, such as the packing density of the powder in the samples used for diffraction, remain constant. It is evident that both 5:3 and 1:1 phase have much larger linear absorption coefficients when using Cu $K\alpha_1$ radiation compared to synchrotron, being approximately one order of magnitude larger. Equally evident is that absorption in the 5:3 phase is higher than that in the 1:1 phase. Thus, when using Cu $K\alpha_1$ radiation it is possible that the small amounts of the 5:3 phase remain undetectable, especially considering that transmitted intensity is proportional to $\exp(-\mu x)$, where x is the distance that X-ray travelled through a sample. Using more energetic synchrotron radiation, the difference between the absorption coefficients of these two phases is not as large, and the absorption in general is much lower. The end result is that both the 5:3 and the 1:1 phases can be detected equally well. The concentration of the 5:3 phase calculated from diffraction data is reasonable given the SEM images and the results of previous work carried out using heat capacity data [38].

Table 4. Linear absorption coefficients μ (in cm^{-1}) of bulk $(Er_{0.9}Lu_{0.1})_5Si_3$ (5:3 phase) and $(Er_{0.9}Lu_{0.1})Si$ (1:1 phase) for the Cu $K\alpha_1$ and synchrotron radiation.

	Cu $K\alpha_1$	Synchrotron
$\mu_{5:3}$	1058.21	137.60
$\mu_{1:1}$	973.27	123.44
$\mu_{5:3}$-$\mu_{1:1}$	84.95	14.16

The volume concentration of the monoclinic 5:4 obtained from conventional XRD is higher than that obtained from synchrotron XRD, being approximately 11 vol.% in the former case as opposed to 8 vol.% in the later case. This difference may be real considering that different pieces of the same arc-melted button have been used to prepare samples for conventional and synchrotron experiments. For example, slight differences in homogeneity in the starting material used for the two diffraction experiments, or differences introduced during sample preparation could easily lead to this discrepancy. However, the most likely explanation again is related to the differences in the linear absorption coefficients of different phases. (N.B. The density and the linear absorption coefficient of the monoclinic 5:4 phase are lower than those of the orthorhombic 5:4 phase, even assuming that their chemical compositions are identical, which follows from Table 1). Considering that the concentrations of phases from Rietveld refinement were determined without correcting for varying absorption, the observed 3 vol.% difference falls within the error limits of the powder diffraction techniques.

It is interesting to compare the powder diffraction results to those obtained by direct observation using the SEM, which shows at least three phases with different compositions in the $(Er_{0.9}Lu_{0.1})_5Si_4$ sample by EDS analysis, namely 5:4, 1:1, and 5:3. As noted above, the dark gray phase seen in Fig.1c using BSE imaging and possessing a 5:4 composition is the monoclinic 5:4 phase, with the slight difference in contrast being due to the different crystal structures. If one carries out quantitative metallography on SEM images from this sample, the relative amounts of phases are 0.5 vol. % of the black phase and 9.9 vol. % of the dark gray phase. These numbers match well with the fractions of the 1:1 and

monoclinic 5:4 phases obtained from XRD techniques. Determining an accurate volume percentage of 5:3 is difficult due to the artifacts discussed in [38]. Measurements obtained from SEM images of regions in the $(Er_{0.9}Lu_{0.1})_5Si_4$ sample that have a high density of 5:3 plates yield a number of ~ 3.6 vol.% of the 5:3 phase. If one applies the same correction factor used in [38] to account for the artificial thickening of the plates, the actual amount can be expected to be close to ~ 1 vol. %. This is much closer to what was calculated using the synchrotron data and is reasonable considering that a high-density region was specifically chosen for the SEM measurements.

Conclusions

Both SEM and XRD using conventional Cu $K\alpha_1$ and synchrotron radiation were used to examine the phase purity of the arc-melted lutetium doped erbium silicide $(Er_{0.9}Lu_{0.1})_5Si_4$. The results show there are three impurity phases coexisting within the orthorhombic 5:4 matrix in this sample, namely, the monoclinic 5:4 phase (~ 10 vol.%), the 1:1 phase (< 1 vol.%) and the hexagonal 5:3 phase (< 1 vol.%). The 5:3 phase was definitely observed in SEM and detected by XRD when using synchrotron radiation, but due to the high X-ray absorption and the high degree of overlap between 5:3 peaks and those of other phases, the 5:3 phase could not be detected when examined by conventional XRD using Cu $K\alpha_1$ radiation. Therefore, high resolution X-ray powder diffraction using synchrotron radiation is more suitable for use when low volume concentrations of highly absorbing phases such as the 5:3 impurity phase considered in this study are present. Additionally, the ability to

discern between the monoclinic and orthorhombic polymorphs of 5:4 phase is possible using backscattered electron imaging in the SEM. However, SEM should be coupled with an XRD technique to ensure accurate identification.

Acknowledgments

This work was performed at Ames Laboratory under contract no.DE-AC02-07CH11358 with the US Department of Energy. This research was supported by the Office of Basic Energy Sciences, Materials Science Division of the US DOE. The high resolution powder diffraction in this study was carried out at the 11-BM synchrotron beamline of APS/ANL. Use of the Advanced Photon Source at Argonne National Laboratory was supported by the U. S. Department of Energy, Office of Science, Office of Basic Energy Sciences, under Contract No. DE-AC02-07CH11358. The authors wish to thank M.Suchomel and other 11-BM staff for their help and work in the high resolution powder diffraction experiments.

References

[1] V. K. Pecharsky, K. A. Gschneidner Jr., Pure. Appl. Chem., 79 (2007) 1383 and references therein.

[2] Y. Mudryk, V. K. Pecharsky, Z. Anorg. Allg. Chem., 637 (2011) 1948 and references therein.

[3] V. K. Pecharsky, K. A. Gschneidner Jr., Phys. Rev. Lett., 78 (1997) 4494.

[4] A. Giguère, M. Foldeaki, B. R. Gopal, R. Chahine, T. K. Bose, A. Frydman, J. A.

Barclay, Phys. Rev. Lett., 83 (1999) 2262.

[5] L. Morellon, C. Magen, P. A. Algarabel, M. R. Ibarra, C. Ritter. Appl. Phys. Lett. 79 (2001) 1318.

[6] L. Morellon, P. A. Algarabel, M. R. Ibarra, J. Blasco, B. Garcia-Landa, Z. Arnold, F. Albertini, Phys. Rev. B, 58 (1998) R14721.

[7] L. Morellon, J. Blasco, P. A. Algarabel, M. R. Ibarra, Phys. Rev. B, 62 (2000) 1022.

[8] E. M. Levin, V. K. Pecharsky, K. A. Gschneidner Jr., P. Tomlinson, J. Magn. Magn. Mater., 210 (2000) 181.

[9] J. B. Sousa, M. E. Braga, F. C. Correia, F. Carpinteiro, L. Morellon, P. A. Algarabel, M. R. Ibarra, Phys. Rev. B, 67 (2003) 134416.

[10] M. Zou, V. K. Pecharsky, K. A. Gschneidner Jr., Y. Mudryk, D. L. Schlagel, T. A. Lograsso, Phys. Rev. B, 80 (2009) 174411.

[11] V. K. Pecharsky, K. A. Gschneidner Jr., Adv. Mater., 13 (2001) 683.

[12] A. O. Pecharsky, K. A. Gschneidner Jr., V. K. Pecharsky, C. E. Schindler, J. Alloys Compd., 338 (2002) 126.

[13] V. K. Pecharsky, A. O. Pecharsky, Y. Mozharivskyj, K. A. Gschneidner Jr., G. J. Miller, Phys. Rev. Lett., 91 (2003) 207205.

[14] C. Ritter, C. Magen, L. Morellon, P. A. Algarabel, M. R. Ibarra, V. K. Pecharsky, A. O. Tsokol, K. A. Gschneidner Jr., J. Phys. Condens. Matter, 18 (2006) 3937.

[15] W. Choe, V. K. Pecharsky, A. O. Pecharsky, K. A. Gschneidner Jr., V. G. Young Jr., G. J. Miller, Phys. Rev. Lett., 84 (2000) 4617.

[16] V. K. Pecharsky, A. P. Holm, K. A. Gschneidner Jr., R. Rink, Phys. Rev. Lett., 91 (2003) 197204.

[17] Z. W. Ouyang, H. Nojiri, S. Yoshii, Phys. Rev. B, 77 (2008) 184426.

[18] Y. C. Tseng, H. J. Ma, C. Y. Yang, Y. Mudryk, V. K. Pecharsky, K. A. Gschneidner Jr., Phys. Rev. B, 83 (2011) 104419.

[19] C. Magen, L. Morellon, P. A. Algarabel, M. R. Ibarra, Z. Arnold, J. Kamarad, T. A. Lograsso, D. L. Schlagel, V. K. Pecharsky, A. O. Tsokol, K. A. Gschneidner Jr., Phys. Rev. B, 72 (2005) 024416.

[20] L. Morellon, Z. Arnold, P. A. Algarabel, C. Magen, M. R. Ibarra, Y. Skorokhod, J.

Phys. Condens. Matter, 16 (2004) 1623.

[21] C. Magen, L. Morellon, Z. Arnold, P. A. Algarabel, C. Ritter, M. R. Ibarra, J. Kamarad, A. O. Tsokol, K. A. Gschneidner Jr., V. K. Pecharsky, Phys. Rev. B, 74 (2006) 134427.

[22] Y. Mudryk, D. Paudyal, V. K. Pecharsky, K. A. Gschneidner Jr., S. Misra, G. J. Miller, Phys. Rev. Lett., 105 (2010) 066401.

[23] Y. Mudryk, D. Paudyal, V. K. Pecharsk, K. A. Gschneidner Jr., Phys. Rev. B, 77 (2008) 024408.

[24] C. Cao, L. S. Chumbley, Mater. Charact., 62 (2011) 737.

[25] J. Szade, G. Skorek, A. J. Winiarski, J. Cryst. Growth, 205 (1999) 289.

[26] J. S. Meyers, L. S. Chumbley, F. Laabs, A. O. Pecharsky, Scripta Mater. 47 (2002) 509.

[27] O. Ugurlu, L. S. Chumbley, D. L. Schlagel, T. A. Lograsso, A. O. Tsokol, Acta Mater., 53 (2005) 3525.

[28] H. Fu, Y. Chen, T. Zhang, M. Tu, J. Rare Earths, 23 (2005) 409.

[29] O. Ugurlu, L. S. Chumbley, D. L. Schlagel, T. A. Lograsso, A. O. Tsokol, Scripta Mater., 53 (2005) 373.

[30] O. Ugurlu, L. S. Chumbley, D. L. Schlagel, T. A. Lograsso, A. O. Pecharsky, 134th TMS (Minerals, Metals and Materials Society) Annual Meeting. Light Metals 2005;1181.

[31] Z. Qian, L. S. Chumbley, S. Misra, G. J. Miller, V. K. Pecharsky, K. A. Gschneidner Jr., K. Ahn, A. S. Chernyshov, N. K. Singh, Acta Mater., 57 (2009) 3374.

[32] C. Cao, L. S. Chumbley, Z. Qian, Intermetallics, 2010 (18) 1021.

[33] O. Ugurlu, L. S. Chumbley, D. S. Schlagel, T. A. Lograsso, Acta Mater., 54 (2006) 1211.

[34] E. Parthe, Acta Crystallogr., 13 (1960) 868.

[35] N. C. Baezinger, J. J. Hegenbarth, Acta Crystallogr., 17 (1964) 620.

[36] J. Arbuckle, E. Parthe, Acta Crystallogr., 15 (1962) 1205.

[37] K. S. V. L. Narasinhan, H. Steinfink, E. V. Ganapathy, J. Appl. Phys., 40 (1969) 51.

[38] L. S. Chumbley, O. Ugurlu, R. W. McCallum, K. W. Dennis, Y. Mudryk, K. A. Gschneidner Jr., V. K. Pecharsky, Acta Mater., 56 (2008) 527.

[39] J. D. Moore, K. Morrison, G. K. Perkins, D. L. Schlagel, T. A. Lograsso, K. A.

Gschneidner Jr., V. K. Pecharsky, L. F. Cohen, Adv. Mater., 21 (2009) 3780.

[40] M. Manekar, M. K. Chattopadhyay, R. Kaul, V. K. Pecharsky, K. A. Gschneidner Jr., J. Phys. Condens. Matter, 18 (2006) 6017.

[41] C. Magen, L. Morellon, P. A. Algarabel, C. Marquina, M. R. Ibarra, J. Phys. Condens. Matter, 15 (2003) 2389.

[42] V. K. Pecharsky, P. Y. Zavalij, Fundamentals of powder diffraction and structural characterization of materials. 2nd ed. New York: Springer; 2009.

[43] 11-BM of Advanced Photon Source: Technical description. Argonne (IL): Argonne National Laboratory (US). [updated Sep 2011]. Available from: http://11bm.xor.aps.anl.gov/description.html#perform

[44] 11-BM of Advanced Photon Source: Sample preparation for mail-in users. Argonne (IL): Argonne National Laboratory (US). [updated Feb 2011]. Available from: http://11bm.xor.aps.anl.gov/users_prep.html

[45] Hunter BA. RIETICA, a visual Rietveld program, Internationals union of crystallography commission on powder diffraction. Newsletter No.20 (1998). Available from: http://www.rietica.org

[46] F. Holtzberg, R. J. Gambino, T. R. McGuire, J. Phys. Chem. Solids, 28 (1967) 2283.

[47] S. P. Luzan, V. E. Listovnichii, Y. I. Buyanov, P. S. Martsenyuk. J. Alloys Compd., 239 (1996) 77.

[48] I. P. Semitelou, J. K. Yakinthos, E. Roudaut, J. Phys. Chem. Solids, 56 (1995) 891.

[49] B. J. Beaudry, K. A. Gschneidner Jr., Preparation and basic properties of the rare earth metals. In: Gschneidner Jr KA, Eyring L, editors. Handbook on the Physics and Chemistry of Rare Earths, New York: North-Holland Publishing Co. (Elsevier); 1978, p.173.

[50] Table of X-Ray Mass Attenuation Coefficients. Gaithersburg (MD): National Institute of Standards and Technology (US). [Online June 1994]. Available from: http://physics.nist.gov/PhysRefData/XrayMassCoef/tab3.html

ACKNOWLEDGMENTS

I would like to take this opportunity to express my sincere thanks to those who helped me throughout this research and the writing of this thesis

First of all, I want to give my deepest appreciation to my advisor, Dr. Scott Chumbley. His remarkable patience and unreserved support have always touched me. His constant enthusiasm, motivation and guidance have encouraged me. His scientific knowledge, technical skills and enlightened views on the research process has left a deep impression on me. To have been a student of him is one of my best experiences in my life.

I would to thank Drs. Vitalij K. Pecharsky and Karl Gschneidner, Jr. for their generous help throughout this research and valuable input into my papers.

Besides the three professors I mentioned above, I also like to thank the rest of my Program of Study (POS) committee members: Drs. Alan M. Russell and Gordon J. Miller for their time and support.

I give my special thanks to Matt Kramer, Fran Laabs, Yaqiao Wu for helping me with the instruments and Deborah L. Schlagel for for the preparation of all the single crystal samples in this thesis study.

My special appreciation extends to the people with whom I have been working in the Ames Laboratory for their help in some of my experiments and data analysis. They are Yaroslav Mudryk, Min Zou, Niraj. K. Singh, Ying Zhang, Yunus Eren Kalay, Hu Zhang.

My thanks also go to my peer students in materials science and engineering department,

especially Zhongyuan Qian, Cheng Ma, Li Li, Jing Liu, Jin Liu, Tugce Karakulak, Taylor Grieve for their support and sharing during my course work and difficult times in my life.

I also thank the Office of Basic Energy Sciences, Materials Sciences Division of the U. S. Department of Energy for their financial support. This work was performed at Ames Laboratory under Contract No. DE-AC02-07CH11358.

Finally, I would like to express my heartfelt gratitude to my parents and my husband Xin Zhao for their unconditional love, constant support and immense faith and encouragement during my graduate studies at ISU.